about for two reasons. The geometric distance to the wall increases with increasing frequency and waves encounter additional retardation in crossing the vertical contours as the wave approaches the reflecting wall. The second effect is to bring the two branches of the loop closer together with increasing frequency. The reason for this is again that the distance between the sounder and wall increases with increasing sounding frequency. If the separation of the contours becomes sufficiently great, the branches may even merge or the effective nose frequency may become so great as to exclude oblique echoes from returning to the satellite. Thus, for a variable spacing in the vertical contours it is possible to get several loops separated by frequency regions of no returned oblique echoes (the two loops in Fig. 1, ionogram C, could be an example of this).

The loops shown in Fig. 1 can now be understood. Each of the loops shows the nose frequency and two branches which tend to merge at the higher frequencies. On ionogram A the nose of the loop is at about 1.03 MHz. Thus, the reflection would occur near the steep part of the $5 \times 10^3$ ($cm^{-3}$) electron density contour shown on Fig. 2 just equatorward of the sounder at point A. On ionogram B the nose frequency is 1.18 MHz so that the reflection occurs near the $8 \times 10^3$ electron density contour. Again the ray would be reflected equatorward of the sounder (point B). Since the sounder at position B is further away from the steep side of the depression than at position A the nose frequency is higher on ionogram B than on ionogram A. On ionogram C there are two loops, whose nose frequencies are about 0.72 MHz and 1.31 MHz. Notice that the extraordinary cutoff is at a much lower frequency on ionogram C, due to the lower electron density at the sounder at point C. The lower and higher frequency loops are reflected from near the $6 \times 10^2$ and $6 \times 10^4$ electron density levels, respectively. The lower frequency loop is reflected equatorward of the sounder from the less dense wall which intersects the sounder path between sounder positions B and C. The higher frequency loop is probably reflected equatorward of the sounder also, since the higher frequency rays can penetrate the less dense wall responsible for the low-frequency loop. However, for the higher frequency loop, reflection from poleward of the sounder cannot be ruled out.

The model discussed in this paper can also be used to understand some echoes from field-aligned sheets of irregularities[8] such as are observed at high magnetic latitudes. For this scattering problem the reflecting wall is stationary and the upper branch of the loop approaches a constant delay time for increasing frequency. Because other ray paths (discussed in studies of spread F[4]) are also possible in this problem the resulting traces are sometimes more diffuse than the traces explained in this paper.

[8] A review of F-region irregularities and a review of topside irregularities are given, respectively, by J. R. Herman, "Spread F and ionospheric F-region irregularities," *Rev. Geophys.*, vol. 4, pp. 255–299, May 1966; and by W. Calvert and J. M. Warnock, "Ionospheric irregularities observed by topside sounders," to be published in *Proc. IEEE*, June 1969.

# Theory and Practice of Ionosphere Study by Thomson Scatter Radar

J. V. EVANS, FELLOW, IEEE

**Abstract—The application of Thomson (or incoherent) Scatter observations to the study of the earth's ionosphere is described. Those aspects of theory of Thomson Scatter that have been put to practical use in ionospheric investigations are reviewed briefly and the type of radar equipment constructed for these investigations is discussed. Methods of measuring electron density, electron and ion temperatures, and ionic composition are then reviewed. Other applications of the technique—to the study of the neutral density and temperature of the upper atmosphere, drift motions, the flux density of fast photoelectrons, and the orientation of the earth's magnetic field—are also described.**

Manuscript received November 21, 1968. This work was sponsored by the U. S. Air Force.

The author is with the M.I.T. Lincoln Laboratory, Lexington, Mass. 02173.

## I. Introduction

DIRECT evidence for the existence of ionized layers in the earth's upper atmosphere has existed since the pioneering experiments of Appleton and Barnett [1] in England in 1925 and those of Breit and Tuve [2] in America in 1926. The basic theory governing the action of solar ultraviolet radiation in forming an ionized layer in the atmosphere was given by Chapman [3] in 1931, and intensive studies of ionospheric electron density were made during and after the second World War. However, major advances in understanding the physics of the ionosphere have been made only since the late 1950's, largely as a result

of new techniques, viz., *in situ* sampling by rockets and satellites and earth-based radar observations of Thomson (or incoherent) Scatter.

The experiments carried out by Appleton and Barnett, Breit and Tuve, and others, depended upon observing a radio signal of frequency $f$ reflected from the ionosphere. This will occur at an altitude at which $f = f_N$ where $f_N$ is the plasma frequency given by [4]

$$f_N = \frac{1}{2\pi}\left[\frac{Ne^2}{m_e\varepsilon_0}\right]^{\frac{1}{2}} \tag{1}$$

where $N$ = electron density/($m^{-3}$), $e$ = charge on an electron ($1.6 \times 10^{-19}$ C), $m_e$ = mass of an electron ($9.1 \times 10^{-31}$ kg) and $\varepsilon_0$ = permittivity of free space ($8.85 \times 10^{-12}$ f/m). When $f_N$ is expressed in MHz, (1) reduces to the well-known relation

$$f_N = 8.97 \times 10^{-6} N^{\frac{1}{2}}. \tag{2}$$

By advancing the frequency $f$ of the exploring signal, it is possible to examine the distribution of density versus altitude up to the peak of the $F2$ layer, which typically might be at 300 km altitude. The ionization lying above the layer peak cannot be detected from the ground by the reflection technique. A second restriction is that only the electron density can be determined. The observed density represents the balance between competing processes of production, loss, and movements, and even today we do not have reliable means of measuring independently these three functions. Thus considerable uncertainty remains concerning the importance of certain effects [5], [6]. However, other properties of the upper atmosphere (neutral density, temperature, and composition) that bear on the formation of the ionosphere are now open to study, thereby eliminating much uncertainty concerning the production and loss terms. Additional properties of the plasma —the ionic composition and temperature—are also measurable, both by *in situ* sampling and by means of high-power radar observations from the ground.

In this paper we attempt to review what can be accomplished using the new technique of high-power radar study. We begin, in the section that follows, by discussing some of the theory of Thomson Scatter. In order to be brief, we simply present, without any derivation, results reached in earlier theoretical papers and limit the review to those predictions of the theory that have been put to practical test and use for ionospheric studies.

In Section III we describe some of the apparatus that has been constructed for Thomson Scatter studies of the ionosphere. At the present time there are four U. S. groups actively engaged in this work, and one group each in England, France, and the USSR. Sections IV–VIII discuss methods of determining, respectively, electron density, electron and ion temperature, ion composition, drift motions, and neutral temperature, and in Section IX other applications of the technique are discussed. In this review it would not be possible to describe all the experimental work that has been performed, and instead, only a few representative results for each of the types of measurement are presented.

## II. Theory

### A. Scatter of Radiation by a Plasma

It was discovered after World War II that, given adequate sensitivity, it is possible to detect signals scattered from the ionosphere at operating frequencies $f \gg f_0F2$ where $f_0F2$ is the plasma frequency $f_N$ at the peak of the $F2$ layer [7]. This scatter arises from the existence of density fluctuations in the medium which give rise to local variations in the dielectric constant $\varepsilon$. If the local deviation is $\Delta\varepsilon$, then the mean square deviation in $\varepsilon$ for any volume $v$ of the medium is

$$\overline{\left|\frac{\Delta\varepsilon}{\varepsilon}\right|^2} = \frac{1}{v}\int_v \left|\frac{\Delta\varepsilon}{\varepsilon}\right|^2 dv \tag{3}$$

and the radar scattering cross section of such a medium per unit volume for given directions of incidence and scattering becomes [8], [9]

$$\sigma = \overline{\left|\frac{\Delta\varepsilon}{\varepsilon}\right|^2}\frac{4\pi^3}{\lambda^4}\sin^2\psi P\left[k(l_2 - l_1), k(m_2 - m_1), k(n_2 - n_1)\right] \tag{4}$$

where $\lambda$ is the radio wavelength and $k$ the propagation constant ($=2\pi/\lambda$). The $(l_1, m_1, n_1)$ is a unit vector in the direction of incidence, and $(l_2, m_2, n_2)$ a unit vector in the direction of scattering, $\psi$ being the polarization angle, i.e., the angle between the incident electric field and the direction to the receiver. The function $P[k(l_2-l_1), k(m_2-m_1), k(n_2-n_1)]$ is a three-dimensional wave-number spectrum of the density variation. Stated differently, this function is the Fourier transform of an autocorrelation function $\rho(x, y, z)$, which specifies the average shape of the irregularities $(\Delta\varepsilon/\varepsilon)$ $(x, y, z)$ in a direction defined by $(l_1, m_1, n_1)$ and $(l_2, m_2, n_2)$. Since the autocorrelation function $\rho(x, y, z)$ must be normalized to unity at the origin, it follows that the wave-number spectrum must be normalized as

$$\int_{-\infty}^{+\infty}\int_{-\infty}^{+\infty}\int_{-\infty}^{+\infty} P\left[k(l_2 - l_1), k(m_2 - m_1), k(n_2 - n_1)\right] d(l_2 - l_1) d(m_2 - m_1), d(n_2 - n_1) = 1,$$

i.e., the volume under the function is unity.

The direction of the vector $(l_2-l_1, m_2-m_1, n_2-n_1)$ is the bisector of the external angle, and defines what may be termed the "mirror direction" for the directions of incidence and scattering. Planes perpendicular to this vector are able to "mirror" the direction of incidence into the direction of scattering [9].

The irregularities in the medium may be Fourier analyzed into plane stratified fractional deviations of $\varepsilon$ having sinusoidal profiles and continuously distributed with regard to both direction and corrugation wavelength. Equation (4) therefore implies that the scattering in a particular direction

depends upon the Fourier content of the irregularities in an associated mirror direction. That is, it depends upon the presence of corrugation wavelengths such as to produce constructive interference in the direction of scattering. For signals to be scattered through an angle $\chi$ there must be a significant Fourier component of corrugation wavelength $\lambda/[2 \sin (\chi/2)]$ in the mirror direction associated with the directions of incidence and scattering. In the particular case of backscattering for which $(l_1, m_1, n_1) = -(l_2, m_2, n_2)$ $[=(l, m, n)$, for example] and $\psi = \pi/2$

$$\sigma = \overline{\left|\frac{\Delta\varepsilon}{\varepsilon}\right|^2} \frac{4\pi^3}{\lambda^4} P(2kl, 2km, 2kn) \tag{5}$$

where $(l, m, n)$ is a unit vector in the direction of incidence. For an ionized medium characterized by a plasma frequency $f_N$ [defined in (1)], it may be shown that [9]

$$\overline{\left|\frac{\Delta\varepsilon}{\varepsilon}\right|^2} = \overline{\left|\frac{\Delta N}{N}\right|^2} \left(\frac{f_N^2}{f^2 - f_N^2}\right)^2 \tag{6}$$

in which $f$ is the radio wave frequency. Thus, in the case when $f \gg f_N$,

$$\overline{\left|\frac{\Delta\varepsilon}{\varepsilon}\right|^2} = \overline{\left|\frac{\Delta N}{N}\right|^2} \left(\frac{f_N}{f}\right)^4. \tag{7}$$

On substituting in (5), this leads to

$$\sigma = \frac{4\pi^3}{c^4} \overline{\left|\frac{\Delta N}{N}\right|^2} f_N^4 P(2kl, 2km, 2kn). \tag{8}$$

As an illustration, suppose that the plasma contains irregularities $\Delta N/N$ that are spherically symmetrical and describable by a Gaussian autocorrelation function with a scale $L$. Then it may be shown that [9]

$$\sigma = \frac{4\pi^3}{c^4} \overline{\left|\frac{\Delta N}{N}\right|^2} f_N^4 (2\pi)^{3/2} L^3 \exp\left[-\frac{8\pi L^2}{\lambda^2}\right]. \tag{9}$$

It is evident from (9) that in this instance the scattering cross section will depend critically upon the ratio $L/\lambda$ which appears in the exponential term. Ionospheric irregularities (associated, for example, with spread $F$) are thought to contain irregularities $\Delta N/N$ of $\sim 1$ percent and have scale sizes $L$ of the order of many tens of meters. Thus they are largely undetectable at radio wavelengths $\lambda \leq 1$m. Under these circumstances, and if no other agent is able to produce density fluctuations in the medium with a scale comparable to $\lambda$, the scattering cross section $\sigma$ will fall to a very low value set by the small density fluctuations arising from the random thermal motion of the particles themselves. This scattering we call Thomson (or incoherent) Scatter.

On substituting from (1) for $f_N$, (8) becomes

$$\sigma = 4\pi \left(\frac{e^2}{\varepsilon_0 m_e c^2}\right)^2 \overline{(\Delta N)^2} P(2kl, 2km, 2kn) \tag{10}$$

$$= 4\pi r_e^2 \overline{(\Delta N)^2} P(2kl, 2km, 2kn)$$

where $r_e$ is the classical electron radius $(= e^2/\varepsilon_0 m_e c^2 = 2.82 \times 10^{-15}$ m).

J. J. Thomson [10], who discovered the electron, also showed that single electrons are capable of scattering electromagnetic waves (X-rays), and that the energy scattered by an electron into unit solid angle per unit incident flux (1 W/m$^2$) is given by $(r_e \sin \psi)^2$ where $\psi$ is the polarization angle, i.e., the angle between the direction of the incident electric field and the direction to the observer. The $(\sin \psi)$ term enters because the scattering polar diagram of each excited electron is similar to that of a Hertzian dipole. It can be seen that the scattering cross section is independent of the wavelength of the incident electromagnetic radiation, and that the total flux reradiated is $8\pi r_e^2/3$. This is known as the Thomson cross section.

Radar engineers have adopted a convention whereby the cross section of a target is stated as the projected area of a perfectly conducting sphere which, if placed in the same position as the real target, would scatter the same amount of energy to the observer. Since perfectly reflecting spheres are isotropic scatterers it follows that the *radar* cross section of an electron $\sigma_e$ should be stated as

$$\sigma_e = 4\pi (r_e \sin \psi)^2 \approx 10^{-28} \sin^2 \psi \text{ m}^2. \tag{11}$$

In the case of backscattering, $\psi = \pi/2$ and thus (10) may be written

$$\sigma = \sigma_e \overline{(\Delta N)^2} P(2kl, 2km, 2kn). \tag{12}$$

Fejer [11] first examined the scattering when the function $P(2kl, 2km, 2kn)$ represents the fluctuation density brought about by the random thermal motion of the particles. He showed that, subject to conditions that will be mentioned, the product

$$\overline{(\Delta N)^2} P(2kl, 2km, 2kn) = N \tag{13}$$

so that the radar cross section of unit volume is $N\sigma_e$. This same result can be reached very simply by classical arguments as follows. The radar signals in any practical experiment will illuminate a finite volume in the ionosphere. Because of their random thermal motion, the electrons will scatter signals whose phases are varying with time and which bear no relation one to another. Thus at the receiver the signal powers (rather than voltages) will add, and on the average the cross section per unit volume will be simply the product of the density $N$ and the cross section per electron $\sigma_e$. It is on the basis of this argument that the term "incoherent scatter" (or "incoherent backscatter") has been used to describe the phenomenon. However, as we shall see, the presence of the ions in the plasma serve to introduce a degree of coherence, and we prefer the name Thomson Scatter.

### *B. Thomson Scatter from a Thermal Unmagnetized Plasma*

The classical argument given above was employed in a paper by Gordon [12], who first showed that modern radar technology had advanced to the point where the Thomson

TABLE I
DEBYE LENGTH AND MINIMUM SATISFACTORY WAVELENGTH AT DIFFERENT ALTITUDES

| Region | Height (km) | Epoch | $N$ ($m^{-3}$) | $T_e$ (°K) | $D$ (cm) | $\lambda_{min}$ (cm) |
|---|---|---|---|---|---|---|
| $E$ | 120 | Winter night $S_{min}$ | $10^{10}$ | 300 | 1 | 25 |
| | | Summer day $S_{max}$ | $10^{11}$ | 300 | 0.4 | 10 |
| $F1$ | 200 | Winter night $S_{min}$ | $10^{11}$ | 2000 | 1 | 25 |
| | | Summer day $S_{max}$ | $5\times10^{11}$ | 3000 | 0.6 | 15 |
| $F2$ | 300 | Winter night $S_{min}$ | $10^{11}$ | 2500 | 1 | 25 |
| | | Summer day $S_{max}$ | $10^{12}$ | 2500 | 0.3 | 7.5 |
| Upper $F2$ | 1000 | | $10^{10}$ | 3000 | 3.8 | 95 |
| Lower exosphere | ≥2000 | | $5\times10^{9}$ | 3000 | 5.6 | 140 |

*Notes:* $S_{min}$ = sunspot minimum.
$S_{max}$ = sunspot maximum.

Scatter from the ionosphere should be detectable. Gordon also predicted that due to their random thermal motion the electrons would scatter signals with a wide variety of Doppler shifts. The spectrum of the reflected signals would be expected to be Gaussian in shape with a center to half-power width of 0.71 $\Delta f_e$, where $\Delta f_e$ is the Doppler shift of an electron approaching the radar at the mean thermal speed, i.e.,

$$\Delta f_e = \frac{1}{\lambda}(8KT_e/m_e)^{\frac{1}{2}} \text{ Hz} \tag{14}$$

where $K$ is Boltzmann's constant ($=1.38\times10^{-23}$ J/°K) and $T_e$ is the electron temperature. If the wavelength $\lambda$ is expressed in meters this reduces to

$$\Delta f_e = \frac{11(T_e)^{\frac{1}{2}}}{\lambda} \text{ kHz.} \tag{15}$$

Gordon [12] proposed to use a wavelength $\lambda = 1.5$ meters for which 0.71 $\Delta f_e \approx 200$ kHz when $T_e = 1600$°K. Thus it was anticipated that the signals would be widely spread in frequency and consequently a very large antenna system would be required for their detection. It was on this basis that the construction of the Arecibo Ionospheric Observatory was proposed (Section III). The first experimental test of these ideas was performed by Bowles [13] using a then newly completed high-power transmitter at Long Branch, Ill., together with a dipole array antenna constructed for the experiment. Bowles [13], [14] observed echoes which resembled the expected ionospheric Thomson scattered signals in most respects except that the bandwidth was considerably less than 0.71 $\Delta f_e$. He correctly surmised that the role played by the ions in the plasma is to narrow the effective spectrum width.

Later theoretical work [11], [15]–[17] has shown that the influence of the ions on the scattering characteristics is important when the exploring wavelength is very much larger than the Debye length. The Debye length or shielding distance $D$ defined for electrons alone is

$$D = (\varepsilon_0 KT_e/4\pi Ne^2)^{\frac{1}{2}} \text{ meters} \tag{16}$$

where $\varepsilon_0$ is the permittivity of free space, $K$ is Boltzmann's constant, $T_e$ is the electron temperature, $N$ the electron density, and $e$ the charge on an electron. Thus,

$$D = 69(T_e/N)^{\frac{1}{2}} \text{ meters} \tag{17}$$

and typically has values in the ionosphere of the order of 1 cm or less below 1000 km, rising to 6 cm at 2000 km altitude (Table I).

It is not possible to sustain organized motion in a plasma on a scale smaller than $D$ [18]. It follows that for exploring wavelengths $\lambda \ll D$, the wave-number spectrum function $P(2kl, 2km, 2kn)$ [in (12)] contains only a term representing the unperturbed motion of the electrons. In this case the total scattering cross section is $N\sigma_e$ as derived above, and the spectrum of the reflected signals will be Gaussian with a half-power width of 0.71 $\Delta f_e$ [see (15)]. Were one to attempt to observe this scattering, say, by operating a radar at a wavelength of 1 cm, the expected spectrum width (when $T_e = 1600$°K) would be ~30 MHz. The energy per unit bandwidth would therefore be extremely small and beyond the detectable limit of present radar systems. Thus, although such scattering has been observed in laboratory plasmas [19] using a laser as the source of the incident light, it is of little practical interest for ionospheric studies at present.

When the exploring wavelength is much larger than the Debye length, the scattering can no longer be regarded as from the individual electrons, but instead is best thought of as arising from density fluctuations brought about by longitudinal oscillations in the plasma. The principal components will be waves introduced by the presence of the ions (ion-acoustic waves) and electron-induced waves at the plasma frequency and electron gyrofrequency. The total amount of power scattered by each of these waves can be obtained by evaluating the wave-number spectrum function $P(2kl, 2km, 2kn)$ for the fluctuation component in question. In Fejer's paper [11] this was carried out for the ion-acoustic and electron plasma waves under assumptions of thermal equilibrium between electrons and ions, no collisions, no magnetic field, and singly charged ions. The problem was also taken up by Dougherty and Farley [15], Salpeter [16], Hagfors [17], and others [20]–[22] with substantial agreement among their results despite a variety of theoretical approaches. When collisions are ignored, but allowance is made for a possible temperature difference between electrons and ions, the power spectrum of the scattered signals is given by

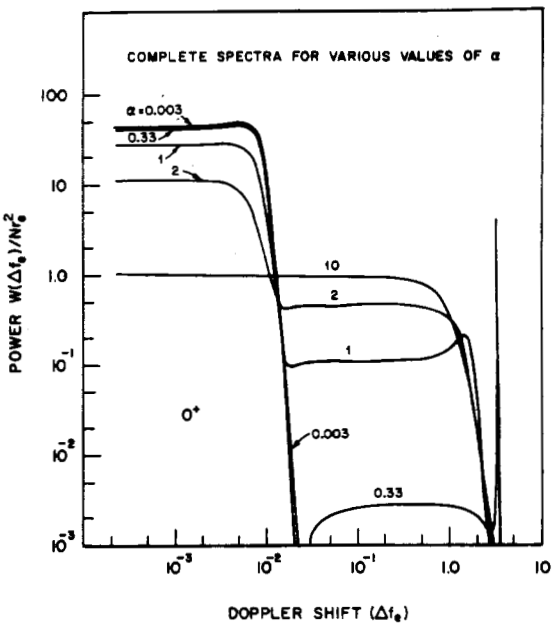


Fig. 1. The variation of the overall spectrum for different values of the ratio $\alpha(=4\pi D/\lambda)$. The ion has been assumed $O^+$. These curves assume that collisions are negligible and that $T_e=T_i$ (after Hagfors [17]).

these terms apply to the ions. The terms in (18) prefaced by summation signs must be evaluated by summing over all the ion species present.

The spectrum function $W(\omega)$ [given in (18)] can be seen to contain two terms, the first of which may be termed the "electronic component" and the second the "ionic component." Fig. 1, taken from a paper by Hagfors [17], shows plots of the logarithm of the echo power versus the logarithm of the Doppler shift in units of $\Delta f_e$ for different values of the parameter $\alpha=4\pi D/\lambda$. The curves in this figure were computed according to (18) for the case $T_e/T_i=1.0$.

When $\alpha\geq 10$, the scattered energy is entirely due to the electronic component and has a Gaussian spectrum with a width proportional to the thermal speed of the electrons as discussed previously [see (15)]. For values of $\alpha$ lying between 0.5 and 2.0, the spectrum appears as the sum of two components (ionic and electronic) which contain approximately equal amounts of power. As $\alpha$ is decreased the amount of power in the *electronic* component decreases and appears in a single line at a Doppler shift approximately equal to the plasma frequency for the medium, $f_N$ [given in (1)]. This plasma resonance line, as it is called, is of great interest and will be discussed further in Sections IV and IX. The largest part of the energy now appears in the ionic component, which, when compared with the electronic spectrum at $\alpha=10$, is narrower by the ratio $(m_i/m_e)^{\frac{1}{2}}$. In the case of $O^+$ ions this is a factor of 171 and thus the width is approximately $2\times 10^{-2}\Delta f_e$. The echo energy is therefore largely concentrated in a relatively narrow spectral line, and it is this feature that renders the earth's ionosphere open to radar investigation using apparatus of lower sensitivity than originally envisaged by Gordon. For $\alpha\to 0$ the total scattered power per electron (in the ionic line) is found to be $\sigma_e/2$ in the case of thermal equilibrium.

$$W(\omega)=\frac{\left|1+\left(\frac{\lambda}{4\pi}\right)^2\sum_i\left(\frac{1}{D_i}\right)^2 F_i(\omega)\right|^2\overline{|N_e^0(\omega)|^2}+\left(\frac{\lambda}{4\pi D_e}\right)^4|F_e(\omega)|^2\sum_i\overline{|N_i^0(\omega)|^2}}{\left|1+\left(\frac{\lambda}{4\pi}\right)^2\left\{\left(\frac{1}{D_e}\right)^2\cdot F_e(\omega)+\sum_i\left(\frac{1}{D_i}\right)^2 F_i(\omega)\right\}\right|^2} \tag{18}$$

where

$\omega$ = angular radio wave frequency displacement from the transmitted frequency
$\lambda$ = radio wavelength
$D_e$ = electron Debye length $=(\varepsilon_0 KT_e/4\pi N_e^2)^{\frac{1}{2}}$
$D_i$ = ion Debye length $=(\varepsilon_0 KT_i/4\pi N_i^2)^{\frac{1}{2}}$

$$F_e(\omega)=1-\omega\int_0^\infty \exp\left(-\frac{16\pi^2 KT_e}{\lambda^2 m_e}\tau^2\right)\sin(\omega\tau)d\tau - j\omega\int_0^\infty \exp\left(-\frac{16\pi^2 KT_e}{\lambda^2 m_e}\tau^2\right)\cos(\omega\tau)d\tau \tag{19a}$$

$$F_i(\omega)=1-\omega\int_0^\infty \exp\left(-\frac{16\pi^2 KT_i}{\lambda^2 m_i}\tau^2\right)\sin(\omega\tau)d\tau - j\omega\int_0^\infty \exp\left(-\frac{16\pi^2 KT_i}{\lambda^2 m_i}\tau^2\right)\cos(\omega\tau)d\tau. \tag{19b}$$

The term $\overline{|N_e^0(\omega)|^2}$ is the fluctuation spectrum of the independent electrons, that is,

$$\overline{|N_e^0(\omega)|^2}=2N\int_0^\infty \exp\left(-\frac{16\pi^2 KT_e}{\lambda^2 m_e}\tau^2\right)\cos(\omega\tau)d\tau \tag{20}$$

and $\overline{|N_i^0(\omega)|^2}$ is the corresponding spectrum for the ions obtained by replacing $N_e$ by $N_i$, $T_e$ by $T_i$, and $m_e$ by $m_i$. Here $N_e$ is the number density of electrons, $T_e$ the electron temperature, $m_e$ the electron mass, and with the subscript $i$,

The ionic component is plotted in Fig. 2 for various values of the ratio $\alpha=4\pi D/\lambda$. In this figure the frequency scale is in units of the Doppler shift $\Delta f_i$ expected for an ion approaching at the mean speed of the ions, i.e.,

$$\Delta f_i=\frac{1}{\lambda}(8KT_i/m_i)^{\frac{1}{2}}\ \text{Hz} \tag{21}$$

where $m_i$ is the mass of the dominant positive ion. For atomic oxygen this reduces to

$$\Delta f_i=65(T_i)^{\frac{1}{2}}/\lambda\ \text{Hz} \tag{22}$$

when $\lambda$ is expressed in meters. It can be seen that when $T_e\to T_i$ the center to half-power width of the spectrum is $\sim 1.6\ \Delta f_i$. Taking $T_i=1600°\text{K}$ and $\lambda=1$ meter, we find $1.6\ \Delta f_i=4.2$ kHz.

The total cross section attributable to the ionic com-

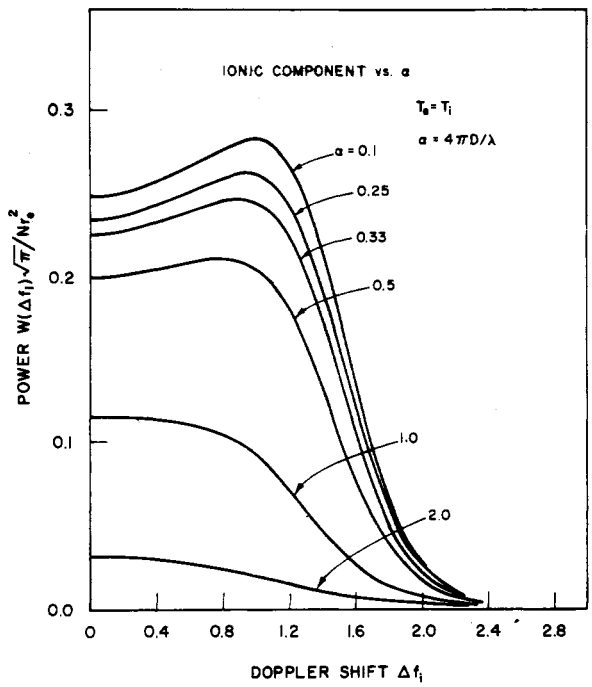


Fig. 2. Spectra of the ionic component of the signal for the case $T_e = T_i$ for different values of $\alpha(=4\pi D/\lambda)$. The frequency scale has been normalized by dividing by the Doppler shift that would be encountered by an approaching ion at the mean thermal speed of the ions (21).

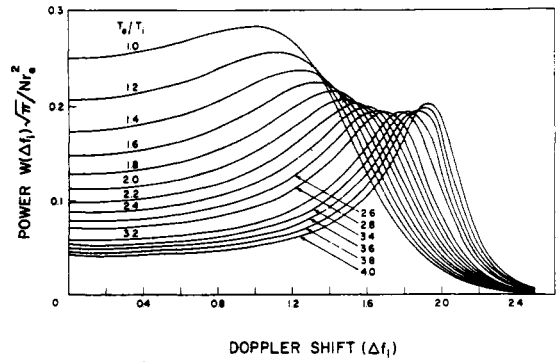


Fig. 3. Spectra of the ionic component for the case $\alpha(=4\pi D/\lambda)=0.1$. The frequency scale is normalized in the same manner as in Fig. 2.

ponent is simply the area under the curves of Fig. 2. Buneman [22] has shown that when $T_e = T_i$ this is given by

$$\sigma = \frac{\sigma_e}{(1+\alpha^2)(2+\alpha^2)} \tag{23}$$

which tends to $\sigma_e/2$ as $\alpha \to 0$, or half that encountered for $\lambda \ll D$ as noted above.

In the ionosphere it is possible for the electrons and ions to be at different temperatures. If it be assumed that both species have Maxwellian velocity distributions, but are characterized by different temperatures, the ionic component of the spectrum will change shape in a way which depends upon the ratio $T_e/T_i$. Fig. 3 illustrates this behavior for the case $\alpha = 0.1$ for $O^+$ ions. The double-humped appearance of the spectra in Fig. 3 lacks any simple explanation. One may choose to regard the humps as reflections from waves traveling toward and away from the observer at the mean thermal speed of fictitious particles having the mass of the ions and the temperature of the electrons, i.e., they occur at $\Delta f_i (T_e/T_i)^{\frac{1}{2}} = 1.0$ (Section VI-B). Values of $T_e/T_i$ outside the range 1 to 4 have not yet been encountered in the ionosphere, though they may be possible in laboratory plasmas.

The effect of varying $T_e/T_i$ on the total echo power can be included in (23) by the following modification [22]:

$$\sigma = \frac{\sigma_e}{(1+\alpha^2)(1+T_e/T_i+\alpha^2)}. \tag{24}$$

Unfortunately, this expression is valid for only a small range of $T_e/T_i$. Renau [23], [24] has pointed out that (24) implies that $\sigma \to 0$ as $T_e/T_i \to \infty$, which is absurd, but did not give the correct result [25]. The failure of (24) for large $T_e/T_i$ stems from the fact that the simplifications made by Buneman are then no longer valid. Moorcroft [26] has computed the exact variation of the effective scattering cross section $\sigma$ as a function of $T_e/T_i$ by integrating the area under the spectrum shape given by Fejer [11]. Fig. 4 shows the result for the case $\alpha \to 0$. It can be seen that the cross section first decreases with increasing $T_e/T_i$, but then as $T_e/T_i \to \infty$, $\sigma \to \sigma_e$. Fig. 5 shows the variation of the total scattering cross section (i.e., ionic plus electronic) with $\alpha(=4\pi D/\lambda)$ for various values of $T_e/T_i$. The range of $T_e/T_i$ encountered in the ionosphere is such that (24) can be used for most ionospheric observations without introducing serious error.

Thus far we have discussed only the effects on the spectrum shape and scattering cross section of varying the parameter $\alpha$ $(=4\pi D/\lambda)$ and $T_e/T_i$. We will defer till later sections the influence of the ionic composition, magnetic fields, and collisions. Before leaving this section, however, it is well to discuss the effect of increasing $\alpha$ on the ability to recover $T_e/T_i$ from the shape of the spectrum [27]. As seen in Fig. 3, the ratio $T_e/T_i$ is characterized by the height of the wing relative to the center of the spectrum. Thus in order to deduce this parameter (assuming $T_i$ is not known), it is necessary that the spectrum have this double-humped appearance. From Fig. 2 this would seem to require that $\alpha \leq 0.5$, which places a limit on the range of useful wavelengths of $\lambda \geq 25D$.

Table I gives likely maximum and minimum values of density and electron temperature (at various altitudes for temperate latitudes) from which $D$ has been calculated. Also listed is the shortest usable wavelength $\lambda_{\min}$ (taken as $25D$) for that altitude. It is evident from this table that a wavelength of $\geq 1$ meter is required if observations are to be conducted to an altitude of 1000 km for all times of day and parts of the sunspot cycle. The *maximum* useful wavelength is set by the need to reduce the relative importance of partially coherent scattering from spread $F$ or other ionospheric irregularities [i.e., make $\lambda \ll L$ in (9)]. Thus if a single wavelength is to be employed for observations over a wide range of heights, the best choice would appear to be in the vicinity of $\lambda = 1$ meter. Table II gives typical values of $T_i$ and $m_i$ that might be encountered at various altitudes in the ionosphere, and the half-width of the signal spectrum

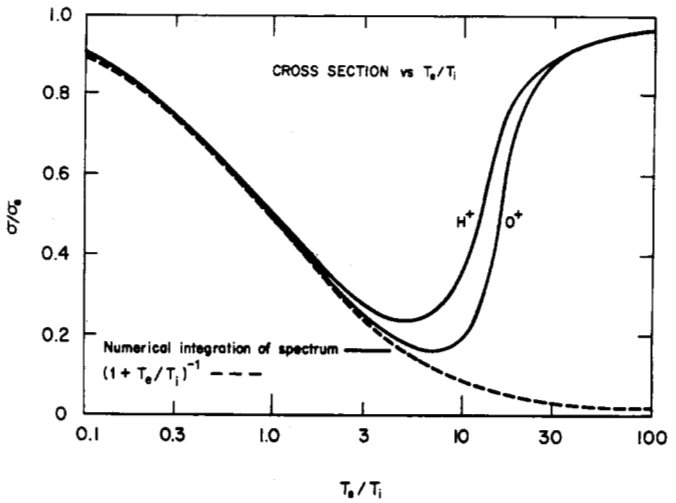


Fig. 4. The variation of the observed electron cross section $\sigma$ divided by the radar cross section $\sigma_e$ given in (11) as a function of $T_e/T_i$ for the case $\lambda \gg 4\pi D$, (after Moorcroft [26]). The dashed curve shows the variation predicted by (24) given by Buneman [22].

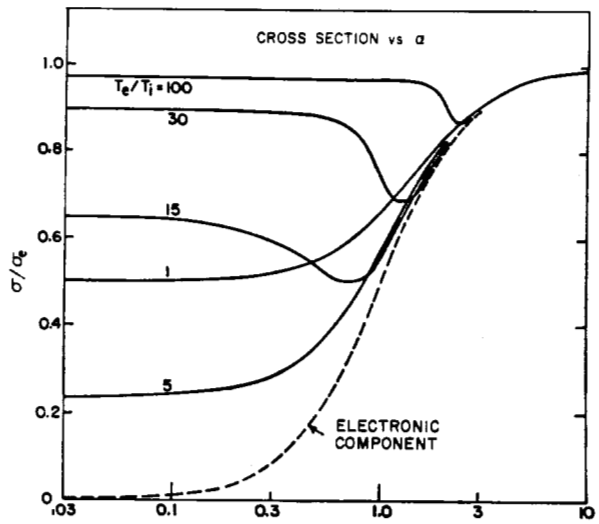


Fig. 5. The variation of the total cross section $\sigma/\sigma_e$ as a function of $\alpha$ $(=4\pi D/\lambda)$ for different values of $T_e/T_i$ (after Moorcroft [26]). The dashed curve shows the amount of power attributable to the electronic component.

TABLE II
SIGNAL SPECTRUM WIDTH AT DIFFERENT ALTITUDES

| Region | Height (km) | Epoch | $T_i$ (°K) | $m_i$ (AMU) | $2\Delta f_i$ (kHz) $\lambda = 1$ meter |
|---|---|---|---|---|---|
| $E$ | 120 | Winter night $S_{min}$ | 300 | 30 | 1.65 |
| | | Summer day $S_{max}$ | 300 | 30 | 1.65 |
| $F1$ | 200 | Winter night $S_{min}$ | 750 | 25 | 2.8 |
| | | Summer day $S_{max}$ | 1500 | 25 | 3.8 |
| $F2$ | 300 | Winter night $S_{min}$ | 1000 | 16 | 4.3 |
| | | Summer day $S_{max}$ | 2000 | 16 | 6.0 |
| Upper $F2$ | 1000 | | 2500 | 4 | 14.3 |
| Lower exosphere | $\geq 2000$ | | 3000 | 1 | 28.6 |

(taken to be $2\Delta f_i$) expected on the basis of these values for this wavelength.

### C. The Radar Equation

In order to define the altitude from which the scattering is occurring, it is necessary either to employ two or more intersecting antenna beams, or to employ a short pulse on transmission. In the latter case the echo power $P_s$ available at the receiver terminals may be shown to be [28]

$$P_s = \frac{P_t L N \sigma c T \lambda^2}{128\pi^3 R^2} \int_\theta \int_\phi G^2(\theta\phi) \sin\theta d\theta\, d\phi \quad \text{watts} \tag{25}$$

where $P_t$ is peak transmitter power (watts), $L$ is a loss factor which allows for such things as ohmic losses in the transmission line systems to the transmitter and receiver, $N$ is the electron density (assumed constant over the height interval $cT/2$ occupied by the pulse), $\sigma$ is the effective cross section per electron [defined in (24)], $c$ is the velocity of light, $T$ is pulse length, $R$ is the range to scattering volume and $G(\theta\phi)$ is the antenna gain over isotropic, where $\theta$ is the angular distance measured from the beam axis and $\phi$ is the azimuthal angle measured with respect to a vertical plane containing the beam axis. In the case where the beam is cylindrically symmetrical, the integration over $\phi$ can be carried out to yield

$$P_s = \frac{P_t L N \sigma c T \lambda^2}{64\pi^2 R^2} \int_\theta G^2(\theta) \sin\theta\, d\theta \quad \text{watts.} \tag{26}$$

For a typical parabolic reflector with 10-dB taper of the illumination over the primary mirror, this may be shown to yield

$$P_s = 0.76 \frac{P_t L N \sigma c T \lambda^2}{64\pi^2 R^2} G(0) \quad \text{watts} \tag{27}$$

where $G(0)$ is the antenna gain on axis. Since $G(0)$ and the effective on-axis collecting area of the antenna $A(0)$ are related through $G(0) = 4\pi A(0)/\lambda^2$, (27) may be written as

$$\begin{aligned} P_s &= \frac{0.76\, P_t L N \sigma c T A(0)}{16\pi R^2} \quad \text{watts} \\ &= \left[\frac{0.76\, P_t A(0) L c T}{16\pi}\right]\left[\frac{N\sigma}{R^2}\right] \quad \text{watts.} \end{aligned} \tag{28}$$

It can be seen that to observe a given density $N$ at a given distance $R$ with a required height resolution (equal to $cT/2$ with beam vertical) the radar designer must optimize the product $P_t A(0)$. Since the scatterers fill the antenna beam, the antenna gain (or collecting area) enters the equation

only once. The designer must also attempt to minimize the amount of competing noise power $P_n = KT_sb$ present in the receiver by reducing the bandwidth $b$ to a value that will just accommodate the spectral width of the echo, and by reducing the system temperature $T_s$ by employing receiving and antenna equipment designed for their low-noise contributions.

In the bistatic situation where two beams are arranged to intersect at an angle $\chi$, the total echo power $P_s$ depends upon the weighting imposed by the two antenna beams. Assuming that both beams are cylindrically symmetrical and that the space where they intersect is represented by an orthogonal coordinate system $x, y, z$, the echo power $P_s$ is

$$P_s = \frac{P_{av}LN\sigma}{4\pi R_1^2 4\pi R_2^2}\int_{-\infty}^{\infty}\int_{-\infty}^{\infty}\int_{-\infty}^{\infty} G_1(\theta_1)A_2(\theta_2)\,dx\,dy\,dz \text{ watts.} \quad (29)$$

Here it is assumed that the transmitter radiates CW with an average power $P_{av}$ and $R_1$ and $R_2$ are, respectively, distances from the center of the scattering volume to the transmitter and receiver. Elsewhere in (29) the subscripts 1 and 2 refer to the parameters of the transmitting and receiving stations, respectively. Equation (29) assumes that the dimensions of the scattering volume are small compared with $R_1$ and $R_2$, i.e., the beamwidths are small. When the widths of the antenna beams are equal at the point of intersection and their included angle $\chi$ is large, we have for typical parabolic antennas [29]

$$P_s = 5.7\,\frac{P_{av}LN\sigma\lambda A_2(0)^{\frac{1}{2}}}{(4\pi)^2 R_2 \sin\chi}. \quad (30)$$

It can be seen that in the bistatic situation with matched beams the echo power varies inversely as the distance $R_2$ of the scattering volume from the receiving antenna (instead of inversely as the square) and only as the half-power of the on-axis collecting area $A_2(0)$ of the receiving antenna. The properties of the transmitting antenna do not enter the equation provided the beams remain matched.

The receiver beam may be wider than the transmitter beam or vice versa and the above integration may be repeated to determine $P_s$ in such cases. Fig. 6 shows the factor by which the right-hand side of (30) must be multiplied for different ratios between the beam diameters at the point of intersection [29]. At first sight it may appear that $P_s$ can be increased by *mismatching* the beam sizes, in violation of one's intuitive reasoning. However, if the receiver beam is, for example, twice as wide as the transmitting beam, this means that $A_2(0)^{\frac{1}{2}}$ can be increased by a factor of 2 when the beams will again match. The total echo power will then increase by $2/1.264 = 1.58$ (or 2 dB). It follows that mismatching the beamwidths does degrade the signal level and, of course, it degrades the height resolution also. The constants appearing in (28) and (30) differ somewhat from earlier ones published by Gordon [12] and Bowles *et al.* [30] where the weighting imposed by the antenna pattern was included in only an approximate manner.

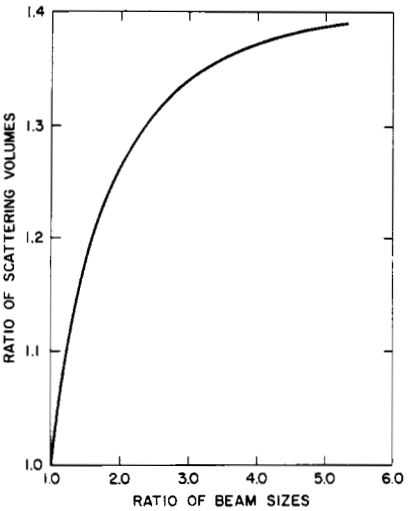


Fig. 6. The variation of the effective scattering volume for a CW radar as a function of the ratio of the diameters of the two beams at the point where they intersect.

## III. Equipment for Ionospheric Thomson Scatter Studies

### A. Introduction

Table III lists the locations of the major radar facilities that have been employed for Thomson Scatter studies of the ionosphere, and their parameters are presented in Table IV. Also in Table IV an attempt has been made to compare their sensitivities by assuming that each system [except the CNET (Centre National d'Études des Télécommunications) radar] is operated with the same pulse length ($T = 100$ μs), same receiver bandwidth ($b = 10$ KHz), and same pulse repetition frequency (50 Hz) though in fact this would be a normal mode of operation for only a few of them. For this reason these relative sensitivities given in Table IV should not be taken too seriously, but do serve to show that the long-wave systems (Jicamarca and Arecibo I) suffer in comparison to the short-wave systems because of the high background noise to which they are exposed. In what follows we describe in greater detail the systems at Jicamarca, Arecibo, and St. Santin. These three differ most widely, and the Malvern and Millstone instruments may be regarded as smaller versions of Arecibo. It should be borne in mind that the three facilities to be discussed were conceived at rather different times and were constructed at differing rates and for widely different costs. Further, the theory outlined in the previous section was but poorly developed when design and construction of Jicamarca and Arecibo began. Despite this, all three have proved remarkably successful instruments.

### B. The Jicamarca Radar Facility

The Jicamarca radar facility was conceived in 1959 and construction began in 1960. The radar was brought into operation in 1961, before full power operation was achieved (mid-1962). Fig. 7 shows a view of the facility, which has been described by Bowles [31]. Following his discovery that the presence of the ions in the plasma serves to narrow

TABLE III
LOCATION OF THOMSON SCATTER RADAR FACILITIES

| Facility | Affiliation | Location | Geographic | | Geomagnetic Latitude |
|---|---|---|---|---|---|
| | | | Latitude | Longitude | |
| Jicamarca Radar Observatory | ESSA Research Laboratories | Near Lima, Peru | 11.95°S | 76.87°W | 2°N |
| Arecibo Ionospheric Observatory | Cornell University | Near Arecibo, Puerto Rico | 18.3°N | 66.75°W | 30°N |
| Stanford | Stanford Research Institute | Stanford, Calif., U. S. | 37.4°N | 122.17°W | 43°N |
| Millstone Hill Ionospheric Radar | Lincoln Laboratory, Massachusetts Institute of Technology | Westford, Mass., U. S. | 42.6°N | 71.5°W | 53°N |
| St. Santin de Maurs | Centre National d'Études des Telecommunication | *Transmitter* St. Santin de Maurs, France | 44.65°N | 2.19°E | 47°N |
| | | *Receiver* Nançay, France | 47.37°N | 2.10°E | |
| RRE Ionospheric Radar | Royal Radar Establishment | Gt. Malvern, Worcester, England | 52.09°N | 2.14°W | 56°N |
| Prince Albert Radar Laboratory | Defence Research Telecommunications Establishment (until 1967) | Prince Albert, Saskatchewan, Canada | 53°N | 105°W | 62°N |

TABLE IV
PARAMETERS OF EXISTING THOMSON SCATTER RADARS

| Location of Facility | Operating Frequency (MHz) | Type | Antenna | Effective Antenna Aperture (dB over 1 m²) | System Temperature (°K) | Peak Power (kW) | Sensitivity* Relative to Millstone I (dB) |
|---|---|---|---|---|---|---|---|
| Jicamarca | 49.92 | Vertical pulse | 290- by 290-m dipole array | 45.0 | 6 000 | 4 000 | −0.2 |
| Arecibo | I 40.12 | Vertical pulse | 300-m spherical | 43.7 | 10 000 | 2 500 | −5.5 |
| | II 430.0 | Vertical pulse | reflector | 41.7 | 300 | 2 000 | +8.8 |
| Stanford | 1300 | Oblique pulse | 27-m parabola | 23.8 | 300 | 5 000 | −8.0 |
| Millstone | I 440.0 | Vertical pulse | 68-m parabola | 32.2 | 200 | 3 000 | 0 |
| | II 1295.0 | Oblique pulse | 25-m parabola | 22.8 | 150 | 4 000 | −7.0 |
| St. Santin | 935.0 | Bistatic CW Transmitter (vertical) | 20- by 100-m reflector | 30.0† | 130 | 75 | −4.0 |
| | | Receiver (oblique) | 40- by 200-m reflector | | | | |
| Malvern | 400.0 | Vertical pulse | 42.5-m parabola | 28.5 | 200 | 10 000 | +2.3 |

* Computed by comparing (peak power) × (aperture) × (pulse repetition)$^{1/2}$ × (system temperature)$^{-1}$. Pulse repetition taken as 50 in all cases except St. Santin.
† Transmitting antenna.

the spectrum of the Thomson scattered signals, Bowles [32] concluded that there should be characteristic fluctuations imparted to the plasma by the motion of the ions gyrating around the field lines. Thus, when the ray path is normal to the field lines, the spectrum of the scattered signals should show a series of peaks separated by the ion gyrofrequency. This phenomenon would be most striking when the exploring wavelength $\lambda$ is of the same order as the ion gyroradius. Accordingly, the Jicamarca facility was constructed near the magnetic equator, the one latitude where a vertically directed radar system would have a beam perpendicular to the field at all heights. Thus it was expected that by studying the spectra of the reflected signals the radar could act as an ion mass-spectrometer. This expectation has largely gone unrealized (Section VI). The choice of location has proved of considerable benefit in other respects, however (Section VII).

The Jicamarca antenna is an array of half-wave dipoles located 0.3 $\lambda$ above a reflecting screen laid on the ground. The array is a square with 96 dipoles along a side. A second array of dipoles orthogonal to that of the first is incorporated into the same physical area and mounted at the same height above the ground. Independent feeds are used for the two orthogonal polarizations. These feeds are

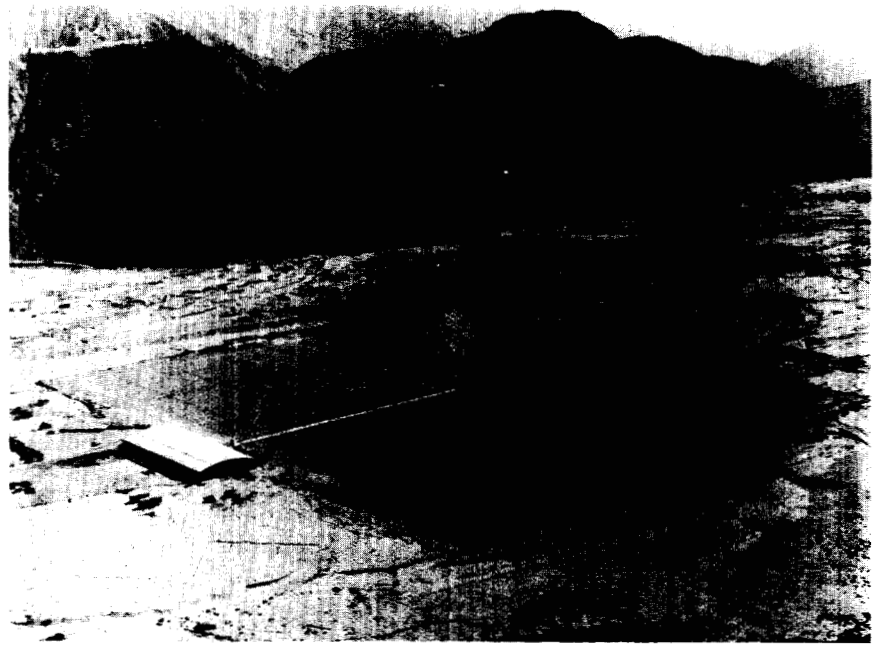

Fig. 7. A view of the Jicamarca radar facility in Peru. The antenna is a square array of dipoles, 300 meters along a side. The building houses the transmitter, receivers, and data processing equipment. (Courtesy of ESSA Research Laboratories, Boulder, Colo.)

coupled at the main feed point through a conventional hybrid coupler. The dipoles in any one array are fed by four feed lines which run from the transmitter to the center of each of four quarters of the antenna. From each of these points, four lines branch to the centers of quarter sections in each sector and this is then repeated so that there is a total of 64 "modules" connected via equal lengths of coaxial cable to the transmitter. By inserting additional lengths of coaxial cable between these 64 modules and their associated feedline terminations, it is possible to phase the antenna beam away from the zenith. Each module contains 144 dipoles of each polarization. Open wire line built of 1-inch-diameter aluminum tubing connects colinear rows of 12 elements to the central feed point of the module. Distribution of power to these radiating elements is accomplished using the inside of each element as a piece of coaxial transmission line. That is, the dipoles may be thought of as constructed from a piece of coaxial transmission line $6\lambda$ in length in which inner and outer conductors are transposed at $\lambda/2$ intervals.

The transmitter is of fairly conventional design and employs four type 15041 shielded-grid-triode tubes mounted in coaxial cavities. Each of these tubes gives about 1 MW peak power. The tubes are phased together in pairs, and under normal circumstances each pair is coupled to one port of the antenna hybrid coupler. Thus, if one pair is energized, a pulse of, for example, left circular polarization is radiated, and by energizing the other pair one obtains a right circular pulse. The transmitter is grid modulated, and can be operated over a very wide range of pulse lengths.

The TR and ATR switches employed in this system are made of coaxial line sections with tungsten rods forming gaps in air between inner and outer conductors. The receivers employed at Jicamarca are of conventional vacuum tube design and are coupled to phase-orthogonal detectors. Data samples can be taken by means of digital voltmeters, and a PB-250 computer is available for controlling the radar and on-line data processing.

In operation the instrument has not been useful for studying altitudes below about 200 km because of interfering echoes from the equatorial electrojet, and is rendered unusable at some $F$ region heights during the presence of spread $F$ irregularities.

### *C. The Arecibo Ionospheric Observatory*

Fig. 8 gives an aerial view of this facility. The antenna has been constructed in a limestone sink-hole in Puerto Rico, and consists of a mesh reflector surface and line-feed. The reflector surface is a section of a sphere with a radius of curvature of 245 meters and a diameter (viewed from above) of 305 meters. Since the surface is spherical, a parallel beam of rays is not brought to a point focus, but instead is made to converge on a line. To collect this bundle of rays, a distributed feed is employed which consists (in the case of the 70-cm radar) of a square waveguide some 30 meters in length with horizontal slots cut in each of its four faces. The 7.5-meter radar employs four dipoles and reflectors arranged in a box-like square around the 70-cm feed. Further details of the system have been published by Gordon and LaLonde [33], Gordon [34], and Carlson [35].

By employing a spherical reflector it is possible to scan the antenna beam by moving the feed. The feed is made to track along an arc of a circle with the same radius as the reflector, thus maintaining the symmetry. This motion is achieved by moving the feed linearly along the bottom surface of a large arm suspended beneath the triangular platform shown in the figure. The bottom of the arm is 144 meters above the reflector surface. By rotating the arm

Fig. 8. The Arecibo Ionospheric Observatory in Puerto Rico. The antenna is a spherical reflector 300 meters in diameter situated in a limestone sinkhole. The feed system is supported by cables which pass over the tops of the three towers. The electronic equipment is located in the building at the bottom of the picture. (Courtesy of Cornell University, Center for Radio Physics and Space Research, Ithaca, N. Y.)

around on a circular track on the underside of the platform, the azimuth of the beam can be changed also. In this fashion the beam can be pointed in any direction up to 20° from the zenith. This motion has been of crucial importance in permitting the instrument to be effective in the fields of radio and radar astronomy, but has not been of major significance in the ionospheric work.

The 70-cm radar feed is connected by a WR 2100 waveguide to the transmitter in the control building at the edge of the reflector. A sliding collector arrangement handles the power transmission between the arm and the movable feed. The 7.5-meter feed is connected to its transmitter via a 9-inch coaxial line, and a scissor type of structure (having several rotating joints) allows for the linear motion of this feed. The 70-cm transmitter employs a pair of Varian VA-842 klystrons as final amplifiers in a coherent transmitter. This transmitter is capable of radiating pulses in the range 10 $\mu$s to 10 ms, and may be run CW at its mean rated power. The 7.5-meter transmitter employs four vacuum tubes in push-pull parallel in its final stage in a lumped-circuit design.

The receiver for 70-cm radar observations employs as first stage an electron-beam parametric amplifier. The TR switch is a coaxial cavity with a gas discharge tube mounted inside. Since circularly polarized waves are transmitted, about 20 dB of isolation between the transmitter and receiver is afforded by the turnstile junction to which the transmit and receive lines are connected. The remaining stages of the receiver are of conventional design. High-speed analog-to-digital converters (digital voltmeters) are available for taking data samples, and these are processed on-line in a CDC 3200 digital computer. The main operating wavelength (70 cm) permits observations throughout the ionosphere, and requires a reflector with a surface tolerance that is not unduly difficult to achieve in such a large suspended reflector. The use of a reflector-type antenna permits multiple-frequency operation, and the second radar at $\lambda = 7.5$ meters should be capable of extending the observations into the exosphere.

The major drawback of the Arecibo design is the line feed. The existing 70-cm feed fails to provide proper illumination of the reflector, with the result that the on-axis gain is some 4 dB less than expected. This value has been given in Table IV, but is in fact misleading. What matters is the integral $\int_0^\theta G^2 \sin\theta d\theta$ [in (26)] and recent measurements (F. Drake, private communication) suggest that the effective collecting area $A(0)$ of Arecibo with the present feed is only one-sixth of the expected value. Plans have been developed to employ an additional remote antenna system so that the Arecibo instrument might be operated bistatically to achieve better height resolution for $E$ region studies and to detect horizontal drift motions (Section VII).

### *D. The CNET Bistatic CW Radar*

Though the Jicamarca and Arecibo radars are basically vertically directed pulse systems, they differ considerably in their cost, flexibility, and utility. The CNET system represents yet a third compromise. This system employs a pair of beams to define the scattering volume and a CW radar system. Of the three systems, the CNET radar is perhaps the best documented. The overall design has been described

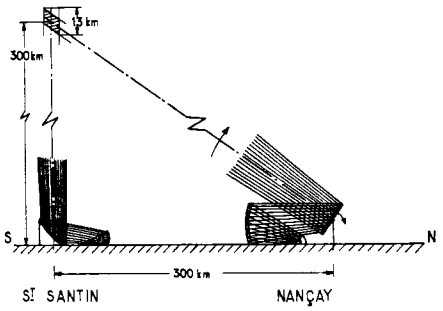


Fig. 9. A diagram of the St. Santin-Nançay CW bistatic radar in France. The receiving antenna (at Nançay) provides a beam which can be steered up or down. The transmitter beam (at St. Santin) is directed vertically. The stations are separated by about 300 km along a north-south baseline.

by du Castel *et al.* [36], the transmitter by Schwab [37], the transmitting antenna design by Tocquec [38], and construction by Parmantier [39]. Petit and Reyssat [40] have described the receiving equipment.

The designers of the CNET system made use of the existence of a large radio astronomy antenna at Nançay to form one element of the bistatic radar (Fig. 9). The transmitter and its antenna were constructed 300 km to the south. The receiving antenna (at Nançay) is based upon a design of J. D. Kraus and consists of a primary reflector arranged vertically and fed from its focal point. A plane mirror some distance away reflects the beam into the sky at the desired angle. The curved section has dimensions 300 meters east-west and is 35 meters high. The plane mirror is 200 by 40 meters. This instrument forms a fan-shaped beam of some 6′ arc east-west and 36′ arc between the half-power points when measured in the meridian plane. This choice was predicated by the radio astronomy requirements. It would of course be preferable from the point of view of obtaining good height resolution to have the fan-beam oriented in the east-west direction rather than in the meridian plane.

The transmitting antenna is basically a section of a Gregorian system. A section of a parabola 100 meters east-west is inclined at 45° to the ground, and when seen in plan the north-south extent is 20 meters. This reflector is fed by a horn feed directed toward a secondary reflector which is a section of an elliptical cylinder 11 meters east-west. In this way the engineers have sought to obtain better control of the illumination of the primary reflector and thus minimize sidelobes, which could permit signals to be obtained from unwanted altitudes. The transmitting antenna provides a vertical beam 1.2° in the meridian and ~12′ east-west, thus providing an approximate match to the receiving beam in the east-west plane at altitudes of the order of 200 km. As the elevation of the receiving beam is raised (by tilting the plane mirror) the height resolution varies (Section V), yet it remains acceptable at all altitudes for which the instrument is useful.

The transmitter employs a single VA-853 klystron as final amplifier and it is anticipated that the power will be doubled by the addition of a second klystron in the near future. The receiver employs a parametric amplifier, and the spectrum analysis of the signals is accomplished using a bank of crystal filters combined with a digital integration and recording system.

The CNET radar system is switched between frequencies of 935.0 and 935.1 MHz at equal intervals of time. At the receiver two filter banks are employed, and the frequency translation in the receiver is such that either one or the other receives a signal, depending upon which of the frequencies the transmitter is radiating. During the "off time" the relative gains of the filters in one bank are established by integrating on noise alone. In this way no information is lost whilst calibrating the filter banks. Frequency and time synchronization between the two sites is accomplished by employing separate 5-MHz frequency standards and comparing a subharmonic via a special telephone line connection.

In order to examine different heights, the large 200- by 40-meter plane mirror must be tilted. Thus, exploring the whole region from which useful echoes can be obtained is a rather slow and tedious process. The results are, however, of special interest, particularly in the $D$ and $E$ regions in view of this system's unrivaled height resolution for spectrum measurements (Section V).

## IV. Altitude Profiles of Electron Density

### A. Power Profile Method of Determination

At first sight, measurements of the echo power $P_s$ as a function of delay using a vertically directed pulse radar system would seem the most obvious way of determining the electron density versus altitude $N(h)$ profile. From (26) we have

$$P_s = \text{const.} \frac{N(h)\sigma(h)}{h^2} \tag{31}$$

where $h$ is the height. The proportionality constant can be established by careful determination of the parameters of the radar, or indirectly by an absolute determination of the density $N$ by some other means. At Millstone [41]–[43] it has been the practice to obtain only the *shape* of the electron density profile via measurements of $P_s$ [in (31)] and to establish the absolute values from measurements of $f_0F2$ using a nearby ionosonde. Unfortunately, as we have seen (Section II-B) the cross section $\sigma(h)$ depends upon both the ratio $\alpha$ $(=4\pi D/\lambda)$ and $T_e/T_i$, which are also functions of altitude. If an extremely long wavelength $\lambda(>1$ meter) is employed (as at Jicamarca), the dependence upon $\alpha$ can be neglected (i.e., $\alpha \to 0$), but that on $T_e/T_i$ remains. In order to remove this dependence, it is necessary to determine the variation of $T_e/T_i$ with altitude via separate measurements of the spectra of the signals reflected from a number of altitudes (Section V). Fig. 10 shows such a set of measurements made at Millstone [44] and in Fig. 11 the corresponding electron density profile is shown after allowing for the variation of $\sigma$ with $T_e/T_i$ according to (24).

At wavelengths where it is not possible to proceed on the assumption that $\alpha \to 0$, a relation pointed out by Moorcroft [27] can prove extremely useful. The arrangement of the terms in (18) describing the signal spectrum is such that

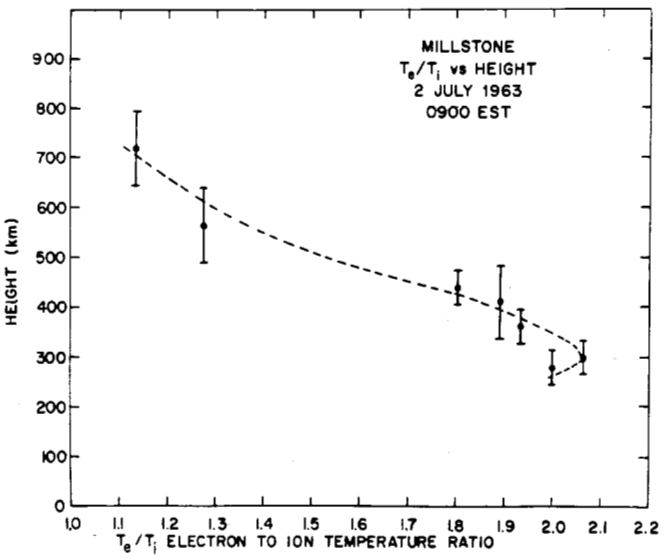


Fig. 10. Variation of the electron-to-ion temperature ratio $T_e/T_i$ deduced from the spectra of the radar signals observed during a period (0921–0926 EST) on July 2, 1963, at Millstone [44].

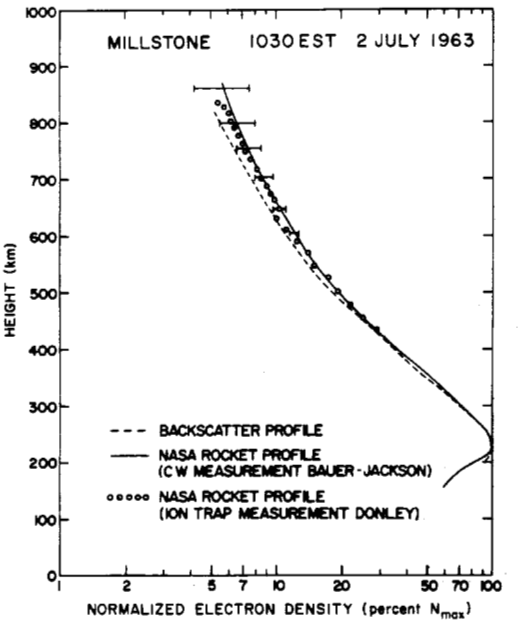


Fig. 11. An electron density profile obtained by combining measurements of echo power versus altitude and $T_e/T_i$ at a number of altitudes (Fig. 10). This profile was obtained at Millstone [44] during the time of launch of a rocket from Wallops Island, and despite the separation between the two places the curves agree well.

the spectrum shape depends upon $\alpha$ in the same way that it depends upon $T_e/T_i$. That is, if the spectrum *shape* is changed due to a change in $\alpha$, the original spectrum can be recovered by a suitable change in $T_e/T_i$. Moorcroft showed that if $T_e/T_i$ is the *true* value of the electron-to-ion temperature ratio and $\beta$ the fictitious temperature ratio that would cause the spectrum to have the same shape if $\alpha$ were zero or extremely small, then

$$\frac{T_e}{T_i} = (1 + \alpha^2)\beta \qquad \alpha \leq 1 \tag{32}$$

and

$$\sigma \approx \frac{\sigma_e}{1 + \beta} \tag{33}$$

where $\sigma_e = 4\pi r_e^2$.

By comparing the shape of the observed spectrum with spectra calculated for the case $\alpha = 0$, the fictitious temperature ratio $\beta$ can be obtained. The scattering cross section of the electrons at that altitude may then be deduced via (33) and the total echo power used to infer the electron density $N$. Thus, whilst this method is less straightforward than might be desired, the echo power versus delay or so-called "power profile" technique can be made to yield good electron density profiles.

At all altitudes the echo power falls inversely as the square of height. Above the peak of the layer the density $N$ falls exponentially with altitude and these two effects then combine to cause the echo power to decrease rapidly. This effect is illustrated in Table V where the signal-to-noise ratio has been computed for the Millstone Hill I radar assuming the radar parameters listed in Table IV and also assuming that $L = 0.8$, $T = 50$ $\mu$s, and the receiver bandwidth is matched to this pulse length (i.e., $b = 20$ kHz). The values of $T_e/T_i$ and density given in Tables I and II were also assumed and the cross section computed according to (24).

Sweep integration may be employed to improve the accuracy of the measurements [41]. Thus by integrating over $n$ sweeps of the radar time base the uncertainty $\Delta P$ in the power at any delay is reduced to

$$\Delta P = \pm \frac{P_s + P_n}{\sqrt{n}}. \tag{34}$$

An estimate of the noise power $P_n$ can be obtained by taking a mean over $m$ points corresponding to altitudes from which virtually no echo power can be expected. This mean can then be subtracted from all other points to yield $P_s$. The uncertainty $\Delta \bar{P}_n$ in the mean noise $\bar{P}_n$ will be $\bar{P}_n/\sqrt{nm}$ and that in the echo

$$\Delta P_s = \pm \sqrt{(\Delta P)^2 + (\Delta \bar{P}_n)^2}. \tag{35}$$

Operating with a pulse repetition frequency of, say, 50 pps, it is possible to determine $P_s$ to an accuracy of $\pm 1$ percent in about 5 minutes, given a reasonable signal-to-noise ratio ($P_s/P_n \gg 1$). When $P_s/P_n$ falls below unity, the percentage error $\Delta P_s/P_s$ increases rapidly and it becomes impossible to achieve an accuracy of better than 10 percent in a reasonable time (e.g., 10 minutes) for $P_s/P_n \leq 0.1$.

In order to overcome the poor signal-to-noise ratio encountered at high altitudes (Table V), it is necessary to lengthen the pulse length $T$ and accept the poorer height resolution that results. Thus at Millstone each electron density profile is constructed using measurements obtained with pulses of 100, 500, and 1000 $\mu$s in length [41]. Fortunately, above the layer peak where it is necessary to employ long pulses the density changes in a smooth monotonic manner and there is little loss of resolution. Similar procedures to those outlined here are employed at Arecibo [35].

TABLE V
SIGNAL-TO-NOISE RATIO AT DIFFERENT ALTITUDES FOR MILLSTONE I
(*Pulse* = 50 μs)

| Region | Height (km) | Epoch | $P_s/P_n$ |
|---|---|---|---|
| *E* | 120 | Winter night $S_{min}$ | 0.43 |
| | | Summer day $S_{max}$ | 4.3 |
| *F*1 | 200 | Winter night $S_{min}$ | 0.67 |
| | | Summer day $S_{max}$ | 3.89 |
| *F*2 | 300 | Winter night $S_{min}$ | 0.31 |
| | | Summer day $S_{max}$ | 6.0 |
| Upper *F*2 | 1000 | | $5.6 \times 10^{-3}$ |
| Lower exosphere | 2000 | | $7.7 \times 10^{-4}$ |

A bistatic radar system may be employed to obtain electron density profiles, but it suffers from a number of operational difficulties. The volume of the region of intersection of the two beams will change with altitude and allowance must be made for this. Also only one density point is obtained per position of the beams and thus it takes a long time to scan over any appreciable altitude range, especially if the beam swinging requires mechanical motion of the antennas. Since the measurements are no longer at the same time it is less easy to be sure that the relative density as a function of height has not been distorted by variations with time of the radar performance or the ionosphere. Additionally, a bistatic radar system does not permit the option of trading height resolution for signal power (although the resolution will inevitably deteriorate with the altitude of the scattering volume). Finally, all other things being equal, the CW bistatic radar suffers because the instantaneous signal-to-noise ratio is less than that achieved by a pulse system of the same average power. To some extent this is compensated by the availability of a greater number of samples per second, but as the above error analysis indicates, it is extremely desirable to keep $P_s/P_n > 1$.

### *B. Faraday Rotation Method*

As we have seen, the echo power versus altitude can be converted to electron density versus altitude only if the variation of $T_e/T_i$ with height is known, and this requires a spectral analysis of the signals. At most wavelengths it is possible to accomplish the two experiments at the same time, i.e., with pulses of a given length, and thus this is not a major drawback. There is, however, one means by which this difficulty can be obviated entirely. In this, use is made of the Faraday rotation of the signals. A plane wave propagated into the ionosphere at a frequency $f$ large compared to the plasma frequency $f_N$ splits into two circular components with opposite senses of rotation and different phase velocities. At any instant the two components may be combined to yield a wave which will have been rotated with respect to the original plane containing the electric field. The amount of rotation is given by [45]

$$\Omega = \frac{1}{4\pi} \frac{e^3 \mu_0}{m_e^2 f^2 c \varepsilon_0} \int_0^R N_r H_r \cos \theta_r \, dr \quad \text{rotations} \tag{36}$$

where $\mu_0$ is the free-space permeability ($= 1.26 \times 10^{-6}$ H/m), $H_r$ is the magnetic field intensity (ampere turns per meter), and $\theta_r$ is the angle between the field and the ray at any distance along the path $r$. For a vertical path, the two-way rotation encountered between the ground and some altitude $h^1$ becomes

$$\begin{aligned} \Omega &= \frac{0.94 \times 10^{-2}}{f^2} \int_0^{h^1} N_h H_h \cos \theta_h \, dh \quad \text{rotations} \\ &\approx \frac{0.94 \times 10^{-2}}{f^2} \overline{H \cos \theta} \int_0^{h^1} N \, dh \quad \text{rotations.} \end{aligned} \tag{37}$$

Evidently $N_h \propto d\Omega/dh$, and thus by determining the Faraday rotation as a function of altitude and differentiating this curve, an absolute electron density profile can be obtained provided only $\overline{H \cos \theta}$ is known.

The earliest report of the observation of Faraday rotation of Thomson scattered signals is that of Millman *et al.* [46] in 1961, and most other observers have sought to avoid the effect by transmitting circularly polarized signals. At Jicamarca, however, the Faraday method has been extensively developed and used routinely for producing electron density profiles [47]. In these observations the antenna is connected to receive and transmit orthogonal circular polarizations. Equal opposite sense circular pulses are transmitted and on reception the phase difference between the reflected pair of pulses is measured by comparing the outputs of receivers connected to the left-hand and right-hand ports of the antenna. Thus if $V_L$ is the voltage at the output of the left-hand receiver and $V_R$ that from the right, the sine and cosine components (obtainable at the outputs of phase detectors driven in quadrature) can be written

$$\begin{aligned} x_R &= V_R \sin \phi \\ y_R &= V_R \cos \phi \\ x_L &= V_L \sin \theta \\ y_L &= V_L \cos \theta. \end{aligned} \tag{38}$$

The means of the products $x_R y_L$ and $y_R y_L$ are formed (by digital sampling and multiplication in a computer) to yield

$$\begin{aligned} \overline{x_R y_L} &= \overline{V_R V_L \sin \phi \cos \theta} \\ &= \overline{1/2 \, V_R V_L} \, \overline{[\sin (\phi + \theta) + \sin (\phi - \theta)]} \\ \overline{y_R y_L} &= \overline{V_R V_L \cos \phi \cos \theta} \\ &= \overline{1/2 \, V_R V_L} \, \overline{[\cos (\phi + \theta) + \cos (\phi - \theta)]}. \end{aligned} \tag{39}$$

Since the angle $(\phi + \theta)$ varies over many radians during the integration process, $\overline{\sin (\phi + \theta)} = \overline{\cos (\phi + \theta)} \to 0$. That is, these terms average out and since $\overline{\sin (\phi - \theta)} = \sin \overline{(\phi - \theta)}$ the Faraday rotation $\Omega$ is given by

$$\Omega = \frac{1}{2} \cdot \frac{1}{2\pi} (\phi - \theta) = \frac{1}{4\pi} \tan^{-1} \frac{\overline{x_R y_L}}{\overline{y_R y_L}}. \tag{40}$$

Note that the rotation of the wave is only half the phase difference between opposite circular components, and hence the factor of one-half in (40). The simplicity and

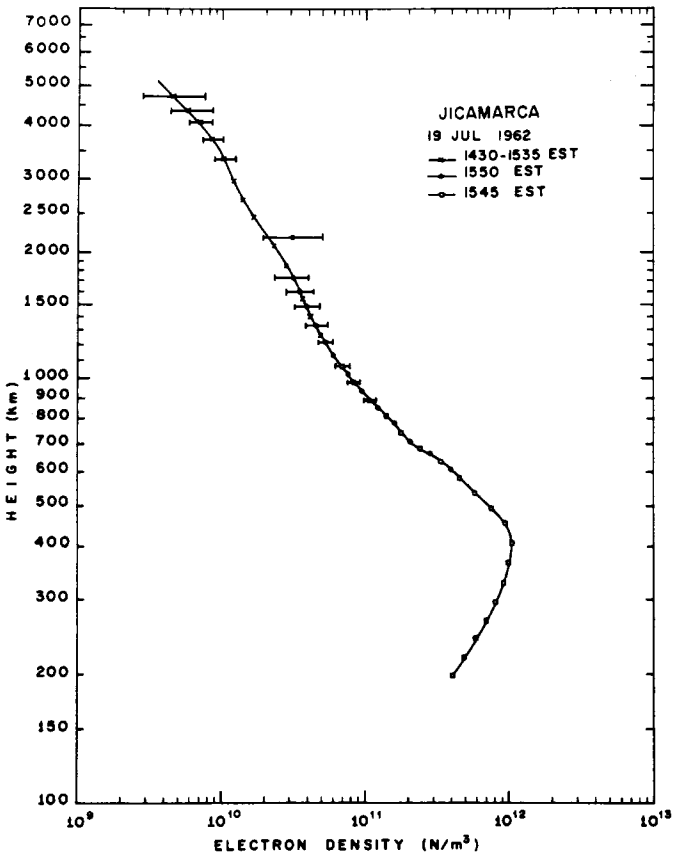


Fig. 12. An electron density profile obtained at Jicamarca that extends to almost one earth's radius [48].

elegance of this method are to some extent offset by a number of practical difficulties. Systematic differences in the gains and orthogonality of the phase detectors must be allowed for by commutating the reference signals on alternate sweeps of the time base. This effectively interchanges sine and cosine components and the computer is instructed to transpose them back before multiplication. Also the coupling between the right and left circular modes of the antenna must be less than $\sim 25$ dB if the separation between the propagated modes is to be kept to an acceptable level [47]. Finally, there is the problem of spurious correlation introduced by polarized noise emission. This can be produced, for example, by synchrotron radiation from the electrons created by the "Starfish" experiment and serves to introduce unwanted correlation between channels. The remedy in this instance is to reverse the phase of one of the transmitted pulses by 180° (on every second pair of sweeps) and reverse the sign of, say, $x_R$ in the computer. Despite all these safeguards the error in the measured electron density becomes unacceptably large at that altitude (typically about 500 km) where $d\Omega/dh$ becomes small. At Jicamarca it is the usual practice therefore to extend to higher altitudes the electron density profile derived by the Faraday method by fitting to it a "power profile" obtained for the region above. It is usually assumed that $T_e/T_i = 1$ above 500 km, based upon a number of studies of the spectra of the signals reflected from these altitudes, so that the power profile requires no modification. Because of the long wavelength employed at Jicamarca ($\lambda = 6$ meters), observations can be made to very great altitudes before the criterion $\lambda \gg D$ is violated, and Fig. 12 gives an early example of one such density profile [48].

### C. Plasma Line Method

For small values of $\alpha (= 4\pi D/\lambda)$ the energy in the electronic component of the spectrum (Section II) appears in a pair of lines displaced from the radar frequency by an amount approximately equal to the plasma frequency $f_N$ [given in (1)]. This feature can be seen in Fig. 1 for the case $\alpha = 0.33$. The actual frequency displacement (in the absence of a magnetic field) is

$$f_r = \pm f_N(1 + 3\alpha^2)^{\frac{1}{2}}. \tag{41}$$

At night the amount of power associated with this line is of the order of $\alpha^2$ times that in the ionic component [see (24)], and is then undetectable to any of the radar systems constructed thus far. During the daytime the line is enhanced by the presence of fast photoelectrons [49]. This enhancement is a factor of about 50 over the nighttime intensity of the line (Section IX-A), and this makes it detectable at certain altitudes by most of the radars listed in Table III [50], [51].

The plasma lines are caused by the scattering from weakly damped longitudinal electrostatic plasma oscillations with frequency $f_r$, wavelength $\lambda/2$ and phase velocity $v_{ph}$, where

$$v_{ph} = \frac{f_r \lambda}{2}. \tag{42}$$

Photoelectrons which travel at the same speed as the waves can transfer energy to them, and it is this process that gives rise to the enhancement seen in the daytime. The energy required of the electrons is

$$E_{ph} = \tfrac{1}{2} m_e (v_{ph})^2. \tag{43}$$

Significant fluxes of photoelectrons exist in the ionosphere with energies approximately in the range 1 to 25 eV. As discussed in Section IX-A, Landau damping by thermal electrons sets a minimum plasma frequency at which the enhanced plasma line may be detected of the order [51]

$$f_{N_{min}} \approx 2/\lambda \text{ MHz} \tag{44}$$

where $\lambda$ is the radar wavelength expressed in meters. A maximum plasma frequency is set by damping of the oscillations due to collisions of the electrons with ions [49] and is of the order of [51]

$$f_{N_{max}} \approx 6/\lambda \text{ MHz}. \tag{45}$$

It follows that, with a suitable choice of wavelength, it is possible to explore the electron density as a function of altitude by offsetting the receiver frequency by an amount $f_r$ and locating the height at which the plasma density is $f_N$ by sweep integration. In the particular case when $f_0F2 \leq f_{N_{max}}$ (45) it is possible by this means to produce an electron density profile over a substantial fraction of the $F$ region, and Fig. 13 shows an electron density profile obtained in this manner at Arecibo [52].

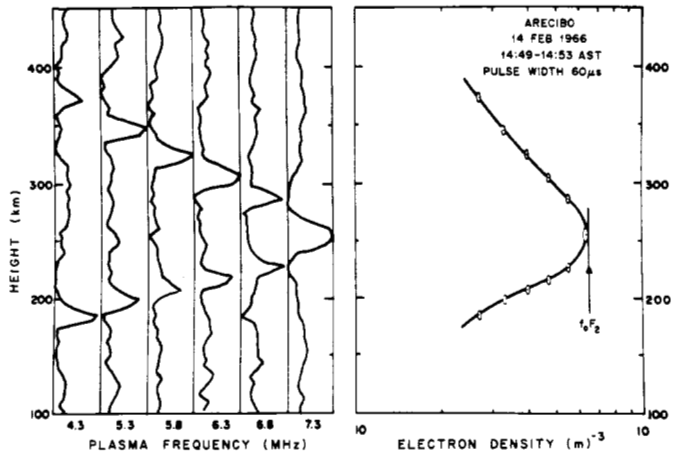


Fig. 13. Method of determining an electron density profile by observing the position of the plasma line [52]. (a) The results of sweep integrations carried out with the frequency of the receiver offset from the transmitter frequency by the amount shown. This serves to establish the altitude at which corresponding plasma frequencies exist. (b) The resulting electron density profile. The arrow gives the value of density obtained for the layer peak from a conventional ionosonde.

## V. Determination of Electron and Ion Temperatures

### A. Spectrum Measurements

We have seen (Section II) that the electron and ion temperatures ($T_e$ and $T_i$) control the shape of the scattered signal spectrum in the case where $\alpha(=4\pi D/\lambda)$ is small. Thus it is possible to determine these parameters from a careful measurement of the shape of the signal spectrum. In the case of a CW bistatic radar, the measurement is fairly straightforward and may be carried out using some form of filter bank as spectrum analyzer (as at St. Santin, Section III), or by digital sampling and computer analysis of the signals [53]. Difficulties of interpretation may arise when a mixture of ions is present (Section VI) or when the value of $\alpha(=4\pi D/\lambda)$ is unknown and cannot be presumed small. To remove the latter dependence one may proceed in the manner suggested by Moorcroft [27] (Section IV-A) and determine a "fictitious" value of the electron-to-ion temperature ratio $\beta$ from the spectrum by assuming $\alpha=0$. This can then be employed in (33) to correct for the effect of nonthermal equilibrium on the scattering cross section and hence derive the local electron density from the total power $P_s$ [via (30)]. By measuring the width of the spectrum to the half-peak-power point, it is possible to determine the ion temperature $T_i$. The value of $T_i$ so obtained is uninfluenced by the value of $\alpha$ and thus with $T_i$, $N$, and $\beta$ known it is possible to solve (32) for $T_e$.

When a pulse radar is employed, it is necessary to select from the radar time base some portion of the echoes for spectral analysis. One technique, employed at Millstone [41], has been to gate the IF signals into a filter bank for a period of time $T$ equal to the transmitted pulse length, at a delay $t_0$ following the transmitted pulse that defines the height of interest. The effect of gating the transmitter and receiver introduces instrumental smearing of the fluctuation spectrum of the medium $W(\omega)$ [given in (18)] such that the observed spectrum $p(\omega')$ is [54]

$$p(\omega') = \int_{\infty}^{+\infty} d\omega W(\omega)_{t_0} j(x) \tag{46}$$

in which $x=\omega-\omega'$ and the convolution function $j(x)$ is

$$j(x) = \frac{2}{\pi T x^2}\left[1 - \frac{\sin(xT)}{xT}\right] \tag{47}$$

where $T$ is the pulse length (seconds). If the filters employed in the filter bank have significant width compared with $1/T$ Hz, it is necessary to compute the additional broadening they introduce. Perkins [54] has shown that for single-pole filters, this can be accomplished analytically by convolving $j(x)$ [see (47)] with the filter transfer function to yield a new convolution function that can be employed in (46).

An alternative scheme currently in use at Millstone is to apply the IF signals without receiver gating to a bank of matched filters (i.e., having a transfer function equal to the distribution of the power in the pulse). In this case it is possible to obtain spectra at a number of delays in the course of a single measurement. With carefully made filters, the instrumental smearing of the spectrum is accurately represented by (46) and (47).

These instrumental effects are of serious concern in all the pulse radar systems (Table IV). In order to recover most of the information in the fluctuation spectrum $W(\omega)$, it is necessary that the spectral width of the pulse be restricted to about one-fifth or one-sixth of the spectral broadening of the medium. This yields

$$T \geq 1.5/\Delta f_i \text{ seconds} \tag{48}$$

which places a restriction on the possible height resolution $\Delta h$ for vertical measurements of

$$\frac{cT}{2} = \Delta h \geq \frac{9\times 10^8}{4\Delta f_i} \text{ meters.} \tag{49}$$

In practical terms this means that the height resolution achievable at altitudes below 250 km is unacceptably poor for all wavelengths that satisfy the relation $\lambda \geq 25\ D$ discussed in Section II. There are two means by which this difficulty can be overcome, namely, 1) by making oblique incidence measurements, and 2) by adopting autocorrelation techniques (Section VII-C).

By tilting the antenna beam, the height resolution improves as the secant of the zenith distance, but the echo power falls [see (28)] as the range to the ionosphere increases. The only real virtue in this approach is that it provides a simple means of eliminating the effects of ground-clutter echoes appearing at the same range as the altitude of the region to be studied.

Table VI lists the height resolution typically achieved for spectrum measurements at various altitudes by the radar systems listed in Table IV. Actually, as shown in Fig. 14(a), the height resolution afforded by the pulse radars is somewhat worse than $cT/2$. This figure shows the altitudes illumi-

TABLE VI
COMPARISON OF THE CAPABILITIES OF VARIOUS THOMSON SCATTER RADARS

| Facility | Operating Frequency (MHz) | Height Resolution (km) for Spectrum Measurements | | | | Electron Density Profile Determination (km) |
|---|---|---|---|---|---|---|
| | | *E* Region (100 km) | *F*1 Region (200 km) | *F*2 Region (>300 km) | Above 1000 km | |
| Arecibo I | 40.12 | ? | ? | ? | 300 | 200–6000? |
| Jicamarca | 49.92 | — | 15 | 30 | 300 | 200–6000 |
| Malvern | 400 | — | — | — | — | 100–600 |
| Arecibo II | 430 | 5 | 15 | 75–150 | 300 | 90–2000 |
| Millstone I | 440 | — | 75 | 75–150 | — | 200–1000 |
| St. Santin | 935 | 4 | 8 | 13 | — | 100–500 |
| Millstone II | 1295 | 35 | 35 | — | — | 100–400 |
| Stanford | 1300 | 35 | 35 | — | — | 100–400 |

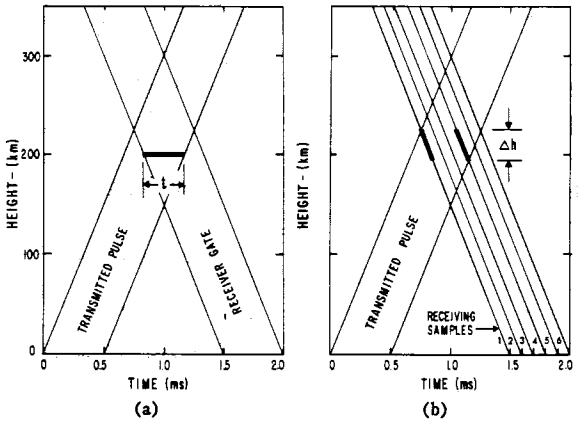


Fig. 14. (a) The filter bank approach to spectrum analysis. Both the transmitted pulse and receiver gate have a duration of 500 $\mu$s. The interval in time that electrons at a given height are both illuminated by the transmitted pulse and have their scattered signal passed through the receiver gate varies with altitude. For an altitude of 200 km, this interval is shown darkened (after Perkins [54]). (b) The sampling method of spectrum analysis. The transmitted pulse has a duration of 500 $\mu$s and the receiver samples are taken at short intervals (drawn here only at 100-$\mu$s intervals for the sake of clarity) over an equal interval of time. The height interval in common to sample 1 and sample 4 is shown darkened (after Perkins [54]).

nated as a function of delay for a pulse of length $T=0.5$ ms. It is evident that in this example, where the receiver gate delay $t_0=1.5$ ms, only the electrons at 225-km altitude are illuminated for the full period that the gate is open. Those at higher or lower altitudes contribute for shorter periods of time. Thus the combined effect of the gating is to weight the echo power reflected between 150 and 300 km in a triangular fashion. Stated otherwise, the height resolution is a poorly defined quantity as the frequency smearing varies with altitude.

A third method of processing the signals is to take samples over the interval $T$ and employ these to compute the echo autocorrelation function. The frequency and height resolution achieved will be the same as in the gated filter-bank scheme if all possible products are formed. If, however, only one pair of samples is employed to compute each mean lagged product and the pair chosen is that closest to the center of the interval, the height resolution will be improved [54]. This is illustrated in Fig. 14(b) which shows the height intervals contributing to the mean lagged product in this case. Though the improvement in height resolution is achieved with no loss of spectral resolution, there is a deterioration in the accuracy of the measurements which depends upon the input signal-to-noise ratio $P_s/P_n$ [54]. Thus this technique is of practical application only when the signals are strong and consequently some of the information in the other possible products is redundant.

Fig. 15 shows temperature measurements obtained with the bistatic radar at St. Santin [55], which may be compared with Fig. 16 in which measurements obtained with the pulse radars Millstone I and II are shown [56]. The vertical bars denote the height interval occupied by the exploring pulse.

In closing this subsection it should be mentioned that the ability to determine simultaneously electron density and electron and ion temperatures as a function of altitude has made the Thomson Scatter radar a most powerful tool in studying the thermal balance of the ionosphere. With measurements of the type described here as guides, the theory of the heating, cooling, and heat transfer processes in the ionosphere has advanced considerably in the last decade, and it would be outside the scope of this article to attempt to review this work.

### *B. Correlation Measurements*

As we have just seen in the case of the pulse radars, the choice of pulse length $T$ determines the frequency resolution, height resolution, and signal-to-noise ratio. For those of the existing pulse radars that operate at wavelengths shorter than 1 meter, an acceptable compromise value of $T$ can be found only for altitudes above about 200 to 300 km. For Jicamarca, single long pulses cannot be employed for spectrum measurements at any altitude below about 1000 km.

One means of obtaining adequate height resolution is to transmit a pair of short pulses separated by an interval $\tau$ and compute the correlation $c(\tau)$ between the echoes from altitudes of interest. By varying the spacing $\tau$ between the pulses over the range $0 \leq \tau \leq (\Delta f_i)^{-1}$ the complete autocorrelation function [i.e., the complex Fourier transform of $W(\omega)$] can be determined. It is of course necessary that the receiver time constant be short compared with the minimum spacing between pulses and this places a limit on the receiver bandwidth of the order of

$$b \geq 10\Delta f_i. \tag{50}$$

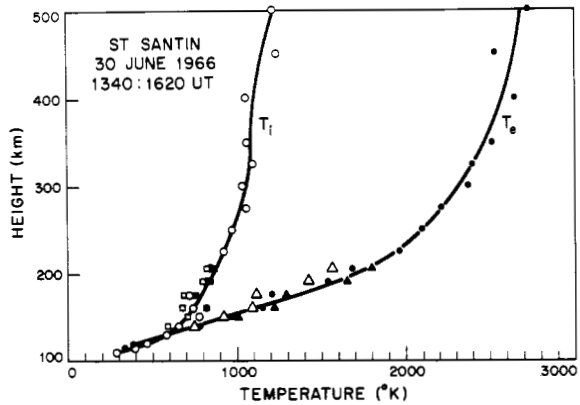


Fig. 15. Electron density and electron and ion temperature observed at St. Santin between 1340 and 1620 UT on June 30, 1966 (Carru *et al.* [55]). In these observations the vertical height resolution is extremely good (Table VI).

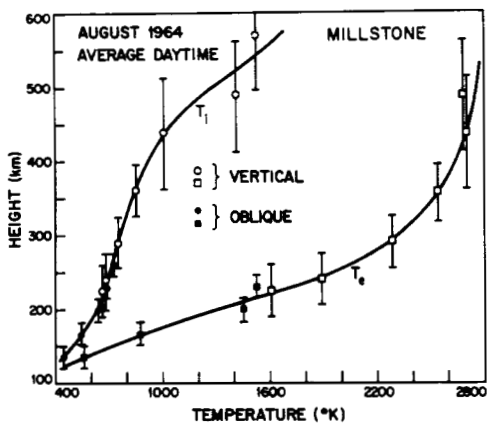


Fig. 16. Electron and ion temperatures observed at Millstone [56] by combining results obtained with the two radar systems (Table IV). The vertical bars denote the height interval occupied by the exploring pulse (Table VI).

This double-pulse technique is employed routinely at Jicamarca and Arecibo. At both stations the range of interesting pulse spacings $\tau$ is such that $\tau \ll 10$ ms, and thus it is inevitable that both pulses will be in the ionosphere simultaneously. To avoid the problem of mutual interference between the two echoes, the Jicamarca group makes use of the two separate modes that can propagate in the ionosphere (Section IV-B). Thus they transmit the pulses with opposite circular polarizations and receive separately the echoes with receivers coupled to orthogonal ports on the hybrid coupler. This elegant scheme has one unfortunate drawback when employed at a station like Jicamarca [57]. This arises because the direction of the beam is close to perpendicular to the magnetic field [i.e., $\cos\theta \to 0$ in (37)] and in consequence there are significantly different amounts of Faraday rotation along different directions within the main beam of the antenna. McClure [57] has termed the resulting decorrelation of the signal "Faraday dispersion." This phenomenon serves to limit the altitude to which it is possible to make electron density profile measurements (Section IV B) as well as make echo correlation determinations and it is serious for Jicamarca at sunspot maximum at high altitudes. At such times it becomes preferable to perform echo correlation measurements by transmitting both pulses with the same polarization and accept the increased statistical uncertainty introduced by mutual interference of the echoes (i.e., self-noise). This latter approach is the one employed at Arecibo and in effect causes the signal-to-noise ratio to fall to unity or less at all altitudes. Fig. 17 shows temperatures obtained at Arecibo for the $E$ and $F1$ regions during the time of a rocket launch [58]. As can be seen, the two techniques yield results that are in good agreement except perhaps at the very lowest altitudes.

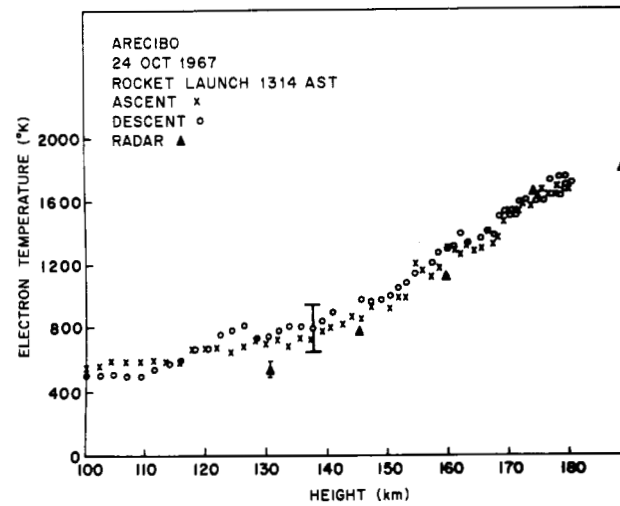


Fig. 17. Comparison of electron temperature profiles from simultaneous radar and rocket observations at the Arecibo Ionospheric Observatory [58].

The bandwidth limitation (50) becomes more severe as the altitude increases (Table II). Indeed in order to offset the rapid decrease in signal strength encountered above the peak of the $F$ layer (Table V) it is usually preferable to transmit single long pulses. In practice, this means that the Arecibo double-pulse observations are confined to altitudes below about 300 km, and the technique could not be used at all with the Millstone II or Stanford radar systems ($\lambda \sim 23$ cm).

### C. Electron-to-Ion Temperature Ratio

If by some means the effective cross section of the electrons $\sigma$ were known at some altitude, $T_e/T_i$ could be deduced via (24) assuming $\alpha \to 0$. This has been the basis of a number of attempts to determine $T_e/T_i$ without embarking upon a spectral analysis of the signals. In order to determine $\sigma$ it is necessary to measure the total echo power and derive the true electron density by an independent method. The technique was first applied for the $F2$ peak using an ionosonde to determine $f_0F2$ [28], [30], [59]. In order to obtain accurate estimates of $T_e/T_i$, it is necessary to calibrate the radar system very carefully. Greenhow *et al.* [59] accomplished this by launching balloon-borne targets of known cross section. Others have established the calibration from nighttime observations (i.e., assuming $T_e/T_i = 1.0$ at night), or by determining the complete power profile and assuming that $T_e/T_i = 1.0$ in the $E$ region and using $f_0E$ to establish the constants of the radar [60].

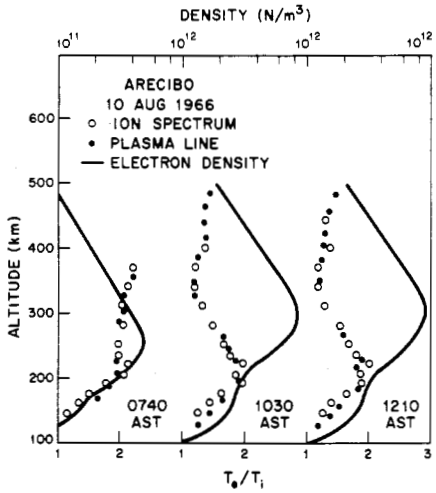


Fig. 18. Electron-to-ion temperature ratios measured by the plasma-line and ion spectrum (double-pulse) methods. (The results for afternoon measurements are very close to the noon measurements.) These measurements were made at Arecibo [64].

Obvious extensions of these studies have been to employ true height (ionosonde) profiles together with Thomson Scatter profiles to yield the variation of $T_e/T_i$ over a range of altitudes [61]. It is possible to dispense with ionosonde methods completely and determine the true density by one of the two absolute methods discussed in Section IV, viz., the Faraday profile [62], [63] method or the plasma-line method. Fig. 18 shows values of $T_e/T_i$ obtained at Arecibo by comparing a power profile with an electron density profile obtained from plasma-line measurements [64]. Also shown in Fig. 18 are $T_e/T_i$ values derived by direct spectrum analysis and, as can be seen, the agreement is very good.

## VI. Determination of Ionic Composition

### A. Effect of Ion Mass on the Spectrum

We have not thus far discussed the effect on the spectrum of the scattered signal of changing the type of ion. As can be seen from (21), the spectrum width varies inversely as the square root of the ion mass $m_i$ and Fig. 19 illustrates this dependence for $O^+$, $He^+$, and $H^+$ ions. If these same spectra are plotted on a normalized frequency scale [i.e., one in units of $\Delta f_i(T_e/T_i)^{\frac{1}{2}}$] they are found to have approximately the same *shape* [27], as shown in Fig. 20. The total power scattered depends slightly upon $m_i$ (Fig. 4), but for the range of values of $T_e/T_i$ encountered in the ionosphere this dependence can safely be ignored.

From the foregoing it is clear that one cannot determine $T_i$ if $m_i$ is not known (or vice versa). Fortunately, there is now enough a priori information concerning the composition of the ionosphere so that this introduces no difficulty provided only a single ion is present.

### B. Mixtures of $O^+$, $He^+$, and $H^+$

When two or more ions are present with comparable abundance, the spectrum of the mixture is not simply the sum of the spectra that these ions would have if present by themselves. Fig. 21 shows the variation of spectrum shapes for an $O^+/He^+$ mixture. When only these two ions are present (or $He^+$ and $H^+$) it would seem that the slope of the spectrum at the half-peak-power point can be used as a measure of the percentage composition [27] provided that observations are available from higher or lower altitudes which can be used to resolve the ambiguity between, say, 20-percent He or 80-percent He (Fig. 21). The case of mixtures of all three ions is more complex, and Fig. 22 shows

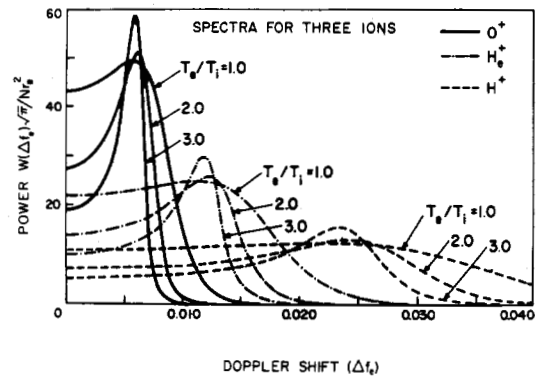


Fig. 19. Spectra for $O^+$, $He^+$, and $H^+$ ions for three values of $T_e/T_i$ (after Moorcroft [27]). The spectra are here plotted on a frequency scale normalized to $\Delta f_e$ and hence appear in their true relative widths.

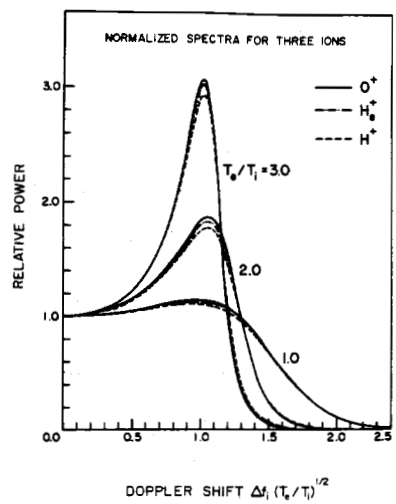


Fig. 20. The spectra shown in Fig. 19 are here replotted on a normalized frequency scale so that their shapes may be compared (Moorcroft [27]).

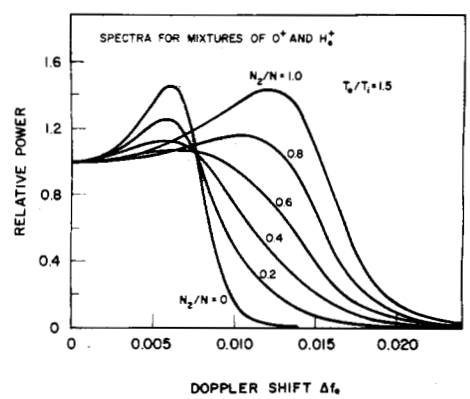


Fig. 21. The variation of the ionic spectrum shape plotted on the same scale as in Fig. 19 for a mixture of $O^+$ and $He^+$ ions. $N_2$ is the number density of $He^+$ ions and $N$ the electron density. Here it has been assumed that $\lambda \gg 4\pi D$ and $T_e/T_i = 1.5$ (after Moorcroft [27]).

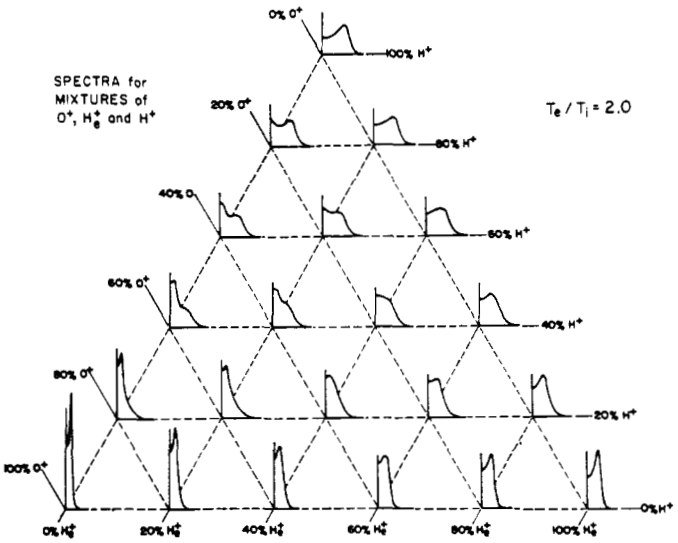


Fig. 22. An array of spectrum shapes computed for a mixture of $O^+$, $He^+$, and $H^+$ ions for the case $\lambda \gg 4\pi D$, $T_e/T_i = 2.0$ (after Moorcroft [27]). It can be seen that the spectra are all different so that it should be possible to determine the composition if $T_e/T_i$ is known.

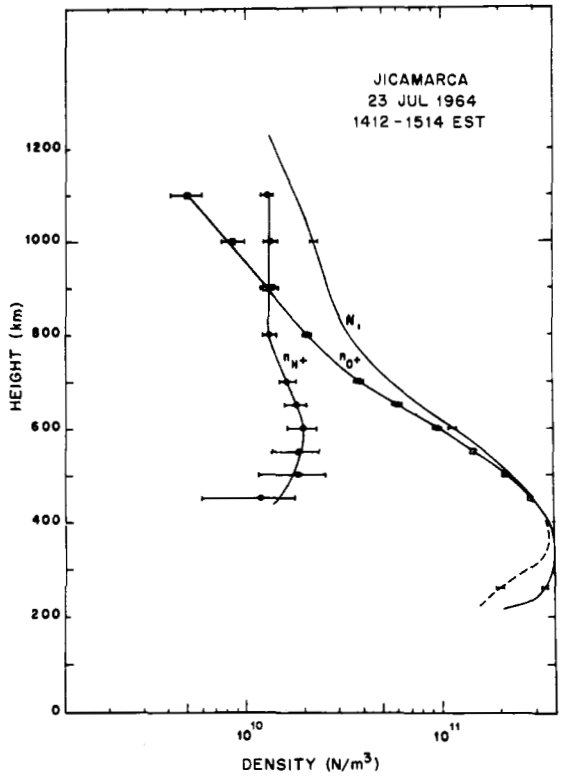


Fig. 23. Typical ionic composition and electron density observed during the day at Jicamarca [62].

an array of spectra computed by Moorcroft [27] for the case $T_e/T_i = 2.0$. If the mixture, $T_e/T_i$, and $\alpha$ are all unknown, then it becomes impossible to make a unique interpretation of the measured spectra.

In practice, two factors have made it possible to simplify the interpretation of high-altitude spectra, at least as recorded at Jicamarca and Arecibo. The first has been the extremely low abundance of $He^+$ encountered thus far. Farley [62], [65] places an upper limit of 10 percent on the amount of $He^+$ observable at any altitude over Jicamarca, while only a slightly larger one is given for Arecibo [66], [67]. This effectively confines the search to the left-hand edge of diagrams such as Fig. 22. Next it transpires that at altitudes at which the transition from $O^+$ to $H^+$ takes place, $T_i \rightarrow T_e$. This results from the fact that at these heights the heat given to the electrons via Coulomb coupling cannot readily be lost to the neutrals via collisions [68]–[70]. Thus at both Arecibo and Jicamarca the approximation $T_e/T_i = 1.0$ is made in analyzing the results.

It has also been possible to proceed on the assumption that $\alpha \rightarrow 0$, and this is questionable only in the case of Arecibo. However, as pointed out by Moorcroft [67], underestimating the value of $\alpha$ is exactly equivalent to overestimating the value of $T_e/T_i$. So this error tends to offset that due to the assumption of thermal equilibrium. These steps reduce the task of interpreting the spectral results to that of finding only $T_i$ and the composition ratio. Fig. 23 shows density and composition profiles obtained for Jicamarca [62]. In this instance the transition altitude between $O^+$ and $H^+$ is at about 900 km.

### C. Mixtures of $O_2^+$, $N_2^+$, and $O^+$

We have seen that at altitudes well above the $F2$ peak, there is a transition from $O^+$ as the dominant ion to lighter ions ($He^+$ and $H^+$). As we go to very low altitudes ($F1$ and $E$ regions), ions heavier than $O^+$ are encountered and the separation of these from $O^+$ presents a greater problem than the light ions. According to rocket measurements, the principal ions in the $E$ region are $NO^+$ and $O_2^+$, and at most altitudes these are present in approximately equal quantities [5], [71]. The masses of $NO^+$ and $O_2^+$ are sufficiently similar that their relative abundance cannot be determined from the shape of Thomson scattered spectra in any measurable way. Indeed, as Petit [72], [73] has shown, $O^+$ and $O_2^+$ (or $NO^+$) are sufficiently alike that it is possible to change their mixture and not be able to distinguish this from some suitable change in $T_i$ and $T_e$. This is particularly unfortunate since the composition changes from predominantly $O_2^+$ and $NO^+$ to predominantly $O^+$ over the altitude range (100 to 250 km approximately) in which $T_i$ and $T_e$ are found to be increasing fastest (Figs. 15 and 16). Thus the interpretation of spectra obtained in this altitude range is extremely difficult and so far has proceeded on the assumption of a model for either the composition or one of the temperatures.

At St. Santin the following approach has been adopted [55], [73]. A model for the ratio of $O^+$ to the sum of $O_2^+$ and $NO^+$ as a function of altitude has been established from the rocket results summarized by Johnson [74] and is shown in Fig. 24. According to this model, $O_2^+$ and $NO^+$ completely dominate below 140-km altitude, and at St. Santin, these ions were represented in the theoretical spectrum calculations by an ion of mass $m_i = 30.5$ AMU (1 AMU $= 1.66 \times 10^{-27}$ kg). The observed spectra are first interpreted on the assumption that the composition dependence is exactly that of the model. They are then reinterpreted assuming that the composition differs by 10

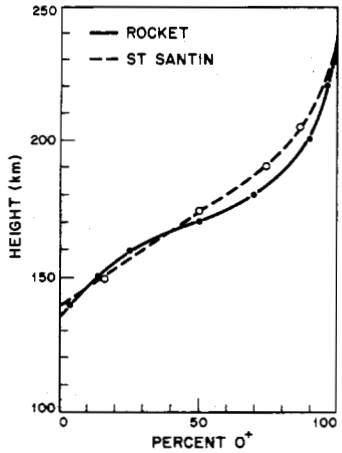


Fig. 24. Comparison of the percentage concentration of $O^+$ ions (the other ions being mainly $NO^+$ and $O_2^+$) as a function of altitude obtained from rocket results [74] and Thomson Scatter measurements at St. Santin [73].

percent in either direction from the model. This leads to three values of $T_i$ and $T_e$ (see Fig. 15) at altitudes between 140 and 240 km where the composition is changing. Smooth temperature curves for $T_i$ and $T_e$ are next drawn through these points to connect to the reliable values established above and below this altitude range, where ions of one mass predominate. From this temperature curve, a new estimate of the composition is made. On this basis a remarkably constant altitude variation of composition is found during the daytime, and Fig. 24 compares the mean variation observed [73] with that assumed in the model [74].

Experimental evidence exists that the composition curve varies between day and night [71], and on theoretical grounds there is reason to believe that there may also be seasonal variations [6]. Accordingly, in analyzing the Millstone results, Evans [56] chose to adopt a model for one of the temperatures. What in fact was done was to assume that $T_i = T_n$, where $T_n$ is the neutral temperature. There is good theoretical evidence [68]–[70] that this must be the case at least up to about 250 km. The variation of neutral temperature in this altitude range was then assumed to be of the form adopted in the CIRA 1965 model atmosphere for sunspot minimum ($\bar{F} = 65$ or $75 \times 10^{-22}$ W/m$^2 \cdot$ Hz), namely,

$$T_n = T_{ex} - (T_{ex} - 355) \exp [-0.0156(h - 120)] \quad (51)$$

where $T_{ex}$ is the exospheric temperature and $h$ is the height in km. This dependence is based upon calculations of the vertical conductivity and has some experimental support from observations of the drag on artificial earth satellites [75]. The temperature $T_{ex}$ was established from the observations by assuming $T_i = T_{ex}$ at altitudes between 250 and 300 km where only $O^+$ was presumed to exist. Equation (51) then gave $T_i$ at all lower altitudes and by an iterative procedure it was possible to recover $T_e$ and the composition ratio from the spectra. This method is open to the objection that the temperature at the lower boundary (120 km) may not be 355°K as assumed in (51) and consequently the composition results will be progressively in error at the lower altitudes.

Yet a third procedure has been adopted at Arecibo [76]. In this, based on rocket results, it is assumed that only $O_2^+$ and $NO^+$ exist at the lowest altitude examined (130 km), and $O^+$ exists above 250 km. Temperatures at these altitudes can then be obtained without ambiguity. At the intervening altitudes the exponential temperature law (51) is assumed except now modified as

$$T_i = T_{i_{250}} - (T_{i_{250}} - T_{i_{130}}) \exp [-s(h - 130)]. \quad (52)$$

Two values of the exponent $s$ were tried, viz., that given in (51) corresponding to the CIRA 1965 models and a value of $\sim 0.028$ employed by Jacchia [75]. The uncertainty in $s$ leads to some uncertainty in the composition curve. Also, Wand (private communication) has found that for some days the method leads to what he believes are spurious variations in the composition curve. These arise because the temperature distribution seems to depart from the steady-state condition given by (52) owing to some form of propagating disturbance. The Thomson Scatter temperatures shown in Fig. 17 were obtained using this simultaneous solution for $T_e$ and composition. The agreement with the rocket results lends support for the method. The disagreement at low altitudes is in keeping with a long-standing discrepancy between Thomson Scatter and rocket results, namely, that the former all indicate $T_e/T_i = 1.0$ for $h \leq 130$ km [55], [56], whereas the latter mostly show $T_e > T_i$ to the lowest altitudes examined.

### *D. Ion Gyroresonance Effects*

In Section III-B the possibility was mentioned that, for propagation directions normal to the lines of force of the earth's magnetic field, characteristic fluctuations will be imparted to the spectrum by the gyro motion of the ions. This idea has been examined theoretically by a number of authors [17], [77]–[79]. In essence, the effect depends upon the fact that when viewed normal to the field lines the ions will all reappear in the same positions at intervals of $1/f_H$ where $f_H$ is the ion gyrofrequency

$$f_H = \frac{\mu_0 eH}{2\pi m_i} \text{ Hz.} \quad (53)$$

Here $H$ is the field intensity in ampere turns per meter, $e$ the charge on the ion (coulomb) and $m_i$ the ion mass (kg). In temperate latitudes at $F$-region altitudes we expect $f_H \sim 50$ Hz for $O^+$ ions.

Previously we have considered the effect of varying the ratio of the exploring wavelength to the Debye length $D$ [defined in (16)]. When magnetic effects are also to be considered, it is necessary to include the ratio of the wavelength to the electron and ion gyroradii $R_e$ and $R_i$, respectively. These are given by

$$R_e = (m_e K T_e)^{\frac{1}{2}}/\mu_0 eH \quad \text{meter} \quad (54)$$

$$R_i = (m_i K T_i)^{\frac{1}{2}}/\mu_0 eH \quad \text{meter.} \quad (55)$$

Values for $R_e$ and $R_i$ as defined in (54) and (55) are given in Table VII for various altitudes in the ionosphere, assuming the ion masses and temperatures given in Tables I and II. It can be seen by comparing Tables I and VII that in the

TABLE VII
GYRORADII FOR IONS AND ELECTRONS

| Region | Height (km) | Epoch | $H$ (A/m) | $T_i$ (°K) | $T_e$ (°K) | $R_i$ (m) | $R_e$ (cm) |
|---|---|---|---|---|---|---|---|
| $E$ | 120 | Winter night $S_{min}$<br>Summer day $S_{max}$ | $5.90 \times 10^{-3}$ | 300<br>300 | 300<br>300 | 1.71 | 0.73 |
| $F1$ | 200 | Winter night $S_{min}$<br>Summer day $S_{max}$ | $5.84 \times 10^{-3}$ | 750<br>1500 | 2000<br>3000 | 1.69<br>2.85 | 1.92<br>2.36 |
| $F2$ | 300 | Winter night $S_{min}$<br>Summer day $S_{max}$ | $5.78 \times 10^{-3}$ | 1000<br>2000 | 2500<br>2500 | 2.35<br>3.32 | 2.18<br>2.18 |
| Upper $F2$ | 1000 | | $5.40 \times 10^{-3}$ | 2500 | 3000 | 1.99 | 2.55 |
| Lower exosphere | ≥2000 | | $5.03 \times 10^{-3}$ | 3000 | 3000 | 1.17 | 2.75 |

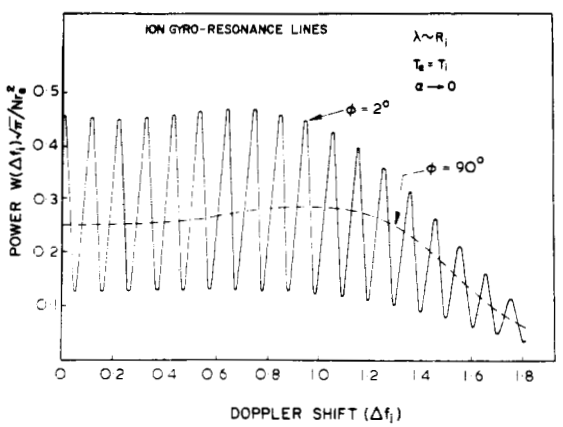


Fig. 25. The appearance of ion gyroresonance lines of $O^+$ in the ionic component of the spectrum. These occur when $\lambda \approx R_i$ and the off-perpendicular angle $\phi$ is small. In this case the ratio $\lambda/R_i = 1.8$ and $\phi = 2°$. The dashed curve shows the spectrum when $\phi \to 90°$ or the field is absent (after Farley *et al.* [78]).

ionosphere $R_e \approx D$ and thus for measurements of practical interest (i.e., when $\lambda/4\pi > D)\lambda \gg R_e$. Thus, whilst a variety of situations have been discussed in the literature, there are only two that need concern us here, namely, $\lambda \sim R_i > R_e$ and $R_i > \lambda > R_e$. The latter condition will be touched upon in Section IX.

When the exploring scale becomes comparable to the ion gyroradius $R_i$, it is possible for modulation to appear in the spectrum at or near the gyrofrequency as originally postulated by Bowles [32]. For an angle $\phi$ between the ray and the normal to the field, the condition required for such resonance effects is that $\sin \phi \ll \lambda/4\pi R_i$. On the basis of numerical calculations Farley *et al.* [78] give $\sin \phi \leq \lambda/35R_i$ as a somewhat more precise criterion of the condition required for gyroresonances to appear in the spectrum. Fig. 25 shows results computed by Farley *et al.* [78] for the case $\lambda = 7.5$ meters with $O^+$ ions for an off-perpendicular angle of $\phi = 2°$. The dotted line shows the spectrum in the absence of a magnetic field (or $\phi = 90°$). Farley *et al.* [78] state that for $\lambda \sim R_i$, the spectrum remains essentially unchanged in the range $90° < \phi < 5°$. As $\phi$ is reduced below 2°, the resonance lines will grow in amplitude, but the overall spectrum width decreases. Finally, at $\phi = 0$ the spectrum collapses into a single line at the radar frequency (Section VII-C).

The positions of the peaks are not precisely equal to multiples of the ion gyrofrequency $f_H$, but in the limit as $\sin \phi \to 0$ are given by [78]

$$\Delta f = n f_H (1 + f_H/\sqrt{\pi}\Delta f_i) \tag{56}$$

where $\Delta f$ is the displacement from the radar frequency and $f_H$ is the gyrofrequency (53). The presence of these lines does not alter the total echo power, i.e., the area under the spectrum remains the same when $T_e = T_i$, but for $T_e > T_i$ the echo power will increase for $\phi \to 0$ [80].

When these gyroresonance phenomena were first considered, it was assumed that collisional damping would be small provided that the ion gyrofrequency $f_H$ is large compared to the electron-neutral collision frequency $\nu_e$. The absence initially of any resonances in the ion spectra observed at Jicamarca led to questions concerning the role played by ion-ion encounters. This problem has been examined by Farley [81]. As noted above, the ion resonance effect occurs because the ions tend to return to their original positions in the plasma at intervals of $1/f_H$ seconds. However, if the ion is deflected from its original orbit due, for example, to an encounter with another ion, the effect will be reduced. Farley [81] shows that ion-ion encounters reduce the modulation depth appearing in the spectrum by a factor $e^{-1}$ when the mean square deviation of the particle displacement $\overline{|(\Delta y)|^2}$ normal to the unperturbed orbit is equal to $\lambda^2/8\pi^2$. Farley gives for $\overline{|(\Delta y)|^2}$

$$\overline{|(\Delta y)|^2} = 1.42 \times 10^{-42} \frac{N \ln \Lambda}{m_i^{3/2} T_i f_H^3} \tag{57}$$

where $\Lambda$ is a slowly varying function of $T$ and $N$ tabulated by Spitzer [82]. An examination of the conditions appearing in the ionosphere shows that $\overline{|(\Delta y)|^2}$ will be comparable with the gyroradius at almost all altitudes below about 1000 km and hence the modulation will be completely destroyed. At altitudes >1000 km where the predominant ion is $H^+$, $f_H$ is increased by a factor of 16 over that for $O^+$, so that there is a net reduction in $\overline{|(\Delta y)|^2}$ by the ratio $(16)^{3/2}$, i.e., by 64 times. In addition, the electron density $N$ will be lower by two to three orders of magnitude. Thus, proton gyroresonances are the only ones likely to be encountered, and these have, in fact, now been observed at Jicamarca [83].

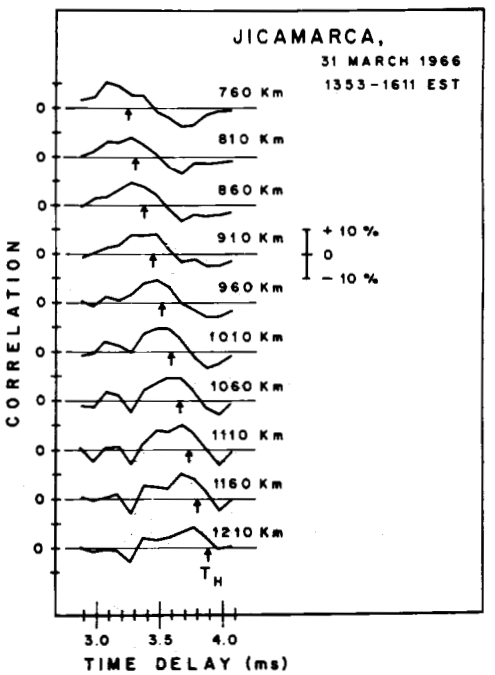


Fig. 26. Correlation functions observed for the signal reflected at various altitudes above Jicamarca [83]. The peaks here arise from the presence of the protons. $T_H$ is the calculated gyroperiod ($=1/f_H$) which varies with altitude because of the reduction of the field intensity $H$.

The gyrofrequency for protons at Jicamarca is in the range 250 to 300 Hz and the search for the resonance was carried out by the correlation technique (Section V-B) by looking for a peak in the correlation function at delays of $1/f_H$ seconds. Fig. 26 shows the peaks observed. In other measurements, peaks at $2/f_H$ and $3/f_H$ have also been detected [83].

## VII. Determination of Drift Velocities

### A. Effect of Particle Drifts on the Spectrum

Up to the present, the principal uses for Thomson Scatter radars have been the determination of electron density, electron and ion temperature, and ion composition. There are obvious reasons for this: these studies complement and extend earlier ground-based measurements and current rocket and satellite programs. In these remaining three sections, we describe other applications of Thomson Scatter, some of which hold considerable promise for advancing our understanding of upper atmosphere physics. Most important of these perhaps is the use of ground-based radar to measure motions within the ionosphere.

The reflection technique has long been employed to study the horizontal drift velocity of ionospheric irregularities at $E$- and $F$-region heights. Thome [84] and others have successfully applied the Thomson Scatter technique to study large traveling disturbances in the $F$ region, and LaLonde [85] has similarly investigated $E$-region irregularities. These studies, by and large, have not shed a great deal of light on the motion of the undisturbed plasma, but rather on the forcing agent (e.g., the neutral atmosphere). Especially needed is information on the vertical drift velocity of the electrons in the $F$ region. Rao [86] and others have attempted to estimate the nighttime vertical velocity from the variation with time of the electron density profiles obtained by Thomson Scatter, but were forced to make certain simplifying assumptions. In point of fact, careful spectrum measurements of the signals are capable of yielding directly the drift velocity of the ambient plasma.

If the electrons and ions at any altitude drift as a whole toward the radar with a velocity $v_d$ m/s, the entire spectrum will be shifted by an amount $\Delta f_d$ where

$$\Delta f_d = \frac{+2v_d}{\lambda} \text{ Hz.} \tag{58}$$

This shift will occur without any change in spectrum shape. If, however, the electrons are moving relative to the ions (i.e., there is a current flow), the spectrum will become asymmetrical [21], [87]. When the ions remain at rest with respect to the radar, this will be the only effect. If, however, the ions are also in motion, the spectrum will be shifted in frequency according to (58), where $v_d$ is now the ion velocity relative to the radar.

Figs. 27 and 28 illustrate the asymmetry that develops when the electrons are moving with respect to the ions [87]. In Fig. 27 spectra are shown for different values of the ratio of the drift speed $v_d$ to the mean thermal velocity of the electrons $\bar{v}_e$ ($=\sqrt{2KT_e/m_e}$). Fig. 28 shows the effect of increasing $T_e/T_i$ for a fixed value of $v_d/\bar{v}_e$. In computing these plots [87], the ions were taken to be at rest with respect to the radar and the velocity $v_d$ of the electrons was in the direction of the receiver. The incident radiation, however, was assumed to be from a direction orthogonal to $v_d$, so that the spectrum width is a factor of $\sqrt{2}$ smaller than that shown in earlier plots where backscattering was the only case considered.

If it were possible to locate the center frequency of the spectrum to an accuracy of, say, 1 percent of the overall width, then any ion drift velocity $v_d$ could be established to an accuracy of the order of 3 percent $\bar{v}_i$, where $\bar{v}_i$ is the mean thermal speed of the ions. This would be about 12 m/s in the $E$ region, rising to about 30 m/s in the $F$-region. Similarly, if the ratio of the two wings could be measured to an accuracy of 1 percent, then the velocity of the electrons with respect to the ions could be determined to an extent that depends critically upon $T_e/T_i$, but in any case better than 1 percent $\bar{v}_e$.

### B. Spectrum Observations

The shape of a typical signal-plus-noise spectrum is sketched in Fig. 29. The spectrum is shown with a center frequency that is displaced by an amount $\Delta f$ from the transmitted frequency. From the shape of the spectrum it is evident that the sharpest features are the edges, and thus the determination of $\Delta f$ rests largely in locating these. In order to estimate the accuracy with which this may be accomplished, it shall be supposed that the measurement consists of comparing the signal level in two identical filters $b$ Hz in width displaced symmetrically in frequency about the transmitted frequency. The difference $\Delta P$ in the powers in the two filters will be

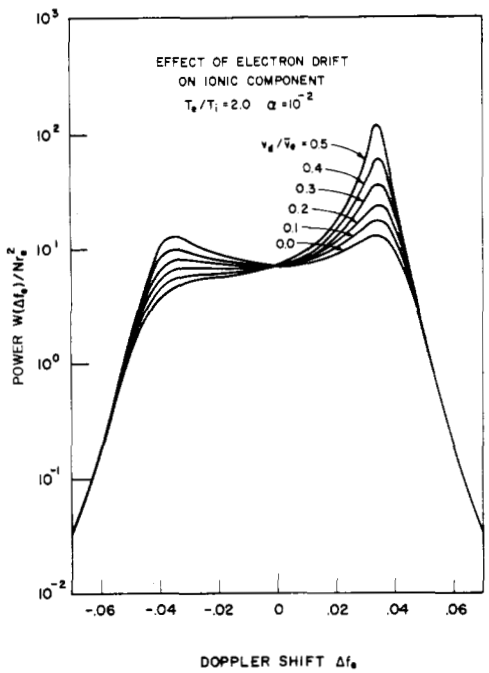


Fig. 27. Spectra showing the asymmetry that develops if the electrons are moving with respect to the ions. In this plot it is assumed that the ions have no bulk velocity with respect to the receiver, but the electrons move toward the receiver with the velocity $v_d/v_e$ shown where $v_e$ is the thermal velocity $\sqrt{2KT_e/m_e}$. The incident radiation is from a direction orthogonal to the direction of the receiver (after Lamb [87]).

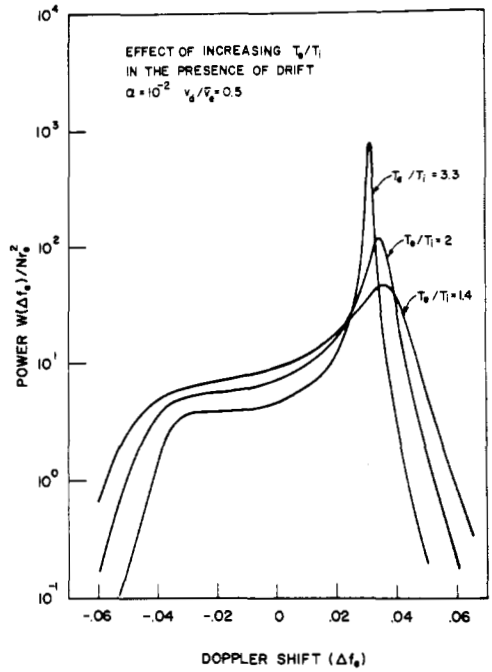


Fig. 28. Spectra for the same conditions as in Fig. 27, showing the effect of increasing the electron temperature above unity. All these curves apply to a ratio of drift to thermal speeds $v_d/v_e = 0.5$ and $\alpha = 10^{-2}$ (after Lamb [87]).

$$\begin{aligned} \Delta P &= 2\Delta f(\text{slope}) \quad \text{watts} \\ &= 2\Delta f\left(\frac{dP_s}{df}\right)_{\text{h.p.}} \quad \text{watts.} \end{aligned} \tag{59}$$

The slope of the spectrum $(dP_s/df)_{\text{h.p.}}$ is approximately linear over a considerable region near the half-peak-power point (Fig. 3), and consequently the filter bandwidths can be quite finite.

The uncertainty in the estimate of the drift velocity $v$ will depend largely upon the uncertainty in $\Delta P$, which may in fact be large enough to mask any difference in the power of the signals in the two filters. The uncertainty in the drift velocity thus becomes [29]

$$\Delta v = \pm \frac{\Delta \bar{P}_s}{\sqrt{2}}\left(\frac{df}{dP_s}\right)_{\text{h.p.}} \lambda \quad \text{m/s} \tag{60}$$

where $\Delta \bar{P}_s$ is the uncertainty in the echo power in each filter, and for pulsed radars may be estimated via (35). If the radar system is a CW bistatic system, then independent echo samples can be obtained at intervals of $1/b$ seconds. Thus after an experiment lasting $t$ seconds, the uncertainty $\Delta \bar{P}_s$ would be

$$\Delta \bar{P}_s \approx \frac{(\sqrt{2}P_n + P_s)}{\sqrt{bt}} \tag{61}$$

depending somewhat on the way in which the noise subtraction is accomplished. Thus, for $P_s \gg P_n$, we have as an approximation

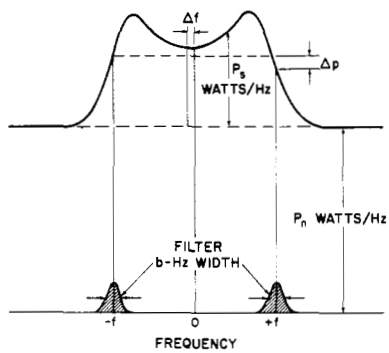


Fig. 29. A model for determining the precise center frequency of the spectrum. The shift in the center frequency $\Delta f$ is determined by measuring the difference $\Delta P$ in the powers contained in identical filters $b$ Hz in width placed symmetrically about the transmitted frequency close to the point of half-peak echo power.

$$\Delta v \approx \pm \frac{P_s}{\sqrt{2bt}}\left(\frac{df}{dP_s}\right)_{\text{h.p.}} \lambda \quad \text{m/s} \tag{62}$$

while for $P_s < P_n$

$$\Delta v \approx \pm \frac{P_n}{\sqrt{bt}}\left(\frac{df}{dP_s}\right)_{\text{h.p.}} \lambda \quad \text{m/s.} \tag{63}$$

In either case it is desirable to set the bandwidth $b$ of the filter as wide as possible consistent with the limitation that the filter only occupy that portion of the spectrum that has a reasonably linear slope. When this is done, (62) and (63) become [29] for $T_e/T_i \approx 2.0$

$$P_s \gg P_n \qquad \Delta v \approx \pm \sqrt{\frac{\Delta f_i}{4t}}\lambda \quad \text{m/s} \tag{64}$$

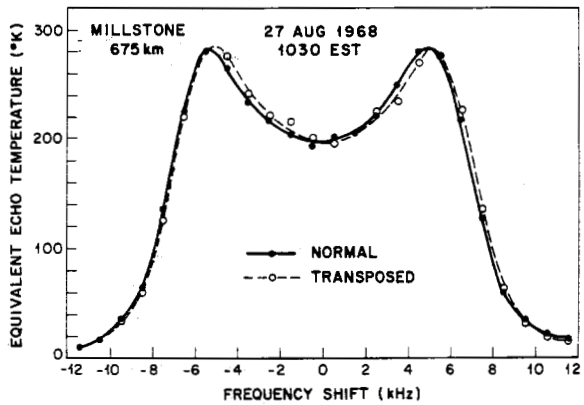


Fig. 30. Spectra observed at Millstone showing evidence of a drift. In this case the "normal" spectrum has been compared with one obtained by transposing the frequency components. This is done by placing one of the receiver local oscillators above the signal frequency. In this instance, the "normal" spectrum is shifted to lower frequencies, indicating an upward drift.

$$P_s < P_n \qquad \Delta v \approx \pm \frac{P_n}{P_s}\sqrt{\frac{\Delta f_i}{2t}}\,\lambda \quad \text{m/s} \qquad (65)$$

and somewhat larger uncertainties hold for lower temperature ratios. For $P_s/P_n \sim 0.1$ and an integration time of 1000 seconds, the velocity uncertainty at $F$-region altitudes would be $\sim \pm 10$ m/s for $\lambda = 1$ meter (Table II). It is evident from (64) and (65) that, provided the signal-to-noise ratio remains unchanged, the accuracy improves as the square root of the operating frequency. Similar equations to these can be obtained for pulse radar systems by replacing $bt$ in (62) and (63) by $nt$ where $n$ is the pulse repetition frequency of the radar. However, in the case of pulse radars the spectrum smearing (Section V-A) will serve to lower the slope at the half-power point and reduce the accuracy achievable.

In practice, systematic errors (i.e., instrumental effects) will often serve to set an ultimate limit to the accuracy obtained in measurements of this type. At St. Santin the method of analysis is to compare the observed spectrum with one computed theoretically and adjusted to yield best fit while allowing for a small frequency offset [88], [89]. An accuracy of the order of $\pm 5$ m/s is thought to be achieved in these measurements.

At Millstone a comparison is made of spectra taken with one of the receiver local oscillator frequencies first set below the signal frequency and then set above the signal frequency by an equal offset. Fig. 30 provides an example of the results obtainable by this method. When 1-m/s pulses are employed, the frequency resolution achieved in a 15-minute observing period is about $\pm 5$ m/s, but of course the height resolution is very inferior to that of the St. Santin bistatic radar.

The St. Santin radar measures the velocity component lying along the bisector of the angle included by the antenna beams (Fig. 9) which lies approximately in the same direction as the lines of force of the earth's magnetic field. Drifts observed at $F$-region altitudes are therefore interpreted as being drifts along the field line [89]. At $E$-region altitudes, however, the interpretation is less straightforward since there is likely to be an appreciable horizontal component.

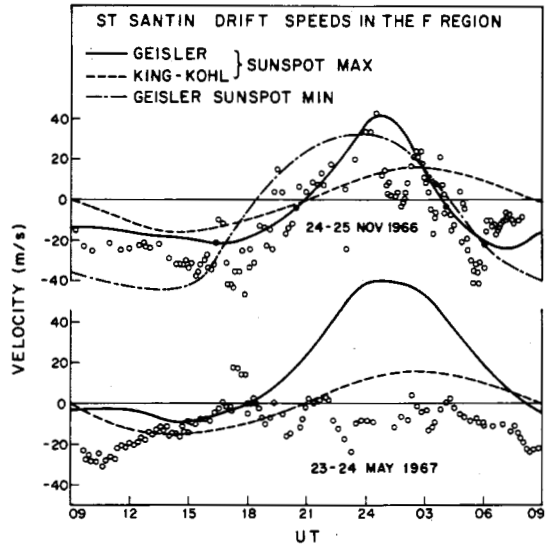


Fig. 31. Measurements of vertical drift in the $F$ region at St. Santin [89]. These points represent the average behavior over the height interval 200 to 400 km, and have been compared with predicted values for the drift velocity that should arise as a result of the drag of the neutral atmosphere which is set in motion by the diurnal heating and cooling cycle [90], [91].

Fig. 31 shows vertical velocity determinations obtained by the French group [89] in which the behavior observed has been compared with predictions by Geisler [90] and Kohl and King [91] for the drifts that should be set up by motion of the neutral air as a result of the diurnal heating and cooling of the upper atmosphere. In later studies the French group has attempted to solve the continuity equation for the ionization at $F$-region heights employing the observed drift velocities to compute the divergence term [92]. They conclude that $\boldsymbol{E} \times \boldsymbol{B}$ drifts *across* the field line (i.e., drifts set up by ionospheric electric fields) are important since the values of loss rate that they derive show a diurnal variation [92]. Unfortunately, as their instrument is not sensitive to a velocity component normal to the field lines, an experimental test of this conclusion is not presently possible. The question of attempting to determine three orthogonal components of the drift velocity is touched upon later in this section.

Bistatic operation of Arecibo is planned as a means of studying one component of $E$-region drifts [93]. An array of fourteen 30- by 30-foot cylindrical parabolic antennas has been erected some 120 km from Arecibo. This instrument will be employed to study the altitude range 110 to 120 km (or 120 to 130 km) with a resolution of about 1.5 km.

### C. Autocorrelation Measurements

In the autocorrelation approach, the information that the signal spectrum is shifted in frequency is contained in the phases of the two reflected pulses. Thus besides determining the echo amplitude correlation it is necessary to determine the phase shift as a function of spacing. We discussed in Section IV-B the method by which the phase shift (due to Faraday rotation) between coincident opposite sense pulses is determined. Using the same techniques it is possible to determine the drift velocity $v$ from

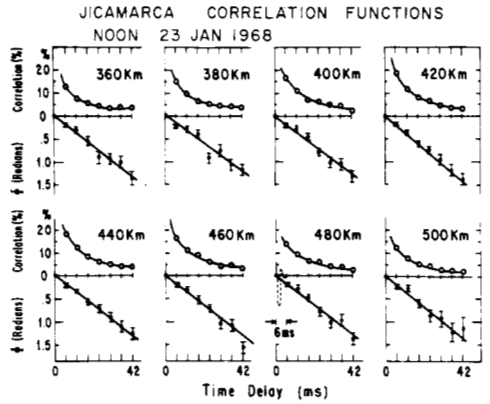


Fig. 32. The amplitude and phase of the echo autocorrelation functions observed at Jicamarca [94]. The constant phase shift with increasing pulse separation indicates the existence of a frequency offset in the spectrum caused by a vertical drift. Good correlation out to very large pulse separations has been made possible by directing the antenna beam normal to the magnetic field lines so that the spectrum narrows to a sharp line.

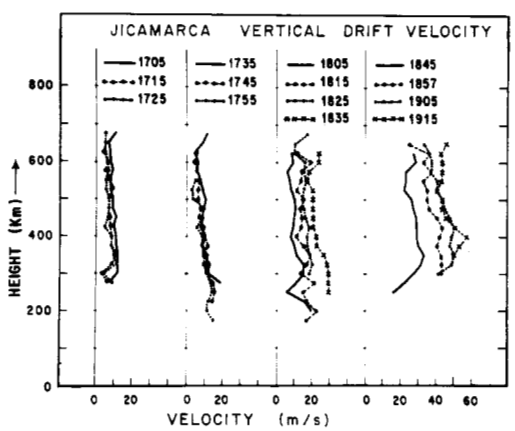


Fig. 33. Drift velocities versus altitude and time observed at Jicamarca [94].

$$v = \frac{\lambda}{4\pi}\left(\frac{d\phi}{d\tau}\right)_{av} \tag{66}$$

where $(d\phi/d\tau)_{av}$ is the average phase change between pulses separated by $\tau$ seconds. Fig. 32 shows the results of measurements of this type performed at Jicamarca [94]. The fact that the slopes of the phase plots are very similar indicates that (in this instance) the vertical velocity was the same at all heights.

One special feature of the Jicamarca radar is the ability to observe perpendicular to the magnetic field. In this direction the spectrum narrows into a single sharp line (Sections VI-D and IX-B). This causes the correlation to persist over extremely long intervals (Fig. 32) thereby permitting very precise velocity estimates. Woodman and Hagfors [95], who have examined the accuracy involved, estimate that for Jicamarca the uncertainty $\Delta v$ is of the order of $\pm 1$ m/s. Fig. 33 provides an illustration of some of the results being obtained by this technique. The interpretation of the drifts in this case seems well established. Since the electrons (and ions) are moving across the field lines, this drift must arise as an $\boldsymbol{E} \times \boldsymbol{B}$ effect, i.e., a vertical drift arising from an east-west electric field. The electric field is believed to be that

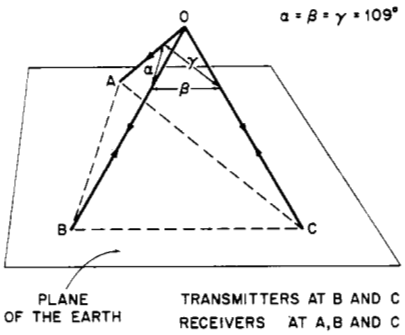


Fig. 34. An arrangement of three stations that yields three orthogonal velocity components. The drift is measured in the direction of the perpendicular bisectors of the angles AOB, BOC, COA. Transmitters are required at two of the stations in order to complete all the paths.

responsible for driving the equatorial electrojet. It would be out of place here to describe the Jicamarca results further and it must suffice to say that they provide convincing evidence in support of the "fountain" theory of the equatorial anomaly [96], [97].

### *D. Determination of Three Orthogonal Components*

We have seen that while Jicamarca and St. Santin are both sensitive to vertical drifts, one measures the velocity component *across* the magnetic fieldlines while the other measures the drift *along* the field. No system has been constructed which measures more than one velocity component, though considerable thought has been given to the matter.

If three antennas are to be employed at the corners of a triangle *ABC*, then their beams must intersect as shown in Fig. 34 in order that the bisectors of the three included angles be mutually perpendicular. It is immediately obvious that 1) none of the beams can be directed vertically, 2) with stations fixed to the ground this property holds for only one altitude, and 3) transmitters are required at two of the stations in order to complete all paths. The problem that three mutually perpendicular directions cannot be obtained at all heights has no ready solution. The best that one can do is arrange that mutually perpendicular bisectors are obtained at an altitude of about 200 km where (at temperate latitudes) drifts along and across the field lines seem equally likely. Above this altitude the instrument will then be more sensitive to vertical drifts than horizontal, and the reverse will be true at lower altitudes. Fig. 35 shows an arrangement in which this is achieved using one transmitting station with a vertically directed beam (at 0) and three receiver stations. If the velocity accuracy for each path is $\Delta v$ [given in (60)], then the accuracy with which the vertical ($z$-component) and components along the $x(OC)$ and $y$ directions can be determined is given in Table VIII in units of $\Delta v$.

Yet a third arrangement is shown in Fig. 36. There the transmitting station is at *C* and transmits CW (to complete the paths *CBA*, *CBD*) in addition to making backscatter measurements (i.e., along *CB*). The relative error estimates in this case are lower than for the four-station scheme (Table IX) provided that the pulse measurement yields the same accuracy of velocity determination as the bistatic measure-

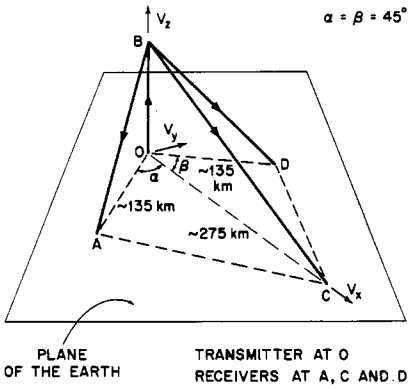


Fig. 35. An arrangement that yields acceptable sensitivity to the three components of the wind velocity [29]. A vertically directed transmitting station (at 0) is employed with three receiving stations.

TABLE VIII

ERROR IN DRIFT VELOCITY AS A FUNCTION OF HEIGHT IN UNITS OF THE VELOCITY ERROR $\Delta V$ OF THE MEASUREMENTS FOR THE FOUR-STATION CW RADAR SHOWN IN FIG. 35

*($C\hat{O}D = C\hat{O}A = 45°$.) In this arrangement the transmitter is at O and receivers are placed at A, C, and D*

| Height (km) | $\Delta V_x$ | $\Delta V_y$ | $\Delta V_z$ |
|---|---|---|---|
| 100 | 1.06 | 1.20 | 1.40 |
| 200 | 2.44 | 1.64 | 1.65 |
| 300 | 3.13 | 2.16 | 1.80 |

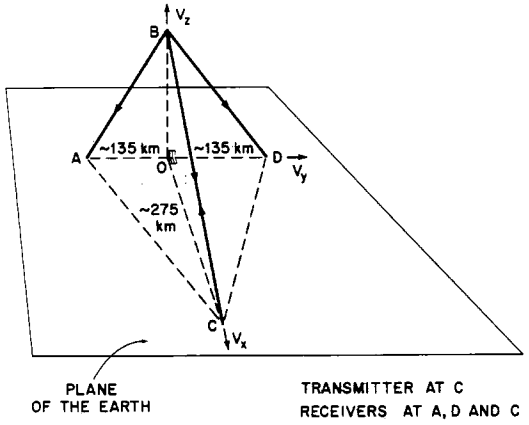


Fig. 36. A three-station arrangement for measuring orthogonal velocity components for a proposed radar in the Midwest [29]. In this scheme the transmitting station is at $C$ and receivers are placed at all three stations. The spacings shown were chosen to make the beam sizes match with antennas at $A$ and $D$ that are only two-thirds the size of that at $C$.

TABLE IX

ERROR IN DRIFT VELOCITY AS A FUNCTION OF HEIGHT IN UNITS OF THE VELOCITY ERROR (ASSUMED EQUAL) IN EACH OF THE THREE MEASUREMENTS

*Here it is assumed that three stations are employed as in Fig. 36 and the station at C makes a monostatic measurement.*

| Height (km) | $\Delta V_x$ | $\Delta V_y$ | $\Delta V_z$ |
|---|---|---|---|
| 100 | 0.92 | 0.85 | 1.605 |
| 200 | 1.20 | 1.18 | 1.08 |
| 300 | 1.48 | 1.59 | 0.97 |

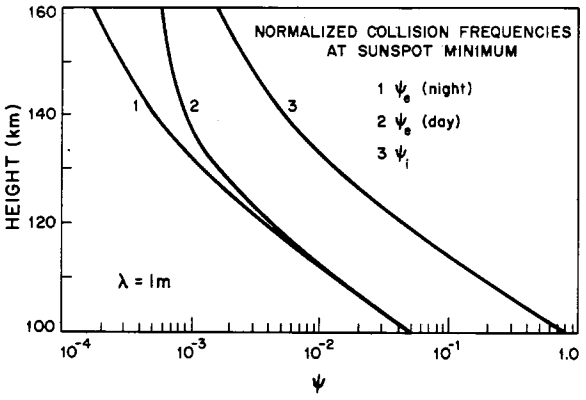


Fig. 37. The normalized ion and electron collision frequencies as a function of altitude at sunspot minimum. The function $\psi_e$ is the wavelength $\lambda$ divided by $4\pi$ times the mean free path of the electrons and $\psi_i$ is the corresponding function for the ions. In this figure the wavelength $\lambda$ has been taken to be one meter (after Dougherty and Farley [99]).

ments. Of the two schemes, the one shown in Fig. 36 requires the lesser number of stations but is capable of examining only one altitude at a time. The arrangement of Fig. 35 offers the opportunity of examining a number of altitudes simultaneously by employing antenna arrays at each receiving station with which multiple beams may be synthesized.

## VIII. DETERMINATION OF NEUTRAL ATMOSPHERE PROPERTIES

### A. Effect of Collisions on the Spectrum

In earlier sections nothing was said concerning the influence of collisions on the spectrum of the scattered signals. This was because collision effects are negligible above about 120-km altitude for all wavelengths of practical interest (10 meters $\geq \lambda \geq$ 0.2 meter). Below this altitude, however, depending somewhat on wavelength, collision effects become important, making it impossible to determine $T_e$ and $T_i$ separately.

The effect of neutral collisions on the spectrum in the case $\lambda \gg 4\pi D$ has been considered by a number of authors [98]–[101]. Of importance is the ratio of the scale of the exploring wavelength $\lambda/4\pi$ to the mean free path of the electrons $l_e$ and ions $l_i$ where

$$l_e = (\nu_e \sqrt{m_e/2KT_e})^{-1} \tag{67}$$

$$l_i = (\nu_i \sqrt{m_i/2KT_i})^{-1} \tag{68}$$

in which $\nu_e$ and $\nu_i$ are the electron-neutral and ion-neutral collision frequencies, respectively. The ratios $\psi_e = \lambda/4\pi l_e$ and $\psi_i = \lambda/4\pi l_i$ are plotted in Fig. 37 based upon data published by Johnson [102] for $\lambda = 1$ meter. It can be seen that $\psi_e \approx 0.1\ \psi_i$ at almost all altitudes, i.e., the mean free path of the electrons is approximately an order of magnitude larger than that of the ions. As a consequence, ion-neutral collisions are more important than electron-neutral encounters.

An obvious approach to describing theoretically the effects of collisions is to introduce in the kinetic equation specifying the dynamics of the ions (i.e., the Vlasov equa-

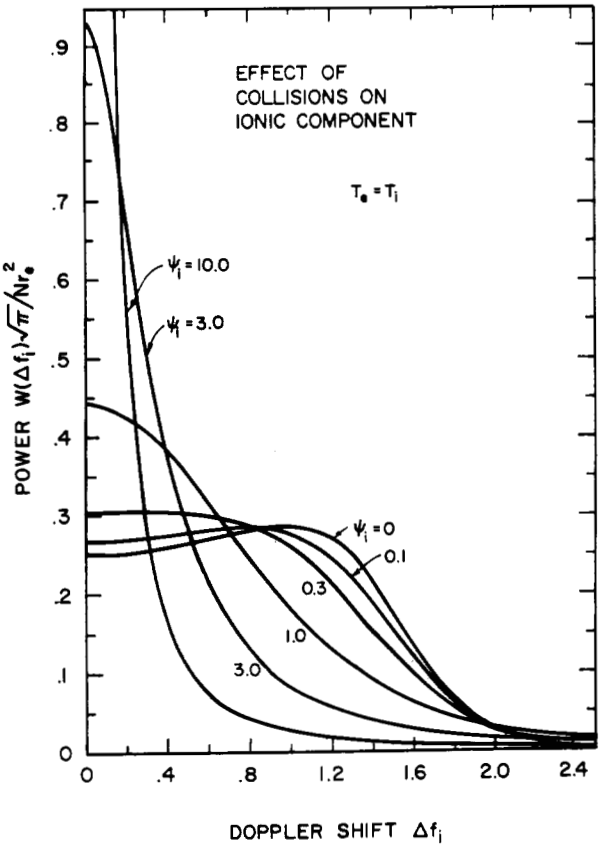


Fig. 38. The effect of collisions on the ionic component in the case $\lambda \gg 4\pi D$ and $T_e/T_i = 1$. The frequency scale is in units of the Doppler shift produced by an ion approaching at its mean thermal speed [(21)]. Plots are given for different values of the ratio $\psi_i$; $\psi_e$ has been taken to be 0.1 $\psi_i$ (after Dougherty and Farley [99]).

tion) a relaxation term $-\nu f(r, v, t)$, where $f(r, v, t)$ is the perturbation in the ion velocity distribution. This modification by itself is not correct because particles in the velocity space "absorbed" by collisions are not reemitted. Thus, Dougherty and Farley [99] employed a collision term suggested by Bhatnagar *et al.* [103]:

$$\left|\frac{df}{dt}\right|_{\text{col}} = -\nu\left[f(r, v, t) - \frac{\Delta N}{N}(r, t)F(v)\right] = -\nu\left[f(r, v, t) - \frac{F(v)}{N}\int f(r, v, t)\, d^3v\right]. \tag{69}$$

Equation (69) attempts to remedy the defect of the simple relaxation term by adding a "reemission" term which reintroduces ions with a Maxwellian velocity distribution $F(v)$. Though this equation does preserve locally (and instantaneously) the density, neither the laws of conservation of energy or momentum are satisfied. Further modifications of (69) are possible which accomplish this and spectra have been calculated [101], [104] using such a collision term.

Results obtained by Dougherty and Farley [99] are plotted in Fig. 38. It can be seen that when the ion mean free path $l_i$ becomes small compared to $\lambda/4\pi$, the spectrum begins to narrow and loses its double-humped appearance. It is then no longer possible to establish if $T_e > T_i$ from the spectrum shape. The total scattered power remains the same, i.e., independent of the collision frequency [99].

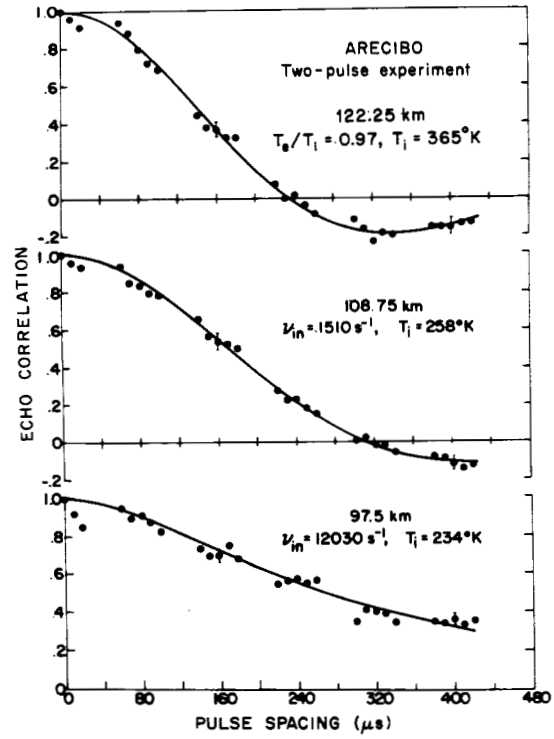


Fig. 39. Sample autocorrelation functions (points) and best fit theoretical curves at *E*-region altitudes above Arecibo [106]. In the upper plot the ion-neutral collision frequency $\nu_i$ has been taken to be zero and both $T_i$ and $T_e/T_i$ have been obtained. In the lower two plots it has been assumed the $T_e = T_i$ and $\nu_i$ and $T_i$ have been measured. For all cases an ion mass $m_i = 30$ AMU was assumed.

### *B. Neutral Properties Between 100 and 120 km*

From Fig. 38 it can be seen that for $\psi_i \leq 1.0$ the spectrum shape is distinctly non-Gaussian and hence two parameters are required in order to characterize it. If it is assumed that $T_e = T_i$ and only a single ion is present, then these two parameters are $T_i$ and $\nu_i$. Given these two parameters it is immediately possible to determine the neutral density if it is further assumed that $T_i = T_n$. This step is accomplished by computing the collision frequency from [105]

$$\nu_{\text{in}} = 2.6 \times 10^3 \sum_j (N_j)(\alpha_j/\nu_j)^{\frac{1}{2}} \quad \text{s}^{-1} \tag{70}$$

where $N_j$ is the density of the $j$th neutral species, $\alpha_j$ is the neutral gas atomic polarizability, and $\nu_j$ the ion-neutral reduced mass. At *E*-region altitudes where $N_2$ and $O_2$ are the principal neutral constituents and $O_2^+$ and $NO^+$ the principal ions (70) can be written [106], [107]

$$\nu_{\text{in}} = 0.9 \times 10^{-15} N(\text{N}_2) \quad \text{s}^{-1}. \tag{71}$$

The assumption that $T_e = T_i = T_n$ seems quite reasonable for the altitude range 100 to 120 km where collision effects become important. Since the masses of $O_2^+$ and $NO^+$ are similar, the assumption of only a single ion is also acceptable. Fig. 39 shows autocorrelation results (Section V-B) obtained at Arecibo by Wand and Perkins [106] for various altitudes in this region. In the upper trace it has been assumed that $\nu_i = 0$ and the function has been interpreted to yield $T_i$ (from the position of the zero crossing) and $T_e/T_i$ (from the depth of the first minimum). In this instance the ion mass was assumed to be $m_i = 30$ AMU. The middle

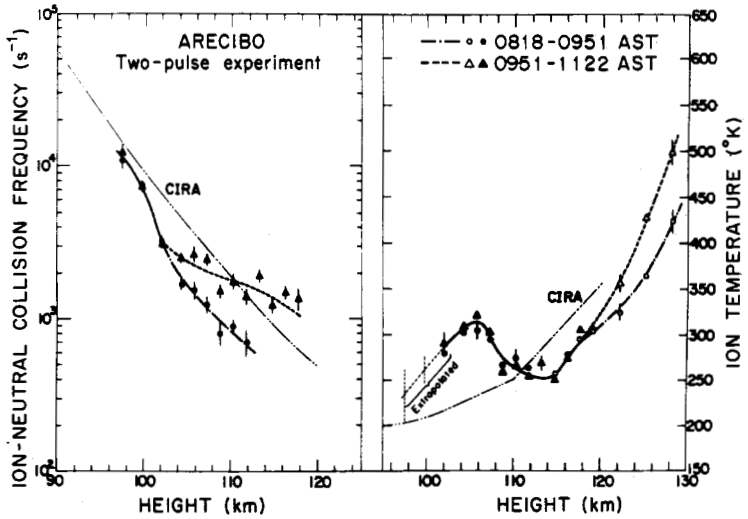


Fig. 40. Values of ion temperature $T_i$ and ion-neutral collision frequency obtained at Arecibo [106] and compared with the CIRA 1965 model atmosphere.

plot shows evidence of collisions and was interpreted to yield $\nu_i$ and $T_i$. It is possible to determine only a single parameter from the lower plot because the spectrum has become completely rounded (Fig. 38) and thus $\nu_i$ was obtained by extrapolating downwards the curve of $T_i$ observed at higher altitudes. Fig. 40 shows the results obtained for $T_i$ and $\nu_i$ [106]. These data are compared in Fig. 40 with the CIRA 1965 model atmosphere. While showing general agreement with the CIRA model, the radar results suggest that the behavior of this region is more complex than implied by the model. Similar work has been attempted by the French group [107] with somewhat different results.

In sum, it seems that Thomson Scatter radar can provide important information on the neutral atmosphere in the region 100 to 120 km, which presently lies above the altitude ($\sim$70 km) explored by the rocket soundings of the meteorological net and below the working altitudes of satellites. The properties (temperature density, etc.) of the upper end of this region are unrealistically assumed to be time invariant in existing model atmospheres, and better information is a prerequisite for improving the models. A word of caution is perhaps in order. The collision theory discussed above has yet to be subjected to careful experimental check and thus radar observations of this region should be tested, perhaps by combined rocket and radar experiments.

### C. Exospheric Temperature

Based upon theory and a number of rocket observations, the temperature of the neutral atmosphere is believed to increase rapidly in the altitude region 120 to 220 km and then become largely isothermal [75]. An isothermal region above about 250 km is expected because of the absence of major heat sources at this and higher altitudes and the high thermal conductivity of the gas (owing to the large mean free paths of the particles). The temperature of the isothermal region is usually called the exospheric temperature $T_\infty$ or $T_{ex}$ [see (51)]. Because of its importance as a means of characterizing the state of the entire upper atmosphere, a number of authors have sought to determine $T_{ex}$ from Thomson Scatter observations [56], [89], [107]–[109].

At altitudes up to about 250 km it appears that the ion and neutral temperatures are equal [56], [70], [75] (also Section VI-C). Thus by measuring $T_i$ at an altitude in the range 250 to 300 km (i.e., where $O^+$ ions predominate, Fig. 24), it is possible to determine $T_{ex}$. At night it seems a sufficient approximation to assume $T_i = T_{ex}$ but during the day it is probably necessary to allow for a small temperature difference $(T_i - T_{ex})$ which depends upon the altitude chosen. This small temperature difference can be computed by equating the heat transferred from the electrons to the ions in Coulomb encounters [107], [108]

$$Q_{ei} = \frac{2.82 \times N^2(T_e - T_i)}{T_e^{3/2}} \text{ J/m}^3\text{/s} \tag{72}$$

to the heat transferred from the ions to the neutrals. The main heat transfer processes here are [105]

1) resonant ion neutral energy loss between $O^+$ and O

$$Q_{in} = 1.23 \times 10^{-8} N(O^+)N(O)(T_i + T_n)^{\frac{1}{2}}(T_i - T_n) \text{ J/m}^3\text{/s} \tag{73}$$

2) elastic collisions with $N_2$

$$Q_{in} = 3.89 \times 10^{-7} N(O^+)N(N_2)(T_i - T_n) \text{ J/m}^3\text{/s} \tag{74}$$

3) combined elastic collisional and charge transfer energy loss to molecular oxygen

$$Q_{in} = 4.0 \times 10^{-7} N(O^+)N(O_2)(T_i - T_n) \text{ J/m}^3\text{/s}. \tag{75}$$

The terms $N$, $T_e$, and $T_i$ in (72) can all be determined directly from the Thomson Scatter observations, but in order to compute the ion-neutral loss, assumptions must be made concerning the number densities of the neutral constituents. Since the difference $T_i - T_n \leq 100°\text{K}$ at 300 km, it seems that the results for $T_{ex}$ will not be very sensitive to these assumptions.

Fig. 41 shows temperature measurements for the exospheric temperature obtained in the manner described [89].

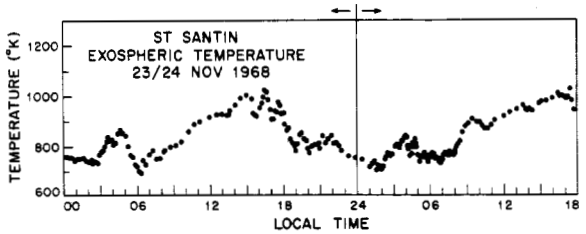


Fig. 41. Examples of the diurnal variation of the exospheric temperature $T_{ex}$ obtained from ion temperature measurements [89]. The increases near dawn probably result from a breakdown of the technique because of the rapid change in $T_e$ at this time. Note that the diurnal maximum occurs later than 1400 hours—the time of peak density derived from satellite drag measurements [75].

It is possible that near dawn the method breaks down for a period when $T_i > T_n$ and ion conduction losses to lower altitudes are important. At other times an approximately sinusoidal variation is found albeit with fine scale fluctuations. The latter may be a manifestation of internal gravity waves. Of special interest in Fig. 41 is that the peak of the diurnal variation occurs between 1600 and 1700 hours local time instead of 1400 hours as inferred from satellite drag observations [75]. This feature has been found at other stations also [107], [108].

It is clear that measurements of $T_{ex}$ near 300 km and measurements of pressure and temperature near 120 km (above) essentially establish the boundary conditions for the neutral atmosphere. As such, Thomson Scatter observations hold the promise of providing almost continuous monitoring of the temperature and pressure of the neutral constituents of the upper atmosphere.

## IX. Further Applications

### A. Fast Photoelectron Flux

We discussed in Section IV-C the plasma lines of the spectrum that are located at approximately $\pm f_N$ with respect to the radar frequency, where $f_N$ is the plasma frequency (1). These lines are normally extremely weak and are not detectable by any existing radar system, except during the daytime when enhanced by the presence of fast photoelectrons. It will be recalled that the electrons which couple to the wave are those which travel with the same phase velocity $v_{ph}$ [see (42)] and which therefore have an energy $E_{ph} = \frac{1}{2} m_e (v_{ph})^2$ [see (43)]. Electrons with energy $E > E_{ph}$ will overtake the wave and feed energy into it, whereas the reverse will be true of electrons with energy less than $E_{ph}$ (Landau damping). Thus the degree of enhancement depends upon the ratio of the number of electrons that serve to support the wave to the number that damp it, i.e., upon the slope of the number $F$ versus velocity $v$ curve at the point $v = v_{ph}$. In the absence of collisions, therefore, the departure from equilibrium can be expressed by a velocity-dependent temperature $T(v)$ which can be defined in terms of a logarithmic derivative of $F(v)$ [49]–[51]

$$T(v) \equiv -(m_e v/K) F(v) (dF/dv)^{-1} \qquad (76)$$

where $m_e$ is the electron mass and $K$ is Boltzmann's constant. The steady-state intensity of the plasma oscillation is then proportional to $T(v)$, and the ratio of the intensity of the plasma line to the ionic component is $(4\pi)^2 \varepsilon_0 KT(v_{ph})/\lambda^2 Ne^2$. As noted in Section IV-C, photoelectrons are continuously produced during the day by solar ultraviolet, mainly in the energy range 1 to 25 eV. In the $F$ region the photoelectrons have a spatial density of the order of $10^{-6}$ of the ambient electron density so that $T(v)$ is almost constant and equal to the ambient electron temperature $T_e$ (2000 to 3000°$K$) for energies up to about 14 $KT_e$. Since $KT_e$ is of the order of 0.2 eV, this means that $T(v)$ and $T_e$ will be the same for velocities corresponding to energies $E(=m_e v^2/2)$ of up to about 3 eV. At higher energies the photoelectrons will dominate and $KT(v)$ will rise rapidly to a value of the order of 10 eV. Thus, an enhancement of the plasma line (neglecting collisions) by a factor $T(v_{ph})/T_e \sim 50$ can be expected at heights where the phase velocity of the wave $v_{ph}$ corresponds to particle energies $E_{ph} \geq 3$ eV.

The effect of the earth's magnetic field upon the plasma wave is important for a wide range of angles $\phi$ between the radar beam and the normal to the field line [49]. This is because the ambient electrons which provide the Landau damping can couple to the wave more readily in the presence of a weak magnetic field, since their gyrorotation about the field lines can cause them to appear to be traveling at $v_{ph}$. That is, an electron may rotate around the field line in a period of $m/f_N$ seconds, i.e., an exact number of cycles of the wave, and hence will reappear in the same position with respect to the wave crest. This effect serves to raise somewhat the minimum energy at which the plasma line is enhanced. Fig. 42 shows the enhancement energy $KT(v_{ph})$ plotted as a function of $f_N$ for wavelengths $\lambda = 0.7$, 0.23, and 2.0 meters and off-perpendicular angles $\phi = 90°$, 50°, and 10° [51]. As $\phi \to 0°$, nulls appear in the function $KT(v_{ph})$ at multiples of the electron gyrofrequency $f_H$ [defined in (53)] which was taken to be 1 MHz in this figure for $\lambda = 0.7$ meter and 1.5 MHz for the other two wavelengths.

The decrease in $KT(v_{ph})$ shown in Fig. 42 for large values of $f_N$ results from electron-ion collision damping which begins to dominate the behavior of the plasma wave at energies $E_{ph} > 25$ eV where the photoelectron density falls to an extremely low value [51].

The first detection of the enhanced plasma line was made at Arecibo [50] and since then it has been observed at most of the other observatories [110], [111] except Jicamarca where, even when enhanced, the line is below the detection threshold owing to the small value of $\alpha(=4\pi D/\lambda)$ (see Section IV-C). The nulls in the enhancement spectrum at harmonics of the gyrofrequency (Fig. 42) have been observed at Stanford [111].

The intensity of the plasma line echo can be computed from the radar equation (28) where the cross section $\sigma$ is multiplied by a factor $\alpha^2[T(v_{ph})/T_e]$ and the number of electrons in the scattering volume $NcT/2$ becomes $2H_e b/f_N$, where $H_e$ is the electron density scale height and $b$ the filter bandwidth [51]. Here it is assumed that the height interval contributing to the echo is set by the combination of the altitude variation of $f_N$ and by the filter bandwidth $b$, and hence is

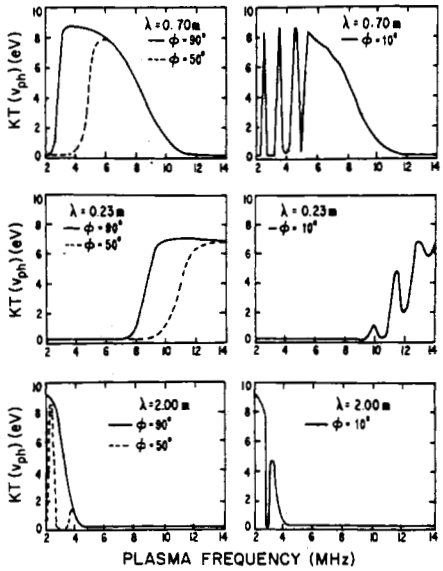


Fig. 42. Numerical calculations of the quantity $KT(v_{ph})$. The electron temperature was assumed to be $T_e = 2000°K$, $\phi$ is the angle of the radar beam with respect to the normal to the magnetic field, and $\lambda$ is the radar wavelength. For $\lambda = 0.70$ meter the electron gyrofrequency $f_H$ was assumed to be $f_H = 1.0$ MHz and for $\lambda = 0.23$ meter and $\lambda = 2.0$ meters, $f_H = 1.5$ MHz. The systematic decrease of $KT(v_{ph})$ for high plasma frequencies results from electron-ion collisions (after Yngvesson and Perkins [51]).

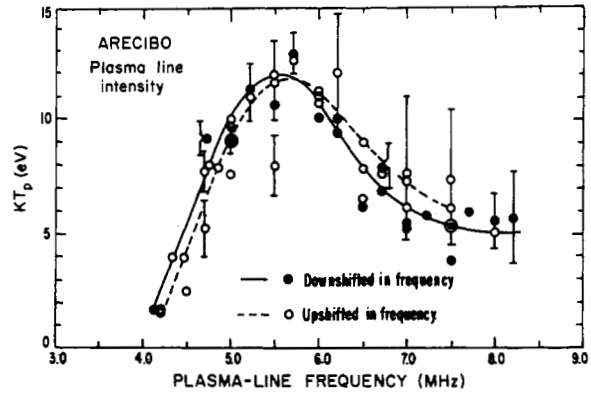


Fig. 43. Measurements of $KT(v_{ph})$ in the topside ionosphere at Arecibo. The open circles are derived from the intensity of the plasma line lying $f_N$ MHz below the radar frequency and hence caused by upward traveling photoelectrons (after Yngvesson and Perkins [51]).

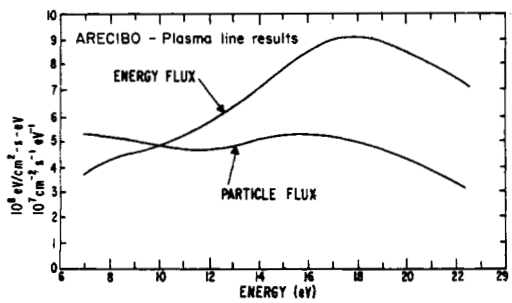


Fig. 44. Differential upward particle and energy fluxes obtained from the curve of Fig. 43 assuming the velocity distribution of (77) (after Yngvesson and Perkins [50]).

much less than $cT/2$. It follows that by measuring the intensity of the plasma lines over a range of values of $f_N$, it is possible to obtain the derivative of the photoelectron velocity distribution $dF/dv_{ph}$ at a number of points in the velocity spectrum.. Unfortunately, this function will in general vary with altitude and since $f_N$ is a function of altitude, the results will not be very meaningful. However, above 300 km, electrons with energies $E \geq 6$ eV can travel a considerable distance (i.e., greater than one scale height $H_e$) before being brought to rest via encounters with other particles, and some electrons can completely escape the local ionosphere. Thus, in the altitude range 300 to 1000 km, the energy spectrum of the escaping and arriving energy fluxes for $E \geq 6$ eV is largely height independent, and hence measurements of $T(v_{ph})$ from many altitudes can be employed to give a single spectrum. The results obtained for $T(v_{ph})$ by Yngvesson and Perkins [51] are shown in Fig. 43.

The results of Fig. 43 determine uniquely the one-dimensional velocity distribution function along the vertical. In order to convert this to a three-dimensional distribution, Yngvesson and Perkins [51] assumed that

$$F(v) = \begin{cases} F^+(|v|^2)\cos\alpha & 0 < \cos\alpha < 1 \\ F^-(|v|^2)|\cos\alpha| & -1 < \cos\alpha < 0 \end{cases} \quad (77)$$

where $\alpha$ is the pitch angle between the velocity vector and the magnetic field and the + and − refer to the upward and downward going fluxes, respectively. This model provides for few electrons with $\alpha \to 90°$ since these are removed by collisions. Fig. 44 shows the energy and particle fluxes that result. The total escaping energy flux appears to be $2 \times 10^{13}$ eV/m$^2$/s (1 eV $= 1.6 \times 10^{-19}$ joule). These observations provide direct experimental evidence in support of conclusions reached on the escape of energy from the ionosphere from the observed thermal behavior [43], [70], [73].

In view of the fact that few satisfactory instruments have been developed for *in situ* examination of fast photoelectrons, these Thomson Scatter radar results are of considerable importance. The inability to determine the energy spectrum for a single altitude is a handicap, which could in principle be overcome by making measurements at many widely spaced frequencies.

### *B. Direction of the Magnetic Field*

There are other applications of Thomson Scatter radar that we shall not attempt to discuss here. We would be remiss, however, if nothing were said about experiments to determine the direction of the earth's magnetic field. There are a number of possible methods by which this may be done. For example, Millman [112] and Cohen [113] have employed the dependence of the amount of Faraday rotation as in (37) on the angle $\theta_h$ between the field and the beam as a means of investigating the direction of the magnetic field. In this process it is necessary to determine the absolute density by some other means, and both these authors used ionosonde records, thus limiting the range of altitudes that could be examined to those below the $F2$ peak.

We have mentioned in earlier sections effects of the magnetic field on the spectrum and intensity of the scattered signals. Any of these may be employed to determine the

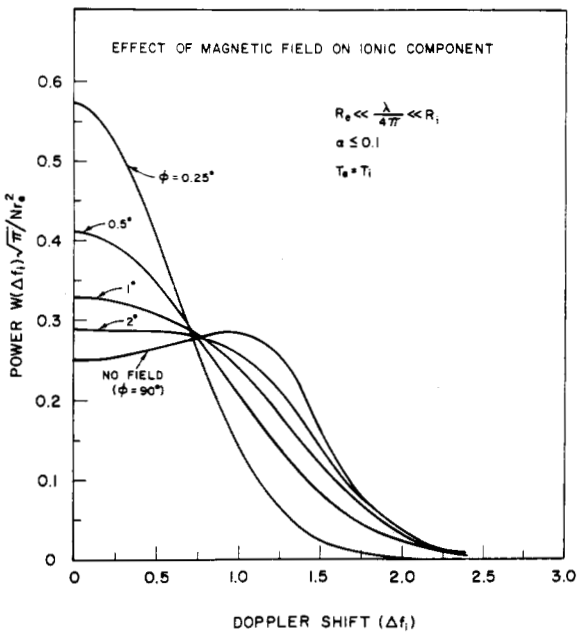


Fig. 45. The effect on the spectrum when the ray path is nearly normal to the field lines in the case where the exploring scale lies between the electron and ion gyroradius. Here $\phi$ is the off-perpendicular angle (after Renau *et al.* [79]).

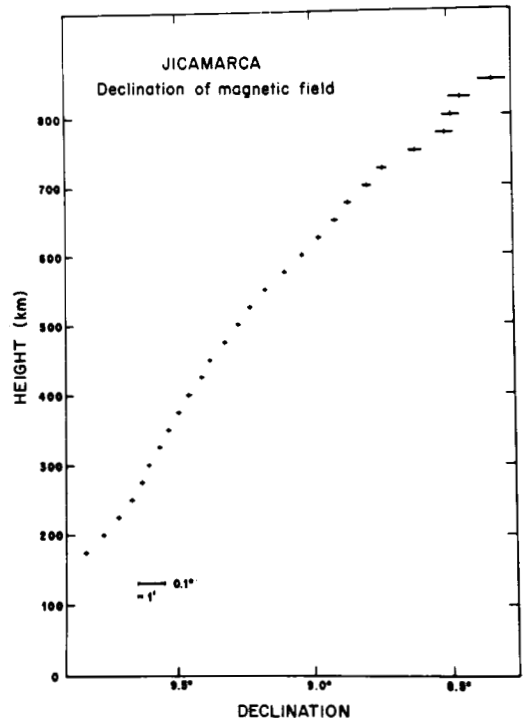


Fig. 46. The declination of the earth's magnetic field above Jicamarca determined by interferometer observations of the direction in which the echo autocorrelation persists over the longest interval (after Woodman [116]).

altitude at which the beam is directed normal to the magnetic field.

The imposition of a magnetic field serves in general to increase the total echo power when $T_e/T_i > 1.0$ [80]. Thus one technique (employed at Stanford [114]) to locate the position where the beam is normal to the field is to measure the echo power as a function of beam position. Historically, the earliest method employed was that of searching for the narrowing of the signal spectrum that should occur in this position. Fig. 45 shows theoretical plots demonstrating this effect for the case where the wavelength scale $\lambda/4\pi$ lies between the electron gyroradius $R_e$ and ion gyroradius $R_i$ [(54) and (55)]. Pineo *et al.* [115] observed this phenomenon using a radar located on Trinidad that could be directed to be normal to the field lines at *F*-region heights. However, since the beamwidth was 2°, these measurements did not define the magnetic field direction very precisely.

At Jicamarca, Woodman [116] has employed the same phenomenon (i.e., the narrowing of the spectrum) in an ingenious way. By splitting the antenna into two halves he has essentially made interferometer measurements to search for the direction in which the spectrum is narrowest. As noted in Section VII-C, the region contributing to the positive correlation of the echoes obtained with widely spaced pulses is that part lying within the beam essentially along a normal to the field line. If now the complex cross correlation is determined of the signals received on two halves of the antenna for long delays in the autocorrelation function, the phase of the cross correlation will indicate the direction of arrival of the signals and hence the normal direction to the field line. Woodman [116] estimates that this technique is potentially accurate to $\sim 1$ arc minute and Fig. 46 shows his results for the declination of the field as a function of altitude above Jicamarca.

## X. Closing Remarks

We believe that the preceding sections should serve to demonstrate the remarkable potential of Thomson Scatter radar systems for investigations of the upper atmosphere. While it has not perhaps been made clear earlier, it should be stressed that many of the observations described can be made *simultaneously* so that the results obtained in a few minutes are often equivalent to what might be accomplished with a successful well-equipped rocket. The ability to repeat the measurements at will is then comparable to a succession of such launches.

It seems increasingly evident that many of the unsolved questions regarding both the neutral and ionized constituents of the upper atmosphere involve the dynamics of these regions. For this reason, the long time history afforded by radar observations is particularly valuable and could not be readily duplicated by rocket launches. The capability of the radar to determine the velocity of the undisturbed plasma is likely to be of increasing importance, and future radar systems are likely to be built with this specifically in mind [117].

In view of the difficulty of extracting from satellite data separately the dependence upon local time, latitude, longitude, season, and geomagnetic coordinates, we believe that a balanced program of ionospheric study would be one in which vertical profiles obtained by Thomson Scatter radars (and rockets) are "tied together" by observations carried out by satellites in circular, near-polar orbits.

## Acknowledgment

The author wishes to express thanks to numerous colleagues for past fruitful discussions and for helpful com-

ments on this paper, which is dedicated to the late V. C. Pineo, who pioneered Thomson Scatter radar studies of the ionosphere at Millstone Hill.

## References


[1] E. V. Appleton and M. A. F. Barnett, "On some direct evidence for downward atmospheric reflection of electric rays," *Proc. Roy. Soc.* (London), vol. 109, pp. 621–641, 1926.

[2] G. Breit and M. Tuve, "A test of the existence of the conducting layer," *Phys. Rev.*, vol. 28, pp. 554–573, 1926; also, "A radio method for estimating the height of the ionosphere conducting layer," *Nature*, vol. 116, p. 357, 1925.

[3] S. Chapman, "The absorption and dissociative or ionizing effect of monochromatic radiation in an atmosphere on a rotating earth," *Proc. Roy. Soc.* (London), vol. 43, pp. 26–45, 1931; also, "The absorption and dissociative or ionizing effect of monochromatic radiation in an atmosphere on a rotating earth. Part II: Grazing incidence," *Proc. Roy. Soc.* (London), vol. 43, pp. 484–501, 1931.

[4] See, for example, J. A. Ratcliffe, *The Magneto-Ionic Theory and Its Application to the Ionosphere*. London: Cambridge University Press, 1959.

[5] T. Yonezawa, "Theory of formation of the ionosphere," *Space Sci. Rev.*, vol. 5, pp. 3–56, 1966.

[6] H. Rishbeth, "On explaining the behavior of the ionospheric F region," *Rev. Geophys.*, vol. 6, pp. 33–71, February 1968.

[7] D. K. Bailey, R. Bateman, L. V. Berkner, H. G. Booker, G. F. Montgomery, E. M. Purcell, and W. W. Salisbury, "A new kind of radio propagation at very high frequencies observable over long distances," *Phys. Rev.*, vol. 86, pp. 141–145, 1952.

[8] H. G. Booker and W. E. Gordon, "A theory of radio scattering in the troposphere," *Proc. IRE*, vol. 38, pp. 401–412, April 1950.

[9] H. G. Booker, "A theory of scattering by non-isotropic irregularities with application to radar reflections from the aurora," *J. Atmos. Terr. Phys.*, vol. 8, pp. 204–221, 1956.

[10] J. J. Thomson, *Conduction of Electricity Through Gases*. London: Cambridge University Press, 1906, pp. 321–326.

[11] J. Fejer, "Scattering of radiowaves by an ionized gas in thermal equilibrium," *Can. J. Phys.*, vol. 38, pp. 1114–1133, 1960; also, "Scattering of radiowaves by an ionized gas in thermal equilibrium," *J. Geophys. Research*, vol. 65, pp. 2635–2636, 1960.

[12] W. E. Gordon, "Incoherent scattering of radio waves by free electrons with applications to space exploration by radar," *Proc. IRE*, vol. 46, pp. 1824–1829, November 1958.

[13] K. L. Bowles, "Observations of vertical incidence scatter from the ionosphere at 41 Mc/sec," *Phys. Rev. Lett.*, vol. 1, pp. 454–455, 1958.

[14] ——, "Incoherent scattering by free electrons as a technique for studying the ionosphere and exosphere: Some observations and theoretical considerations," *J. Research NBS*, vol. 65D, pp. 1–13, 1961.

[15] J. P. Dougherty and D. T. Farley, "A theory of incoherent scattering of radio waves by a plasma," *Proc. Roy. Soc.* (London), vol. A259, pp. 79–99, 1960.

[16] E. E. Salpeter, "Electron density fluctuations in a plasma," *Phys. Rev.*, vol. 120, pp. 1528–1535, 1960; also, "Scattering of radiowaves by electrons above the ionosphere," *J. Geophys. Research*, vol. 65, pp. 1851–1852, 1960.

[17] T. Hagfors, "Density fluctuations in a plasma in a magnetic field with applications to the ionosphere," *J. Geophys. Research*, vol. 66, pp. 1699–1712, 1961.

[18] D. Pines and D. Bohm, "A collective description of interactions II: Collective vs. individual particle aspects of the interactions," *Phys. Rev.*, vol. 85, pp. 338–353, 1952.

[19] See, for example: G. Fiocco and E. Thompson, "Thomson scattering of optical radiation from an electron beam," *Phys. Rev. Lett.*, vol. 10, pp. 89–91, 1963; A. W. DeSilva, D. E. Evans, and M. J. Forrest, "Observations of Thomson and co-operative scattering of ruby laser light by a plasma," *Nature*, vol. 203, pp. 1321–1322, 1964.

[20] J. Renau, "Scattering of electromagnetic waves from a non-degenerate ionized gas," *J. Geophys. Research*, vol. 65, pp. 3631–3640, 1960.

[21] M. N. Rosenbluth and N. Rostoker, "Scattering of electromagnetic waves by a non-equilibrium plasma," *Phys. Fluids*, vol. 5, pp. 776–788, 1962.

[22] O. Buneman, "Scattering of radiation by the fluctuations in a non-equilibrium plasma," *J. Geophys. Research*, vol. 67, pp. 2050–2053, 1962.

[23] J. Renau, "The cross section for scattering of electromagnetic waves from an ionized plasma in thermal non-equilibrium," *J. Geophys. Research*, vol. 67, pp. 3624–3626, 1962.

[24] ——, "Notes on number density fluctuations and the scattering cross section for electromagnetic waves scattered from a thermal nonequilibrium plasma," *Z. Physik*, vol. 177, pp. 458–494, 1964.

[25] E. E. Salpeter, "Density fluctuations in a non-equilibrium plasma," *J. Geophys. Research.*, vol. 68, pp. 1321–1333, 1963.

[26] D. R. Moorcroft, "On the power scattered from density fluctuations in a plasma," *J. Geophys. Research*, vol. 68, pp. 4870–4872, 1963.

[27] ——, "On the determination of temperature and ionic composition by electron backscattering from the ionosphere and magnetosphere," *J. Geophys. Research*, vol. 69, pp. 955–970, 1964.

[28] J. V. Evans, "Studies of the F region by the incoherent backscatter method," M.I.T. Lincoln Lab., Lexington, Mass., Tech. Rept. 274, 1962.

[29] J. V. Evans and Y. T. Lo, "Antenna design for a Thomson scatter radar," University of Illinois, Aeronomy Lab., Urbana, Ill., Rept. 23, 1967.

[30] K. L. Bowles, G. R. Ochs, and J. L. Green, "On the absolute intensity of incoherent scatter echoes from the ionosphere," *J. Research NBS*, vol. 66, pp. 395–407, July/August 1962.

[31] K. L. Bowles, "Measuring plasma density in the magnetosphere," *Science*, vol. 139, pp. 389–391, 1963.

[32] ——, NBS, Boulder, Colo., Rept. 6070, 1959 (unpublished).

[33] W. E. Gordon and L. M. LaLonde, "The design and capabilities of an ionospheric radar probe," *IRE Trans. Antennas and Propagation*, vol. AP-9, pp. 17–22, 1961.

[34] W. E. Gordon, "Arecibo Ionospheric Observatory," *Science*, vol. 146, pp. 26–30, 1964.

[35] H. C. Carlson, "Ionospheric heating by magnetic conjugate point photoelectrons as observed at Arecibo," Cornell University, Ithaca, N. Y., CRSR 212, 1965.

[36] F. H. du Castel, M. Petit, and P. Waldteufel, "Le sondeur ionosphérique à diffusion du CNET," *L'Onde Élec.*, vol. 46, pp. 1–4, March 1966.

[37] P. Schwab, "L'émmeteur du sondeur ionospherique à diffusion," *L'Onde Élec.*, vol. 46, pp. 5–7, March 1966.

[38] Y. Tocquec, "L'Antenne d'émission du sondeur ionosphérique," *L'Onde Élec.*, vol. 46, pp. 9–14, March 1966.

[39] M. Parmantier, "Realisation de l'antenne d'émission du sondeur ionosphérique à diffusion du CNET," *L'Onde Élec.*, vol. 46, pp. 15–19, March 1966.

[40] M. Petit and M. Reyssat, "La station de réception du sondeur ionosphérique à diffusion français," *L'Onde Élec.*, vol. 46, pp. 21–24, March 1966.

[41] J. V. Evans and M. Loewenthal, "Ionospheric backscatter observations," *Planet. Space Sci.*, vol. 12, pp. 915–944, 1964.

[42] J. V. Evans, "Ionospheric backscatter observations at Millstone Hill," *Planet. Space Sci.*, vol. 13, pp. 1031–1074, 1965.

[43] ——, "Midlatitude F-region densities and temperatures at sunspot minimum," *Planet. Space Sci.*, vol. 15, pp. 1387–1405, 1967.

[44] ——, "Ionospheric temperatures during the launch of NASA Rocket 814 on July 2, 1963," *J. Geophys. Research*, vol. 69, pp. 1436–1444, 1964.

[45] I. C. Browne, J. V. Evans, J. K. Hargreaves, and W. A. S. Murray, "Radio echoes from the moon," *Proc. Phys. Soc.*, vol. B69, pp. 901–920, 1956; also, J. V. Evans, "The measurement of the electron content of the ionosphere by the lunar radio echo method," *Proc. Phys. Soc.*, vol. B69, pp. 953–955, 1956.

[46] G. H. Millman, A. J. Moceyunas, A. E. Sanders, and R. F. Wyrick, "The effect of Faraday rotation on incoherent backscatter observations," *J. Geophys. Research*, vol. 66, pp. 1564–1568, 1961.

[47] D. T. Farley, J. P. McClure, D. L. Sterling, and J. L. Green, "Temperature and composition of the equatorial ionosphere," *J. Geophys. Research*, vol. 72, pp. 5837–5851, 1967.

[48] K. L. Bowles and Staff of Jicamarca Radio Observatory, Instituto de Geofisico del Peru, "Profiles of electron density over the magnetic equator obtained using the incoherent scatter technique," NBS, Boulder, Colo., Tech. Note 169, March 1963.

[49] F. W. Perkins and E. E. Salpeter, "Enhancement of plasma density fluctuations by non-thermal electrons," *Phys. Rev.*, vol. 139A, pp. 59–69, 1965.

[50] F. W. Perkins, E. E. Salpeter, and K. O. Yngvesson, "Incoherent

scatter from plasma oscillations in the ionosphere," *Phys. Rev. Lett.*, vol. 14, pp. 579–581, 1965.
[51] K. O. Yngvesson and F. W. Perkins, "Radar Thomson Scatter studies of photoelectrons in the ionosphere and Landau damping," *J. Geophys. Research*, vol. 73, pp. 97–110, 1968.
[52] K. O. Yngvesson (unpublished).
[53] See, for example, R. B. Blackman and J. W. Tukey, *The Measurement of Power Spectra*. New York: Dover, 1959.
[54] F. W. Perkins, "Physical and computational considerations in the interpretation of Thomson Scatter spectra," in *Thomson Scatter Studies of the Ionosphere—An Informal Conference Record*, University of Illinois, Aeronomy Lab., Urbana, Ill., Rept. 19, 1967.
[55] H. Carru, M. Petit, and P. Waldteufel, "Mesures de températures électroniques et ioniques par diffusion incohérente," *J. Atmos. Terr. Phys.*, vol. 29, pp. 351–366, 1967.
[56] J. V. Evans, "Electron temperature and ion composition in the $F_1$ region," *J. Geophys. Research*, vol. 72, pp. 3343–3355, 1967.
[57] J. P. McClure, "Faraday dispersion loss at Jicamarca," in *Thomson Scatter Studies of the Ionosphere—An Informal Conference Record*, University of Illinois, Aeronomy Lab., Urbana, Ill., Rept., 19, 1967.
[58] R. C. Sagalyn, M. Smiddy, W. P. Sullivan, R. Wand, G. Thome, L. M. LaLonde, and H. C. Carlson, "Rocket borne and backscatter measurements of charged particle temperatures in the lower ionosphere," presented at the Spring URSI Meeting, Washington, D. C., 1968.
[59] J. S. Greenhow, H. K. Sutcliffe, and C. D. Watkins, "The electron scattering cross-section in incoherent backscatter," *J. Atmos. Terr. Phys.*, vol. 25, pp. 197–207, 1963.
[60] J. V. Evans, "Incoherent backscatter studies of the ionosphere at Millstone Hill," in *Electron Density Distribution in the Ionosphere and Exosphere*, E. Thrane, Ed. Amsterdam: North Holland Publ. Co., 1964, p. 266.
[61] L. A. Maynard and E. D. DuCharme, "A new technique for the measurement of the electron/ion temperature ratio at high altitudes," *Can. J. Phys.*, vol. 43, pp. 2088–2092, 1965.
[62] D. T. Farley, "Observations of the equatorial ionosphere using incoherent backscatter," in *Electron Density Profiles in the Ionosphere and Exosphere*, J. Frihagen, Ed. Amsterdam: North Holland Publ. Co., 1966, p. 446.
[63] C. D. Watkins, G. N. Taylor, and J. B. A. Roberts, "Some preliminary $F_2$ region studies at Malvern." in *Thomson Scatter Studies of the Ionosphere—An Informal Conference Record*, University of Illinois, Aeronomy Lab., Urbana. Ill., Rept. 19, 1967.
[64] K. O. Yngvesson and F. W. Perkins, "Plasma line observations," in *Research in Ionospheric Physics*, Cornell University, Ithaca, N. Y., CRSR Rept. 70, 1967.
[65] D. T. Farley, "Ionospheric temperature and composition measurements at the magnetic equator," *Ann. Géophys.*, vol. 22, pp. 448–453, 1966.
[66] H. C. Carlson and W. E. Gordon, "Radar spectrographic estimates of ionic composition from 225 to 1400 kilometers for solar minimum winter and summer conditions," *J. Geophys. Research*, vol. 71, pp. 5573–5578, 1966. Also, S. S. Prasad, "Nightime ionic composition and temperature over Arecibo," *J. Geophys. Research*, vol. 73, pp. 6795–6807, 1968.
[67] D. R. Moorcroft, "Nighttime, topside, ionic composition and temperature over Arecibo, Puerto Rico," *J. Geophys. Research*, in press, 1969.
[68] W. B. Hanson, "Electron temperatures in the upper atmosphere," in *Space Research*, vol. 3, W. Priester, Ed. Amsterdam: North Holland Publ. Co., 1963, p. 282.
[69] P. M. Banks, "Ion temperature in the upper atmosphere," *J. Geophys. Research*, vol. 72, pp. 3365–3385, 1967.
[70] J. V. Evans and G. P. Mantas, "Thermal structure of the temperate latitude ionosphere," *J. Atmos. Terr. Phys.*, vol. 30, pp. 563–577, 1968.
[71] J. C. Holmes, C. Y. Johnson, and J. M. Young, "Ionospheric chemistry," in *Space Research*, vol. 5, D. G. King-Hele, P. Muller, and G. Righini, Eds. Amsterdam: North Holland Publ. Co., 1965, p. 756.
[72] M. Petit, "Application de la diffusion 'quasi-incohérent' à la mesure de la température, de la composition ionique et de la concentration électronique de l'ionosphère," *Ann. Géophys.*, vol. 19, pp. 63–71, 1963.
[73] ——, "Mesures de températures, de densité électronique et de composition ionique dans l'ionosphère par diffusion de Thomson, Étude du déséquilibre thermodynamique dans l'ionosphere diurne," *Ann. Géophys.*, vol. 24, pp. 1–38, 1968.
[74] C. Y. Johnson, "Ionospheric composition and density from 90 to 1200 kilometers at solar minimum," *J. Geophys. Research*, vol. 71, pp. 330–332, 1966.
[75] For example, see J. V. Evans, "Ground-based measurements of atmospheric and ionospheric particle temperatures," in *Solar Terrestrial Physics*, J. W. King and W. S. Newman, Eds. London: Academic Press, 1967, ch. 9.
[76] F. W. Perkins and R. H. Wand, "$E$ and $F_1$ region composition and temperature measurements at Arecibo," in *Thomson Scatter Studies of the Ionosphere—An Informal Conference Record*, University of Illinois, Aeronomy Lab., Urbana, Ill., Rept. 19, 1967.
[77] J. A. Fejer, "Scattering of radiowaves by an ionized gas in thermal equilibrium in the presence of a uniform magnetic field," *Can. J. Phys.*, vol. 39, pp. 716–740, 1961.
[78] D. T. Farley, J. P. Dougherty, and D. W. Barron, "A theory of incoherent scattering of radio waves by a plasma. II: Scattering in a magnetic field," *Proc. Roy. Soc.* (London), vol. A263, pp. 238–258, 1961.
[79] J. Renau, M. Camnitz, and W. Flood, "The spectrum and the total intensity of electromagnetic waves scattered from an ionized gas in thermal equilibrium in the presence of static quasi-uniform magnetic field," *J. Geophys. Research*, vol. 66, 2703–2732, 1961.
[80] D. T. Farley, "A theory of incoherent scattering of radio waves by a plasma. IV: The effect of unequal electron and ion temperatures," *J. Geophys. Research*, vol. 71, pp. 4091–4098, 1966.
[81] ——, "The effect of Coulomb collisions on incoherent scattering of radio waves by a plasma," *J. Geophys. Research*, vol. 69, pp. 197–200, 1966.
[82] L. Spitzer, Jr., *Physics of Fully Ionized Gases*. New York: Interscience, 1956.
[83] D. T. Farley, "Proton gyroresonance observed in incoherent scattering from the ionosphere," *Phys. Fluids*, vol. 10, pp. 1584–1586, 1967.
[84] G. D. Thome, "Incoherent scatter observations of travelling ionospheric disturbances," *J. Geophys. Research*, vol. 69, pp. 4047–4049, 1964.
[85] L. M. LaLonde, "Incoherent backscatter observations of sporadic E," *J. Geophys. Research*, vol. 71, pp. 5059–5063, 1966.
[86] P. B. Rao, "Night-time plasma transport in the topside ionosphere using backscatter $N_h$ profiles," *J. Atmos. Terr. Phys.*, vol. 30, pp. 1415–1427, July 1968.
[87] G. L. Lamb, "The scattering of electromagnetic waves by non-equilibrium plasma," Los Alamos Sci. Lab., Los Alamos, N. Mex., Rept. LA 2715, 1962.
[88] H. Carru, M. Petit, and P. Waldteufel, "Mise en évidence de mouvements dans l'ionosphère au moyen de la diffusion incohérente," *Compt. Rend. Acad. Sci. Paris*, vol. 264, pp. 560–563, 1967.
[89] H. Carru, M. Petit, G. Vasseur, and P. Waldteufel, "Résultats ionosphériques obtenus par diffusion de Thomson 1966–1967," *Ann. Gèophys.*, vol. 23, pp. 455–465, 1967.
[90] J. E. Geisler, "Atmospheric winds in the middle latitude $F$ region," *J. Atmos. Terr. Phys.*, vol. 28, pp. 703–720, 1966.
[91] H. Kohl and J. W. King, "Atmospheric winds between 100 and 700 km and their effects on the ionosphere," *J. Atmos. Terr. Phys.*, vol. 29, pp. 1045–1062, 1967.
[92] G. Vasseur and P. Waldteufel, "Étude par diffusion de Thomson de la production et de la recombinaison dans la région $F$ de l'ionosphère diurne,"CNET, Issy-les-Moulineaux, France, Tech. Note GRI/NTP/21, 1968.
[93] L. M. LaLonde, "Bistatic station," in *Research in Ionospheric Physics*, Cornell University, Ithaca, N. Y., CRSR Rept. RS74, 1968.
[94] J. P. McClure, "Observations of vertical drifts in the ionosphere near the magnetic equator," presented at the Spring URSI Meeting, Washington, D. C., 1968.
[95] R. F. Woodman and T. Hagfors, "Methods for the measurement of vertical ionospheric motions near the magnetic equator by incoherent scattering," *J. Geophys. Research*, in press, 1969.
[96] W. B. Hanson and R. J. Moffett, "Ionization transport effects in the equatorial $F$ region," *J. Geophys. Research*, vol. 71, pp. 5559–5572, 1966.
[97] D. F. Martyn, "Theory of height and ionization density changes at the maximum of a Chapman-like region, taking account of ion production, decay, diffusion and total drift," in *Proc. Cambridge Conf.* London: Phys. Soc., 1955, p. 254.
[98] R. Benoit, "Le spectre de diffusion incohérent dans un plasma avec ou sans collisions," in *Proc. Internatl. Conf. on Ionosphere*, A. C. Strickland, Ed. London: Phys. Soc., 1963.

[99] J. P. Dougherty and D. T. Farley, "A theory of incoherent scattering of radio waves by a plasma. III: Scattering in a partly ionized gas," *J. Geophys. Research*, vol. 66, pp. 5473–5486, 1963.
[100] E. C. Taylor and G. C. Comisar, "Frequency spectrum of thermal fluctuations in plasmas," *Phys. Rev.*, vol. 132, pp. 2379–2384, 1963.
[101] P. Waldteufel, "Sur le terme de collision dans l'équation de Boltzmann d'un gaz—Application à la diffusion d'une onde électromagnétique par un plasma," *Compt. Rend. Acad. Sci. Paris*, vol. 257, pp. 3835–3837, 1963.
[102] *Satellite Environment Handbook*, F. S. Johnson, Ed. Stanford, Calif.: Stanford University Press, 1961.
[103] P. L. Bhatnagar, E. P. Gross, and M. Krook, "A model for collision processes in gases. I: Small amplitude process in charged and neutral one-component systems," *Phys. Rev.*, vol. 94, pp. 511–525, 1954.
[104] P. Waldteufel, "Introduction de l'effect des collisions élastiques sur l'équation de Boltzmann d'un gaz faiblement ionizé—Application à la diffusion incohérent d'une onde électromagnétique par l'ionosphère," *Ann. Géophys.*, vol. 21, pp. 106–120, 1965.
[105] P. Banks, "Collision frequencies and energy transfer:Ions," *Planet. Space Sci.*, vol. 14, pp. 1105–1122, 1966.
[106] R. H. Wand and F. W. Perkins, "Radar Thomson Scatter observations of temperature and ion-neutral collision frequency in the *E* region," *J. Geophys. Research*, vol. 73, pp. 6370–6372, 1968.
[107] P. Waldteufel, "Thomson Scatter measurements concerning the neutral atmosphere," in *Thomson Scatter Studies of the Ionosphere —An Informal Conference Record*, University of Illinois, Aeronomy Lab., Urbana, Ill., Rept. 19, 1967.
[108] J. S. Nisbet, "Neutral temperatures from incoherent scatter observations," *J. Atmos. Sci.*, vol. 24, pp. 586–593, September 1967.
[109] K. K. Mahajan, "Diurnal variation of the ion temperature," *J. Atmos. Terr. Phys.*, vol. 31, pp. 93–101, 1969.
[110] H. Carru and G. Lejeune, "Caractéristiques des raies de plasma observées en France par sondage à diffusion de Thomson," *Compt. Rend. Acad. Sci. Paris*, vol. 266, pp. 890–892, March 1968.
[111] E. J. Fremouw and J. Petriceks, "Observations of the incoherent scatter plasma line at large and small angles to the geomagnetic field," presented at the Spring URSI Meeting, Washington, D. C., 1968.
[112] G. H. Millman, "Magnetic field measurements by the incoherent scatter technique," *J. Atmos. Terr. Phys.*, vol. 27, pp. 586–591, 1965.
[113] R. Cohen, "Determination of electron concentration and magnetic field inclination from the Faraday rotation of an incoherently scattered signal," in *Thomson Scatter Studies of the Ionosphere—An Informal Conference Record*, University of Illinois, Aeronomy Lab., Urbana, Ill., Rept. 19, 1967.
[114] M. Baron and J. Petriceks, "Incoherent scattering at perpendicular intersection with the earth's magnetic field," *J. Geophys. Research*, vol. 72, pp. 5325–5329, 1967.
[115] V. C. Pineo, D. P. Hynek, and G. H. Millman, "Geomagnetic effects on the frequency spectrum of incoherent backscatter observed at 425 megacycles per second at Trinidad," *J. Geophys. Research*, vol. 68, pp. 2695–2706, 1963.
[116] R. Woodman, "Measurement of the direction of the magnetic field using incoherent scatter techniques," presented at the Spring URSI Meeting, Washington, D. C., 1968.
[117] J. V. Evans, "Design considerations for a Thomson Scatter radar," University of Illinois, Aeronomy Lab., Urbana, Ill., Rept. 17, 1967.

# Optical Doppler Measurement of Microscale Wind Velocity

JAMES C. OWENS, MEMBER, IEEE

**Abstract—A system analysis of the feasibility of optical heterodyne measurement of Doppler shifts as a method for the remote determination of vector wind velocity is carried out. It is found that with a 50-mW laser at 6328 Å, naturally occurring aerosols in clear air will permit measurements at distances of only a few tens of centimeters, but haze and dust will extend this range to a few tens of meters and fog to 75 meters. By generating smoke to enhance the scatter, a range of about 40 meters will be achievable. The use of a 1-watt argon laser will extend the clear-air and smoke-plume ranges by a factor of 48 and the ranges in uniform dust or fog by smaller amounts. Hence useful measurements in the boundary layer of the atmosphere are possible although they will require some artificial contamination of the air to give consistently good results. Remote temperature measurement is not possible using this technique.**

## I. Introduction

MONOSTATIC microwave Doppler radar techniques are commonly used for tropospheric measurements of wind velocity in storms and for ionospheric studies of electron and ion densities and temperatures. The mean velocity component of the scattering elements along the beam direction is given by the mean Doppler shift of the received signal, while the spectral width of the signal provides a measure of the range of scattering element velocities within the scattering volume. In the case of ionospheric Thomson scatter, this spectral width can be used to calculate the kinetic temperatures of the scattering elements. Because the fractional Doppler shifts are very small, coherent detection is required. The development of lasers has made possible the extension of these techniques to the optical spectral region. The principal advantage of this extension is that with the very short wavelength of visible light much greater spatial resolution is possible than with radio or microwave systems; when the beam is focused, volumes as small as $1 \times 10^{-6}$ cm$^3$ can be examined at a distance of a meter or more. In addition, although the fractional Doppler shift is independent of carrier frequency, the absolute shift is much larger at optical than at radio frequencies, thus offering the possibility of improved precision in the velocity measurement. For these reasons, optical Doppler measurements of fluid velocity [1] and of the ve-

Manuscript received January 3, 1969.
The author is with the ESSA Research Laboratories, Boulder Colo. 80302.

Fig. 7. A view of the Jicamarca radar facility in Peru. The antenna is a square array of dipoles, 300 meters along a side. The building houses the transmitter, receivers, and data processing equipment. (Courtesy of ESSA Research Laboratories, Boulder, Colo.)

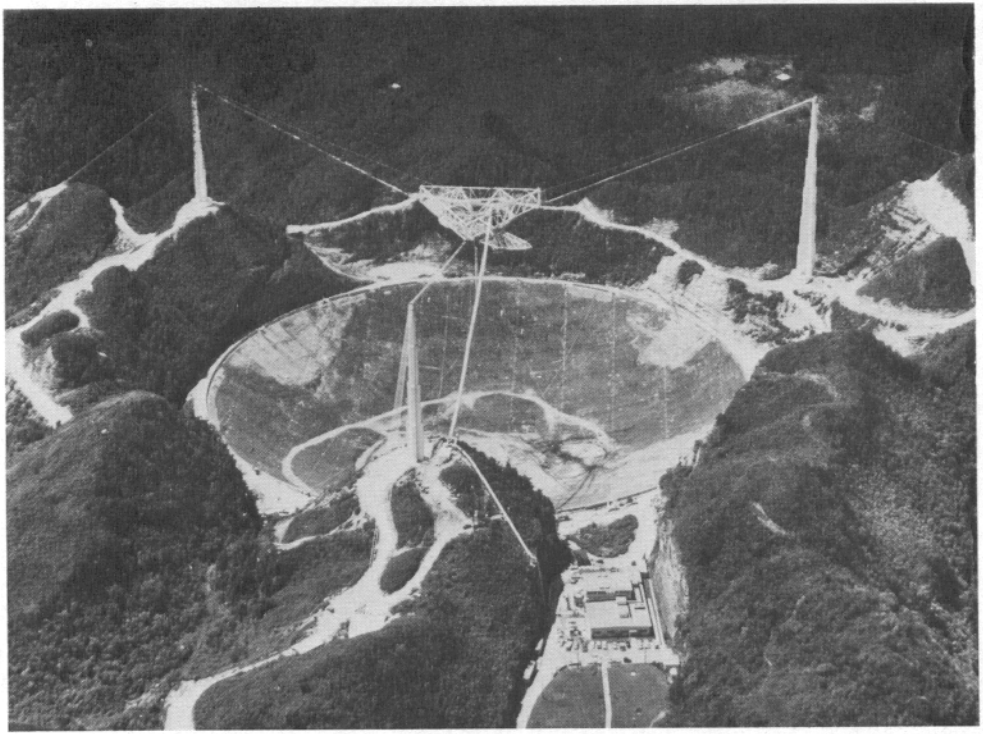

Fig. 8. The Arecibo Ionospheric Observatory in Puerto Rico. The antenna is a spherical reflector 300 meters in diameter situated in a limestone sinkhole. The feed system is supported by cables which pass over the tops of the three towers. The electronic equipment is located in the building at the bottom of the picture. (Courtesy of Cornell University, Center for Radio Physics and Space Research, Ithaca, N. Y.)